UNCLASSIFIED

(2)

REPORT DOCUMENTATION PAGE

Form Approved
OMB No. 0704-0188

1. AGENCY USE ONLY (Leave blank)	2. REPORT DATE	3. REPORT TYPE AND DATES COVERED
	December 26, 1990	Final Report: May 1, 1986 - October 31, 1990

AD-A232 714

4. TITLE AND SUBTITLE
Unsteady Flow Structure from Swept Edges Subjected to Controlled Motion

5. FUNDING NUMBERS
AFOSR-86-0177
2307/A3

6. AUTHOR(S)
Professor Donald Rockwell

7. PERFORMING ORGANIZATION NAME(S) AND ADDRESS(ES)
Lehigh University
354 Packard Laboratory #19
Bethlehem, Pennsylvania 18015

8. PERFORMING ORGANIZATION REPORT NUMBER
LU-AFOSR-FR-90

AFOSR-TR- 91 0139

9. SPONSORING/MONITORING AGENCY NAME(S) AND ADDRESS(ES)
Air Force Office of Scientific Research
AFOSR/NA Fluid Mechanics Program
Bolling Air Force Base
Building 410
District of Columbia 20332-66448

10. SPONSORING/MONITORING AGENCY REPORT NUMBER
AFOSR-86-0177

11. SUPPLEMENTARY NOTES

DTIC
ELECTE
MAR 12 1991
D

12a. DISTRIBUTION/AVAILABILITY STATEMENT
Approved for public release,
distribution unlimited

12b. DISTRIBUTION CODE

13. ABSTRACT (Maximum 200 words)

This program addresses the unsteady flow structure and loading of delta wings subjected to controlled pitching motion. Efforts are focussed on three primary areas: generation of computer-aided techniques for quantitative interpretation of flow structure; development of new types of experimental instrumentation and facilities; and characterization of the unsteady flow structure on delta wings.

Computer-aided techniques of quantitative visualization of the vortex structure involve tracking of hydrogen bubble timelines and particles illuminated by scanning lasers. These techniques are integrated with active control systems that generate prescribed pitching motion of delta wings.

Characterization of the unsteady flow structure addresses: response of the vortex breakdown to the motion of the wing; and preliminary consideration of the instantaneous cross-sectional structure of the leading-edge vortices. The phase lag of these features of the flow structure, relative to the wing motion, is a central consideration.

14. SUBJECT TERMS	15. NUMBER OF PAGES
Leading-edge vortices; vortex breakdown; laser diagnostics	26
	16. PRICE CODE

17. SECURITY CLASSIFICATION OF REPORT	18. SECURITY CLASSIFICATION OF THIS PAGE	19. SECURITY CLASSIFICATION OF ABSTRACT	20. LIMITATION OF ABSTRACT
Unclassified	Unclassified	Unclassified	UNCLASSIFIED

NSN 7540-01-280-5500

Standard Form 298 (Rev. 2-89)
Prescribed by ANSI Std. 239-18

91 3 06 196

GENERAL INSTRUCTIONS FOR COMPLETING SF 298

The Report Documentation Page (RDP) is used in announcing and cataloging reports. It is important that this information be consistent with the rest of the report, particularly the cover and title page. Instructions for filling in each block of the form follow. It is important to ***stay within the lines*** to meet ***optical scanning requirements***.

Block 1. Agency Use Only *(Leave blank)*.

Block 2. Report Date. Full publication date including day, month, and year, if available (e.g. 1 Jan 88). Must cite at least the year.

Block 3. Type of Report and Dates Covered. State whether report is interim, final, etc. If applicable, enter inclusive report dates (e.g. 10 Jun 87 - 30 Jun 88).

Block 4. Title and Subtitle. A title is taken from the part of the report that provides the most meaningful and complete information. When a report is prepared in more than one volume, repeat the primary title, add volume number, and include subtitle for the specific volume. On classified documents enter the title classification in parentheses.

Block 5. Funding Numbers. To include contract and grant numbers; may include program element number(s), project number(s), task number(s), and work unit number(s). Use the following labels:

C	- Contract	PR	- Project
G	- Grant	TA	- Task
PE	- Program Element	WU	- Work Unit Accession No.

Block 6. Author(s). Name(s) of person(s) responsible for writing the report, performing the research, or credited with the content of the report. If editor or compiler, this should follow the name(s).

Block 7. Performing Organization Name(s) and Address(es). Self-explanatory.

Block 8. Performing Organization Report Number. Enter the unique alphanumeric report number(s) assigned by the organization performing the report.

Block 9. Sponsoring/Monitoring Agency Name(s) and Address(es). Self-explanatory.

Block 10. Sponsoring/Monitoring Agency Report Number. *(If known)*

Block 11. Supplementary Notes. Enter information not included elsewhere such as: Prepared in cooperation with...; Trans. of...; To be published in.... When a report is revised, include a statement whether the new report supersedes or supplements the older report.

Block 12a. Distribution/Availability Statement. Denotes public availability or limitations. Cite any availability to the public. Enter additional limitations or special markings in all capitals (e.g. NOFORN, REL, ITAR).

- DOD - See DoDD 5230.24, "Distribution Statements on Technical Documents."
- DOE - See authorities.
- NASA - See Handbook NHB 2200.2.
- NTIS - Leave blank.

Block 12b. Distribution Code.

- DOD - Leave blank.
- DOE - Enter DOE distribution categories from the Standard Distribution for Unclassified Scientific and Technical Reports.
- NASA - Leave blank.
- NTIS - Leave blank.

Block 13. Abstract. Include a brief *(Maximum 200 words)* factual summary of the most significant information contained in the report.

Block 14. Subject Terms. Keywords or phrases identifying major subjects in the report.

Block 15. Number of Pages. Enter the total number of pages.

Block 16. Price Code. Enter appropriate price code *(NTIS only)*.

Blocks 17. - 19. Security Classifications. Self-explanatory. Enter U.S. Security Classification in accordance with U.S. Security Regulations (i.e., UNCLASSIFIED). If form contains classified information, stamp classification on the top and bottom of the page.

Block 20. Limitation of Abstract. This block must be completed to assign a limitation to the abstract. Enter either UL (unlimited) or SAR (same as report). An entry in this block is necessary if the abstract is to be limited. If blank, the abstract is assumed to be unlimited.

Final Technical Report for AFOSR-86-0177 Grant

UNSTEADY FLOW STRUCTURE FROM SWEPT EDGES SUBJECTED TO CONTROLLED MOTION

Program Monitors: Captain H. Helin and Dr. J. McMichael, May 1, 1986 - October 31, 1990

Principal Investigator: Professor Donald Rockwell, Department of Mechanical Engineering and Mechanics, Lehigh University, Bethlehem, PA

SUMMARY

This program addresses the unsteady flow structure and loading of delta wings subjected to controlled pitching motion. Efforts have focussed on three primary areas: generation of computer-aided techniques for quantitative interpretation of flow structure; development of new types of experimental instrumentation and facilities; and characterization of the unsteady flow structure on delta wings.

In the area of computer-aided techniques of quantitative flow visualization of vortex structure, emphasis has been on generation of new methods of two and three-dimensional image construction. Such images are produced by tracking hydrogen bubble timelines in three-dimensional space or by obtaining a large number of particle images in a given plane or contiguous planes of the three-dimensional flow.

In the area of experimental instrumentation and facilities, novel types of integrated, active control systems have been developed for simultaneously forcing delta wings and quantitatively determining the instantaneous flow structure. Development of new quantitative visualization techniques has involved flying hydrogen bubble wires, direct particle tracking, and particle image velocimetry employing laser scanning and pulsed-laser techniques.

Characterization of the unsteady flow structure on delta wings subjected to various forms of pitching motion addresses the substantial time shift (or phase lag) between the response of location of vortex breakdown and the wing motion, even at very low values of reduced pitching rate. Moreover, the instantaneous structure of the cross-section of the leading-edge vortices during the pitching motion has been addressed. Preliminary attempts to control the vortex structure using local and global control methods shows several promising possibilities.

TABLE OF CONTENTS

COMPUTER-AIDED TECHNIQUES FOR QUANTITATIVE INTERPRETATION OF FLOW STRUCTURE

I. *COMPUTER-AIDED RECONSTRUCTION OF THREE-DIMENSIONAL FLOWS BY LAGRANGIAN TRACKING OF TIMELINES (Lawson, Magness)*

OBJECTIVES

✓ Construct global, isometric views of flow structure on an oscillating delta wing as a function of time-dependent angle of attack.

✓ Technique: generate, via the pulsed wire method, timelines of bubbles. Track these bubble lines in two orthogonal views to allow construction of instantaneous three-dimensional views.

PRINCIPAL FINDINGS/PROGRESS

✓ A new CAD technique has been developed for determining three-dimensional curves from two-dimensional line projections. This capability involves techniques such as intersection of projected surfaces generated from two-dimensional lines. The resultant three-dimensional lines then can be connected using a bicubic spline technique to form a three-dimensional surface.

✓ Use of this technique has revealed that:

- At given angle of attack, the rate of development of the vortical structure on the wing and the rate of entrainment of the surrounding irrotational fluid are highly dependent on the reduced frequency of oscillation.
- At higher reduced frequency, vortical distortions of different form occur along the surface of the wing at a given instantaneous angle of attack; the timeline surfaces show regions of both positive and negative curvature over the extent of the wing.
- At low reduced frequency, it appears that the three-dimensional shape of the vortical surface tends toward conical similarity; at a threshold (higher) value of reduced frequency, there is departure from this type of similarity along with severe chordwise distortions of the vortical surface.

II. *COMPUTER-AIDED ANALYSIS OF THREE-DIMENSIONAL EVOLUTION OF VORTEX FLOW ON OSCILLATING DELTA WING: APPLICATION OF A NEW LASER-INDUCED REFLECTION TECHNIQUE (Magness, Utsch, Curtis, Lawson)*

OBJECTIVES

- ✓ Using a laser-scanning technique in conjunction with the generation of multiple bubble surfaces, determine the three-dimensional, time-dependent evolution of the flow structure on oscillating, three-dimensional wings.
- ✓ Proposed techniques:
  - Generate laser sheets to define the desired cross-section of the unsteady vortical motion;
  - Determine, in the plane of the laser sheet, the distortion of the multiple bubble surfaces;
  - Track, in non-real-time at a defined angle of attack, the distortion of a defined bubble surface extending from the apex of the wing to its trailing-end. In doing so, use the instantaneous position of the wing as a phase reference.
  - Construct the three-dimensional surfaces representing the instantaneous flow distortion at a given angle of attack using a newly developed CAD technique.

PRINCIPAL FINDINGS/PROGRESS

- ✓ An experimental technique has been developed to generate multiple bubble-timeline surfaces. A three-dimensional adjustable laser-scanning system has also been perfected.
- ✓ A CAD method has been implemented to form three-dimensional surfaces from the individual planes of the flow visualized by laser sheets.

III. *DEVELOPMENT OF NEW METHODS OF THREE-DIMENSIONAL IMAGE CONSTRUCTION FROM PLANES OF PARTICLE IMAGES (Robinson)*

OBJECTIVES

- ✓ Construct three-dimensional images from velocity fields in arbitrarily-spaced and -oriented planes in an unsteady flow field.
- ✓ Apply the technique to unsteady flow past a delta wing using a phase-referencing technique to construct the three-dimensional vortex structure at successive instants of time.

PRINCIPAL FINDINGS/PROGRESS

This technique involves two principal phases: development of accurate interpolation techniques for the velocity fields within the planes of acquired data; and determination of the out-of-plane velocity field and the associated three-dimensional streamline pattern fields within the planes of acquired data; and determination of the out-of-plane velocity field and the associated three-dimensional streamline pattern.

- ✓ For interpolation of the velocity field within each plane, two techniques have been developed: an adaptive Gaussian window (AGW) method; and a spline, thin shell (STS) technique. Both of these techniques have been tested for specified flows, and have been shown to give results that are in good agreement.

- ✓ The technique for determining the three-dimensional field is as follows:

  - Applying the continuity equation at each node of three-dimensional grid, the derivatives in the x and y directions of the in-plane (x,y plane) velocity components (u,v) are fitted by a finite cosine series. The integrated form of this continuity equation is approximated by a modified finite sine series.

  - Applying inverse discrete cosine and sine transforms, using a Fast-Fourier Transform technique, the values of the out-of-plane velocity components at each node are computed.

  - With the three-dimensional velocity field at hand, a tri-cubic spline interpolation is employed to obtain the three-dimensional streamline pattern.

IV. *INVERSE APPROACHES FOR ASSESSING THREE-DIMENSIONAL CONSTRUCTION USING THEORETICAL SOLUTIONS (Robinson)*

OBJECTIVES

- ✓ Using known theoretical solutions of three-dimensional flows, simulate particle tracking occurring in laboratory flows, and reconstruct the known three-dimensional velocity field from the velocity vectors corresponding to the simulated particle images.

- ✓ Feedback inadequacies of the reconstruction technique to the computational scheme in order to optimize the accuracy and speed of the image construction process.

PRINCIPAL FINDINGS/PROGRESS

- ✓ Two classes of theoretical solutions have been considered: a columnar vortex which contains the basic elements of a leading-edge vortex on a delta wing; and a Hill's spherical vortex having highly distributed vorticity and representing many of the features of the bubble mode of vortex breakdown of a leading-edge vortex.

- ✓ For the case of the columnar vortex, the streamlines are not closed, and the flow structure is invariant with the x direction. As a consequence, it is possible to reconstruct the principal features of this vortex with minimum information. Near the central portion of the vortex, where the wavelength of the spiral motion is minimum, it is possible to obtain a faithful representation of the streamline pattern for a distance between data planes corresponding a half wavelength of the spiral of the vortex.

- ✓ For the case of Hill's vortex, the streamlines are closed and the flow structure is variant with streamwise distance. In this case, it is necessary to employ a sufficiently large number of planes (approximately twenty evenly distributed along the axis of the vortex) in order to accurately reproduce the inner portions of the closed streamline pattern.

V. *THREE-DIMENSIONAL IMAGE CONSTRUCTION OF LEADING-EDGE VORTICES FROM PARTICLE IMAGE DATA (Robinson, Magness)*

OBJECTIVES

- ✓ Determine the velocity distribution over defined planes of arbitrary spacing and location along the leading-edge of a delta wing. Develop a technique for determining the separation line from the leading-edge of the wing from the raw particle velocity data.

- ✓ Determine the three-dimensional streamline pattern corresponding to a leading-edge vortex on a stationary delta wing.

- ✓ Using phase-referencing techniques, extend the foregoing procedures to the unsteady leading-edge vortex on a pitching delta wing.

PRINCIPAL FINDINGS/PROGRESS

- ✓ A method has been developed for determining the velocity field over the cross-section of the leading-edge vortex. The separation streamline from the edge of the wing is evaluated by application of either the adaptive Gaussian window (AGW) or spline thin shell (STS) interpolation technique to the raw particle image data. A critical assessment of the accuracy of the two techniques shows that they give very close agreement for the separation streamline. The separation streamline is interpreted as a line cutting across the three-dimensional streamsurface of the leading-edge vortex, coincident with the plane of the original particle image data. In

the event that vortex breakdown occurs within the core of the leading-edge vortex, interpolation is not valid within the breakdown region. The boundary of the (noncircular) domain of breakdown is determined by the interface between the random and organized velocity vector orientations of the original particle image data. This technique has been applied to both a leading-edge vortex from a stationary wing and its corresponding counterpart from a wing undergoing pitching motion.

- ✓ The velocity fields in seven planes covering a chordwise domain of approximately two-thirds the chord of a delta wing have been employed to determine the three-dimensional streamline pattern. In order to accomplish this, the velocity field in a plane angled with respect to the freestream is used to initiate the out-of-plane construction process. Use of the three-dimensional image construction method allows determination of the chordwise streamline pattern.

VI. *TOPOLOGICAL METHODS FOR INTERPRETATION OF FLOW STRUCTURE ON A PITCHING DELTA WING*

OBJECTIVES

- ✓ Develop a streamline construction technique, to be applied to instantaneous velocity fields, that allows interpretation of the primary characteristics of the instantaneous flow structure on the basis of critical point theory.

- ✓ With the critical point theory concepts at hand, and use of a previously-developed three-dimensional construction technique, develop methods for constructing the three-dimensional and streamline and streamsurface patterns along the chord of a pitching delta wing.

PRINCIPAL FINDINGS/PROGRESS

- ✓ An interactive process has been developed for determining the saddle points and foci over an entire plan of data at a three-dimensional flow. This method allows construction of the instantaneous streamline pattern or any cross-section and has particular merit for interactively determining the locations of saddle points and constructing the intersecting streamline patterns in the vicinity of them. This software allows ready identification of the foci (vortex centers) and whether they exhibit stable or unstable characteristics.

- ✓ A method has been developed for construction of the three-dimensional streamline patterns and streamsurfaces at any instant (i.e. given angle of attack) along the entire chord of the delta wing. This method takes advantage of the previously developed techniques involving spectral and finite difference methods to determine the out-of-plane velocity component, and has a number of new, additional features that allow for proper smoothing of streamline patterns in three-dimensional space.

VII. *INTERACTIVE FLOW VISUALIZATION-THEORETICAL SIMULATION (Gursul)*

OBJECTIVES

- ✓ Determine the relationship between visualized flow patterns of unsteady shear flows and the underlying vorticity fields.

- ✓ Formulate criteria for pattern recognition schemes in two- and three-dimensional unsteady flows and characterize fallacies in interpreting visualization of these flows.

PRINCIPAL FINDINGS/PROGRESS

- ✓ The fundamental case of an unsteady free shear flow in the form of a row of simple vortices having the same orientation has been considered using Stuart's exact nonlinear solution. This formulation allows specification of arbitrary concentration of vorticity for a given value of circulation. The evolution of streaklines along the critical layer has been considered for several values of the vorticity concentration parameter.

- ✓ An increased concentration of vorticity actually results in a larger cross-stream extent of the visualized streakline pattern for a given value of circulation.

- ✓ Essentially identical streakline patterns can be obtained for drastically different combinations of vorticity concentration parameter and circulation.

EXPERIMENTAL INSTRUMENTATION AND FACILITIES: NEW TECHNIQUES

VIII. *INTEGRATED ACTIVE CONTROL/QUANTITATIVE FLOW VISUALIZATION/FORCE MEASUREMENT (Magness, Fredriksson)*

OBJECTIVES

- ✓ Develop a computer-controlled system that allows simultaneous control of: the pitching motion of a delta wing; flow visualization using laser-scanning and pulsed-laser illumination of particles; and measurement of the unsteady forces on the oscillating delta wing.
- ✓ Develop a phase-referencing technique that will allow acquisition of velocity and force information that cannot be secured simultaneously. This phase referencing is to be specified by the digital format of the motor controller system.

PRINCIPAL FINDINGS/PROGRESS

- ✓ A new, large-scale apparatus for pitching delta wings has been designed and constructed. It allows, in principle, arbitrary pitching motion and variation of the pitching axis. It is controlled by a Compumotor controller system, which is driven by the central microcomputer. Corresponding software in "C" language has been developed in order to allow forcing of the pitching wing in various ramp-type maneuvers.
- ✓ A laser scanning system for illumination of particles allows quantitative visualization. The camera recording the visualization is fired by the microcomputer-controlled system, allowing images to be acquired at desired phases of the pitching motion of the wing.
- ✓ A high sensitivity force measurement system has been developed using high sensitivity strain gauges. Force signals are in the form of modulated carrier signals in order to improve accuracy.

IX. *DIRECT PARTICLE TRACKING VIA LASER SCANNING (Magness, Kuo)*

OBJECTIVES

- ✓ Develop a technique for illuminating suspended particles. Requirements are: an intensity of illumination an order of magnitude higher than that attainable with conventional chopper (rotating disk) arrangements; and a variable frequency of illumination.
- ✓ Obtain a sufficiently high concentration of illuminated particle images and values of displacement of particle images that will allow accurate

characterization of the flow field by direct determination of displacements of successive particle images.

PRINCIPAL FINDINGS/PROGRESS

- ✓ A galvanometer-driven rotating mirror system, externally controlled by a function generator, undergoes successive ramp-type oscillations at rates as high as 500 c/s. The intensity and duration of the scanning rate is sufficiently high to allow generation of as many as three to five multiple exposures of a typical particle image during displacement on the film negative. These multiple exposures allow verification of the in-plane motion of each particle.

- ✓ As many as three hundred to five hundred particle trajectories are typically acquired over a given cross-section of the flow using Pliolite particles having characteristic diameters of the order of 50 to 75 microns. These successive displacements of a given particle are digitized using a Tektronix digitizing tablet from very large prints of the particle images.

- ✓ Determination of the randomly located velocity vectors, followed by application of either an adaptive Gaussian window (AGW) or spline thin shell (STS) interpolation scheme provides the instantaneous velocity field over a cross-section of the flow.

- ✓ The unsteady flow structure on the delta wing can be selectively sampled using computer-generated firing pulses transmitted to the camera.

- ✓ For both stationary and unsteady flows, it is possible to construct the instantaneous streamline pattern. Moreover, the separation streamlines can be determined by using a tracking algorithm.

X. *PARTICLE IMAGE VELOCIMETRY VIA LASER SCANNING AND PULSED LASER TECHNIQUES (Magness, Kuo, and Konak)*

OBJECTIVES

- ✓ Aim for high spatial resolution, instantaneous velocity fields over a defined cross-section of the flow field. Use small particles (two to ten micron diameter), in conjunction with illumination of high-powered YAG lasers having a pulse width of the order of nanoseconds, in order to ensure that the particles do not drift on the film negative during successive illumination pulses.

- ✓ Establish a means of interrogating the film negative showing the successive locations of the particle images due to multiple exposure of the film. Employ a Young's Fringe Technique involving an optical Fourier Transform Technique, in order to determine the magnitude and direction of the velocity at a given location of the film negative.

- ✓ Develop data evaluation techniques that will allow evaluation, transformation and display of the large data sets (approximately four to five thousand velocity vectors per cross-section of the flow), including methods for determining the instantaneous streamline patterns and contours of constant vorticity.

PRINCIPAL FINDINGS/PROGRESS

- ✓ A new water channel system, made entirely of plastic so that foreign particles will not contaminate the marker particles, has nearly been completed. It has fine filtration systems for properly conditioning the water.

- ✓ The first goal has been to determine a method for effectively combining the beams from two YAG lasers into a single colinear beam. Design of this aspect has been completed, including use of a beamsplitter cube especially fabricated for high-powered laser applications.

- ✓ An optical method, unique to our laboratory, for forming a laser sheet from a cylindrical beam cross-section, and translating it to desired locations in the flow, has been designed. It involves use of beam steering optics in conjunction with spherical and cylindrical lenses, all of which must be specially selected to account for the high laser power of the order of one Joule/cm^2.

FLOW STRUCTURE AND LOADING: PHYSICAL FINDINGS

XI. *FLOW STRUCTURE ON OSCILLATING WING SEGMENTS (Utsch)*

OBJECTIVES

- ✓ Determine basic classes of three-dimensional vortex generation from interacting wing segments with application to: wing-flap configurations; and adjustable wings. Investigate new concepts of lift generation associated with controlled motion of wings and wing segments.
- ✓ Examine effects of relative frequency, phase, and amplitude of oscillating wing segments on three-dimensional flow structure. This characterization of the flow structure will include: trajectories of the generated three-dimensional vortices; characteristic scale and circulation of vortical structures; and definition of vortex interference phenomena.

PRINCIPAL FINDINGS/PROGRESS

- ✓ Vortices can coexist on both the interior and exterior surfaces of an oscillating wing segment.
- ✓ At a given value of streamwise (chordwise) location, the spanwise position of the interior or exterior vortex remains nearly invariant. This invariance persists despite large excursions in the angle between the oscillating wing segments, including the limiting case where the wing segments come into contact during the oscillation cycle.
- ✓ At a threshold value of dimensionless oscillation frequency, the interior region of the wing segments takes on a fully turbulent character. At this same frequency, large-scale vortices are generated at closure of the wing segment system.

XII. *FLOW STRUCTURE ON PITCHING DELTA WING BY USE OF LASER-SCANNING TECHNIQUES (Magness)*

OBJECTIVES

- ✓ Determine the character of the vortical flow structure as a function of mean angle of attack, reduced frequency, and sweep angle of the delta wing.
- ✓ Define the hysteresis of the three-dimensional vortex formation as a function of streamwise (chordwise) distance from the apex of the airfoil by tracking the streamwise development of the vortex from the apex of the wing as a function of pitch angle $\alpha(t)$.

- ✓ Investigate the extent to which the vortex formation process can be suppressed for certain types of excitation; consider whether this so-called suppression occurs over the entire wing or over a limited range of streamwise (chordwise) distance along the wing.

PRINCIPAL FINDINGS/PROGRESS

- ✓ Hysteresis of the vortex formation relative to the wing motion extends to relatively low values of reduced frequency. Moreover, this hysteresis process emanates from the apex region of the wing and is evident at all locations along the wing from the apex to the trailing-edge.

- ✓ At sufficiently high reduced frequency, and over a certain interval of chordwise distance along the wing, there is no vortex on either the upper or lower side of the wing, despite the fact that such vortex formation does occur on the corresponding stationary wing.

- ✓ At sufficiently high reduced frequency, and over a certain interval or chordwise distance along the wing, there is no vortex on either the upper or lower side of the wing, despite the fact that such vortex formation does occur on corresponding stationary wing.

- ✓ Strongly distorted (suppressed) vortex patterns are evident as the trailing-edge is approached when the wing is excited at sufficiently high reduced frequency. This distortion is due to the integrated effect of the upstream development of the flow.

XIII. *FLOW STRUCTURE ON A PITCHING DELTA WING BY LAGRANGIAN TRACKING TECHNIQUES EMPLOYING A FLYING WIRE (Atta)*

OBJECTIVES

- ✓ Determine the distortion of the flow structure entering the plane of the wing at its apex; in doing so, employ a wire oriented in the plane of the wing and located close to the apex of the wing. This wire is to "fly" at the same velocity as the apex of the wing.

- ✓ Relate the local flow structure at the apex of the wing to that along the entire wing, extending into the near-wake region. Characterize the basic types of three-dimensional vortex formation in the near-wake of the delta wing.

- ✓ Interpret the hysteresis of the initial stages of vortex formation near the apex to the manner in which flow is swept above and below the apex of the wing during the oscillation cycle.

- ✓ Characterize the above-described aspects of the flow structure in terms of mean angle of attack and reduced frequency.

PRINCIPAL FINDINGS/PROGRESS

- ✓ Due to dynamic effects, the flow entering the plane of the wing at the apex can pass below, in contrast to above, the wing surface; this effect occurs even at relatively high positive values of angle of attack α.

- ✓ Flow entering the plane of the wing and passing by the apex shows substantial hysteresis, even at the lower values of reduced frequency examined herein. These hysteresis patterns can be characterized by an effective sweep angle of the timeline pattern in the region of the apex. This effective sweep angle of the flow structure, relative to the geometrical sweep angle of the wing, shows substantial hysteresis.

- ✓ At a threshold (relatively high) value of reduced frequency, at any instant during the wing motion, the flow passes above the wing over a certain portion of the wing, and below the wing over another portion of the wing.

- ✓ The foregoing types of flow distortion at the apex and along the entire surface of the wing lead to several different classes of three-dimensional vortex formation from the trailing-edge of the wing.

XIV. *STRUCTURE OF VORTEX CORE DEVELOPMENT AND BREAKDOWN IN A PITCHING DELTA WING (Atta)*

OBJECTIVES

- ✓ Determine the mechanism of formation of the vortex core on an oscillating delta wing as a function of angle of attack and reduced frequency.

- ✓ Identify the classes of instability and breakdown of the vortex core relative to the vortex core on a static wing. Quantify these observations by determining the axial velocity of the centerline of the vortex core.

- ✓ Define the hysteresis of vortex core breakdown, relative to the motion of the wing.

PRINCIPAL FINDINGS/PROGRESS

- ✓ At a threshold value of reduced frequency, there is no vortex core along the surface of the wing over a significant portion of the oscillation cycle.

- ✓ The onset of vortex core development is distinctly different at low reduced frequency and high reduced frequency. At low reduced frequency, there is simultaneous development of the entire column of the vortex core along its entire streamwise extent. At higher reduced frequency, there is rapid ejection of the leading-edge of the core from the apex region of the wing.

- ✓ Irrespective of the mechanism of development of the vortex core, the axial velocity of the core remains constant during the development process.

- ✓ The eventual breakdown of the core of the vortex can be grouped into four basic classes, ranging from a spiral-like mode similar to that appearing on a static wing to a rapid, column-type collapse of the entire core.

- ✓ A secondary vortex, along the leading-edge of the wing, can develop simultaneously with the primary vortex. Its core displays the same principal features of development and breakdown as that of the primary vortex.

XV. *RESPONSE OF VORTEX BREAKDOWN TO TYPE OF PITCHING MANEUVER (Magness)*

OBJECTIVES

- ✓ Implement active control techniques that allow maneuver of the delta wing in the pure pitching mode at a desired pitching rate for several types of maneuver: simple pitch-up; simple pitch-down; and continuous pitch-up and pitch-down motions.

- ✓ Observe, with the use of hydrogen bubble and dye injection techniques, the location of the occurrence of vortex breakdown with respect to the instantaneous position of the wing during the course of a given maneuver, in order to provide a basis for studying the detailed structure of the vortex while the wing is in motion.

PRINCIPAL FINDINGS/PROGRESS

- ✓ Dye injection and hydrogen bubble techniques have been developed to allow movement of the location of marker injection with the motion of the wing. Notable is the technique for manufacturing the segmented hydrogen bubble wire and its installation along the leading-edge of the wing. Both high speed video and 35 mm camera techniques have been employed to characterize the vortex breakdown during the maneuver.

- ✓ Some of the principal features of the movement of the vortex breakdown location with respect to the wing motion are as follows:

  - Irrespective of whether one considers pitch-up or pitch-down motion, the axial location has its lowest value when the location of vortex breakdown is at its furthest upstream location, coinciding with the existence of large-scale vortex breakdown over a substantial portion of the wing surface. Higher velocities tend to occur when the breakdown is on the downstream portion of the wing.

  - When the continuous pitch-up-down motion of the wing is invoked, the breakdown location remains downstream of the midchord and low values of the axial velocity of the breakdown location are avoided.

XVI. *RELATION OF INSTANTANEOUS FORCE TO TYPE OF PITCHING MANEUVER (Fredriksson)*

OBJECTIVES

- ✓ Design and implement a high sensitivity force measurement system for characterizing the unsteady lift and moment on a delta wing undergoing unsteady pitching motion in water.
- ✓ Determine the variation of lift as a function of instantaneous angle of attack for various values of pitching rate and initial and terminal angles of attack during ramp-type maneuvers. If possible, extend these same characterizations to unsteady moment on the wing.
- ✓ Compare the variations of lift and vortex breakdown position with angle of attack to determine the correlation between them.

PRINCIPAL FINDINGS/PROGRESS

- ✓ A specially-designed force measurement system for use in water has been completed and implemented. The strain gauge system is integrated with a signal processing system that employs a modulated-carrier concept in contrast to traditional DC measurement of forces. Data acquisition and reduction software have been developed in order to allow characterization of the instantaneous forces as a function of time or angle of attack. Moreover, method for ensemble-averaging successive force measurements has been developed.
- ✓ The instantaneous lift vs. angle of attack has been determined for several values of pitching rate. Characteristics of the dynamic lift such as overshoot of the static characteristic and hysteresis of the lift vs. angle of attack have been determined. Increasing the value of pitching rate substantially increases the area of the hysteresis loop via maintain low values of lift during the pitch-down portion of the pitching motion. However, the overshoot above the static lift characteristic does not seem to be significantly influenced by pitching rate.
- ✓ Correlation of the instantaneous location of vortex breakdown with the instantaneous lift on the wing suggests, contrary to the assumed behavior, that there is not a direct relationship between movement of the vortex breakdown position along the surface of the wing and changes in lift. This aspect is currently under investigation.

XVII. *INSTANTANEOUS FLOW STRUCTURE ACROSS LEADING-EDGE VORTEX IN RELATION TO TYPE OF PITCHING MANEUVER (Magness)*

OBJECTIVES

✓ Determine the detailed flow structure at selected cross-sections on a stationary delta wing, including the detailed velocity distribution across the specified cross-section as well as the separation line emanating from the leading-edge of the wing.

✓ Obtain similar information for the case of a wing undergoing unsteady pitching motion, and directly compare with the corresponding stationary case, in order to determine the underlying physical basis for the time shift of the response of the vortex structure with respect to the motion of the wing. Use this information to aid in interpretation of the nature of the chordwise movement of the vortex breakdown location during a typical maneuver.

PRINCIPAL FINDINGS/PROGRESS

✓ A laser scanning system, which allows movement of the laser sheet to arbitrary chordwise location and its orientation with respect to the freestream, has been implemented in conjunction with the active controller system with the wing motion. During this first phase of the investigation, efforts have focussed on the characterization of the structure of the vortex at the midchord of the wing, coincident with the location of the pitching axis. Direct comparisons of the detailed structure of the leading-edge vortex have been made for the pitch-down (ramp-type) motion and compared directly with the structure of the vortex existing on a stationary wing at the same angle of attack.

✓ Preliminary observations of the instantaneous structure of the vortex cross-section on the pitching wing, in comparison with the stationary wing, are:

- In absence of any breakdown within its core, the detailed structure of the vortex cross-section relaxes to its steady state value within approximately one convective timescale C/U_∞ after cessation of the wing motion.

- The existence of vortex breakdown within the core of the vortex precludes significant relaxation of the detailed structure of the vortex cross-section within time scales of the order of C/U_∞.

XVIII. *RESPONSE OF LEADING-EDGE VORTEX TO TRANSIENT SUCTION (Parmenter)*

OBJECTIVES

- ✓ Determine the effectiveness of localized suction, simulating a point sink, located well downstream of the onset of vortex breakdown. Determine the minimum suction amplitude for which the vortex core can be restabilized.
- ✓ Characterize the transient response of the restabilization and destabilization of the vortex core due to abrupt onset and abrupt cessation of the suction respectively.
- ✓ Determine the nature of the unsteady restabilization of the vortex core from the state of full breakdown to no breakdown.

PRINCIPAL FINDINGS/PROGRESS

- ✓ Experiments have focussed on the process of restabilization of the vortex core over a distance of about one-half chord of the wing. Vortex breakdown in its natural state occurs at midchord and the tip of the suction probe is located approximately at the trailing-edge of the wing. In this case, it is possible to stabilize the vortex core with a suction coefficient C_μ as low as 0.035. Substantially lower values of suction coefficient should be attainable when the location of the probe tip is closer to the location of naturally-occurring vortex breakdown.
- ✓ When there is abrupt cessation of the suction after the vortex core has been stabilized, there occurs substantial hysteresis of the vortex breakdown location x_b versus time t, relative to that occurring for the abrupt onset of suction. The magnitude and direction of this hysteresis depends upon the amplitude of the suction coefficient C_μ.
- ✓ When the suction coefficient C_μ reaches a sufficiently high amplitude for the (transient) onset of suction, the total time elapsed for restabilization of the vortex core is invariant with amplitude of the coefficient C_μ. On the other hand, when the amplitude C_μ is sufficiently small, the overall response time increases rapidly with increasing C_μ.

XIX. *RESPONSE OF LEADING-EDGE VORTEX TO TRANSIENT BLOWING (Kuo, Gu)*

OBJECTIVES

- ✓ Determine the response of the vortex breakdown to localized blowing applied at critical locations on the leading-edge of the delta wing; at the apex; along, and in line with the leading-edge of the wake; and along the axis of the vortex.

- ✓ Since the possibility for restabilization, i.e. downstream movement of the vortex breakdown position, for the case of blowing applied tangentially along a rounded leading-edge.

- ✓ For the forgoing types of blowing, apply transient blowing, in order to characterize the overall response time until restabilization of the vortex core is attained.

- ✓ Determine the time-dependent cross-sectional structure of the vortex during the process of the transient blowing as well as during the relaxation of the vortex core after the cessation of blowing.

PRINCIPAL FINDINGS/PROGRESS

- ✓ A large scale half delta wing has been designed and constructed. It allows arbitrary angle of attack, while maintaining the location and orientation of the localized blowing at a fixed location and orientation in space. For the case of distributed blowing in the tangential direction along the entire leading-edge of the wing, a special leading-edge, variable slit arrangement has been designed. For all types of blowing, a transient function generator has been developed. It involves a piston-like arrangement, driven by a stepping motor, which, in turn, is linked to the laboratory microcomputer. This function generator allows various forms of time-dependent blowing to the applied.

- ✓ Although all of the forgoing types of blowing described in the objectives are effective, and can produce, to varying degrees, downstream movement at the location of vortex breakdown, the most effective technique seems to be the application of tangential blowing from the rounded leading-edge of the delta wing. Particularly interesting is the fact that when this tangential blowing is applied with an alternating so-called blowing/suction cycling, at a dimensionless frequency of the order of a convective time scale, effective restabilization of the vortex core can be attained over a distance of the order of one-half the chord of the wing.

- ✓ Corresponding particle tracking of the cross-sectional development of the vortex chord during the process of alternate blowing and suction is underway. At a given cross-section of the leading-edge vortex, located downstream of the original breakdown position, a complete recovery of the non-broken down leading-edge vortex is obtainable by the application of alternating blowing/suction.

PUBLICATIONS AND PARTICIPANTS

XX. PUBLICATIONS

The major thrust of this research program has been determination of the flow structure on swept edges subjected to controlled motion. Emphasis has been on techniques of quantitatively visualizing the flow, while simultaneously subjecting the wing to various types of active control. Using these techniques, it is possible to directly relate the flow structure to the excitation conditions. Several basic types of control have been implemented. These control approaches encompass:

(a) low frequency, sinusoidal motion of swept wings, focusing on study of the phase shift between the evolution of the leading-edge vortex and the motion of the wing;

(b) high frequency perturbations of the leading-edge of the wing, leading to alteration of the structure of the separating shear layer and modification of the time-mean structure and location of vortex breakdown;

(c) large-amplitude motion of segmented, delta-wing flaps allowing generation of substantial circulation and lift at zero mean angle of attack;

(d) ramp-type motion of delta wings, allowing description of the very long time scales of the vortex responses; and

(e) application of unsteady source-like transients to fully stalled wings, providing substantial extensions of the length of the vortex core prior to occurrence of breakdown.

Parallel to these investigations, formulation and instrumentation of new techniques of quantitatively interpreting the flow structure with use of computer-aided methods have been addressed. Concepts of pattern recognition and three-dimensional construction have been pursued.

The following list of publications provides synopses of progress to date.

✓ *"Hysteresis of Vortex Development and Breakdown on an Oscillating Wing" by R. Atta and D. Rockwell, AIAA Journal, Vol. 25, No. 11, 1987, pp. 1512-1513.*

A delta wing subjected to sinusoidal pitching motion exhibits vortex formation from the leading-edge having several distinguishing features relative to the case of vortex formation from a stationary wing. There is substantial phase shift of the onset of vortex breakdown relative to the instantaneous position of the wing such that maximum breakdown length may occur near or at the maximum angle of attack. Moreover, it is possible for the core of the vortex to disappear over a portion of the oscillation cycle. These observations occur at moderate and high values of reduced frequency; further studies are addressing the vortex behavior at very low reduced frequencies.

✓ *"Ensemble-Averaging and Correlation Techniques for Flow Visualization Images" by P. J. M. Kerstens and D. Rockwell, Experiments in Fluids, Vol. 6, 1988, pp. 409-419.*

Flow visualization using marking techniques such as timelines provides a basis for quantitative analysis of macroscale features of unsteady flows by global

ensemble-averaging and correlation techniques. In the visual-ensemble-averaging technique described herein, the timeline positions are tracked and averaged in successive images. The phase reference for the averaging process can take the form of an analog pressure, velocity, or displacement signal, or a recurring coherent portion of the image. Global correlations of the timeline patterns are obtained using the same timelines defined for the ensemble-averaging process. A new type of visual correlation function, giving the correlation between two timelines in a given image or successive images, is proposed.

√ *"Estimation of Velocity Eigenfunction and Vorticity Distributions from the Timeline Visualization Technique" by D. Lusseyran and D. Rockwell, Experiments in Fluids, Vol. 6, 1988, pp. 228-236.*

For the case of quasi-periodic flow, it is demonstrated that use of the hydrogen bubble timeline method leads to reasonable estimates of the eigenfunction of the streamwise velocity fluctuation. Both amplitude and phase distributions across an unstable wake flow are well-approximated. It is shown that the vorticity extrema, as well as the degree of concentration of vorticity, are in good agreement with those calculated from linear stability theory.

A critical assessment is given of the possible uncertainties associated with this technique; the existence of a finite, but unknown cross-stream velocity component; bubble rise due to buoyancy effects; wake defect created downstream of the bubble wire; and resolution of the digitized image. Furthermore, the uncertainty in the streamwise velocity, arising from existence of a finite cross-stream velocity component, is actually less than that corresponding to a single-element hot film probe over certain regimes of operation.

√ *"Flow Visualization Via Laser-Induced Reflection from Bubble Sheets" by C. Magness, T. Utsch, and D. Rockwell, AIAA Journal, Vol. 28, No. 7, 1990, pp. 1199-1200.*

The structure of steady and unsteady aerodynamic flows can be characterized by generating fluid markers at desired locations in the flow and tracking them in three-dimensional space. The hydrogen bubble technique allows localized injection of both continuous and interruptive fluid markers. The technique described herein employs multiple sheets of hydrogen bubbles in conjunction with laser sheet illumination. Arbitrary cross-sections of the unsteady flow past an oscillating delta wing can be characterized. Using a phase-referencing technique, it is possible to relate the visualization of various cross-sections along the wing at a given value of instantaneous angle of attack.

√ *"Leading-Edge Vortices on a Pitching Delta Wing" by R. Atta and D. Rockwell, AIAA Journal, Vol. 28, No. 6, 1990, pp. 995-1004.*

Flow past a stationary delta wing of moderate sweep angle gives rise to leading-edge vortices having non-circular (quasi-elliptical) cross-section, with the inclination of the vortex cross-section changing the streamwise distance along the wing. Representations of vortex swirl angle are compared with angle of attack and change of position in vortex breakdown. Vortex breakdown consistently occurs in an organized spiral mode; the corresponding maximum values of swirl angle approximate those of vortex breakdown in axisymmetric internal flows.

When the wing undergoes pitching motion, there occur two basic types of vortex development. At low frequencies, the vortex core develops in the upstream

direction towards the apex; at high frequencies, there is ejection of the leading-edge of the vortex core from the apex in the downstream direction. At sufficiently high frequencies, the classes of vortex breakdown are distinctly different from those occurring in steady flow.

The evolution in time of the leading-edge vortices shows pronounced dynamic hysteresis: the flow structure of the vortex is different during the up- and downstroke motion of the wing, even for very low values of reduced frequency. The direction of the dynamic hysteresis loop (clockwise or counterclockwise) can be related directly to the type of vortex development.

During unsteady development of the vortex core, the axial velocity on the centerline of the vortex is constant with distance from the apex of the wing. As the location of vortex breakdown is approached, there is abrupt deceleration over a distance of the order of ten percent of the chord of the wing. The distributions of velocity in this region suggest a universal form for a wide range of angle of attack in reduced frequency.

✓ *"Transient Response of Leading-Edge Vortices to Localized Suction" by K. Parmenter and D. Rockwell, AIAA Journal, Vol. 28, No. 6, 1990, pp. 1131-1132.*

This investigation addresses the restabilization of a leading-edge vortex on a delta wing by transient suction. Suction is applied through a probe well downstream of the onset of vortex breakdown. Of particular interest is the overall time required for stabilization of the vortex and hysteresis of the vortex response. The focus of this investigation is the response of the vortex in relation to the abrupt onset and cessation of suction. The following aspects are addressed: visualization of the unsteady evolution of the vortex core; the nature of the hysteresis of the core development; and the overall response time from the onset of suction to the stabilization of the core as a function of suction amplitude and suction probe location.

✓ *"Flow Structure Generated by Oscillating Delta Wing Segments" by T. Utsch and D. Rockwell, AIAA Journal of Aircraft, Vol. 27, No. 6, 1990, pp. 574-576.*

Oscillation of two delta wing segments about a common axis by a concentric drive train arrangement allows forcing of each wing segment in an arbitrary manner. The resultant flow structure is visualized using a new technique of laser-induced reflection from small hydrogen bubbles generated upstream of the moving wing segments. The scanning laser sheet, which is translated in the direction of flow, allows instantaneous slices of the flow structure to be captured. This approach leads to phase-locked, instantaneous velocities, allowing evaluation of the circulation of the leading-edge vortices.

For the case of sinusoidal motion of the wing segments, it is possible to generate, at zero angle of attack, substantial values of circulation. Oscillation of the wing segments at finite angle of attack produces drastic hysteresis of the vortex formation during the upstroke and downstroke motions of the wing. Correspondingly, the circulation during the upstroke motion is much higher than that during the downstroke.

PUBLICATIONS SUBMITTED

✓ *"Control of Vortex Structure on a Delta Wing by Small Amplitude Perturbations of Angle-of-Attack," by C.-H. Kuo, C. Magness, and D. Rockwell, submitted to Journal of Fluid Mechanics*

Small displacement amplitude of the leading (one degree) sinusoidal variations in angle of attack can substantially alter the structure of the leading-edge vortices on a highly-swept delta wing. These perturbations are applied over a frequency range which includes the inherent instability frequencies of: the shear layer separating from the leading-edge; and the vortex breakdown process. Both upstream and downstream movement of the location of vortex breakdown can be affected. Correspondingly, the ratio of the characteristic swirl and axial velocities can change by as much as a factor of two from that value for the unperturbed wing.

Detailed characterization of the spectral content of the unsteady vortex upstream and downstream of location of vortex breakdown show highly organized spectral components at the controlled excitation frequency; moreover, as many as ten higher order harmonics can occur. This highly coherent, phase-locked structure persists along the entire axial extent of the vortex breakdown region.

The foregoing observations of the instantaneous and mean flow are interpreted with the aid of flow visualization of the instantaneous flow structure.

PUBLICATIONS IN PREPARATION

✓ *"Quantitative Visualization of Unsteady and Separated Aerodynamic Flows" by D. Rockwell, R. Atta, R. Curtis, C. Hefele, A. Klink, R. Lawson, C. Magness and T. Utsch (submitted to Experiments in Fluids)*

Tracking of hydrogen bubble markers in steady and unsteady three-dimensional flows can lead to quantitative information on the flow structure in terms of velocity fields, streamlines, streamsurfaces, and timeline surfaces. This flow structure is obtained by dual-image and single-image techniques, employing diffuse stroboscopic lighting and a scanning laser sheet respectively. Vortex flows on stationary and oscillating delta wing segments are addressed using these approaches.

These investigations make use of an integrated active control-quantitative flow visualization system with: high resolution stepping motors that force the wing/wing segments; a custom-designed bubble generator for producing hydrogen bubble markers in terms of pulsed grids or arrays of bubbles; and a movable optics system that translates the scanning laser sheet. All three of these elements of the integrated system are controlled by a central computer in the laboratory.

Construction of three-dimensional flow images is done with image processing techniques and computer-aided methods applied to slices of the three-dimensional flow field. In turn, these images can be displayed in real time from arbitrary perspectives on systems in the CAD laboratory.

✓ *"Response of Vortex Breakdown on a Pitching Delta Wing Subjected to Arbitrary Forms of Pitching Motion" by C. Magness and D. Rockwell*

This manuscript will address the principal features of the vortex breakdown response on a pitching delta wing. In particular, the form of the pitching motion, involving simple, pitch-up or pitch-down maneuvers, in comparison with continuous (successive) pitch-up and pitch-down maneuvers will be addressed. To complement these overall observations of the response of the vortex breakdown, velocity fields and separation, streamlines of the cross-sectional structure of the vortex will be presented. The time lags of the vortex structure for a pitching wing, relative to that of a corresponding stationary wing, will be addressed.

✓ *"Unsteady Topology in the Leading-Edge Vortex" by C. Magness and D. Rockwell*

Using critical point theory, the instantaneous topology is defined for a delta wing undergoing pitching motion. This approach allows identification of the saddle points and foci of the instantaneous streamline pattern at given cross-sections of the flow at a defined angle of attack. Although analysis is still underway, it appears that the unsteady topology is substantially different from what one would expect on the basis of quasi-steady interpretation.

✓ *"Unsteady Crossflow on a Delta Wing Using Particle Image Velocimetry" by C. Magness and D. Rockwell*

A technique of laser scanning is employed to illuminate micron-sized particles; photographs of these particles provide the instantaneous velocity distribution over the entire plane of the flow. Using this approach, it is possible to characterize the instantaneous flow structure over the entire crossflow plane. Although data reduction is still underway, it appears as though it will be possible to characterize the well known hysteresis effect during pitch-up and pitch-down motion in terms of degree of coherence (unstalled vs. stalled) of the leading-edge vortex.

NON-JOURNAL ARTICLES

✓ *"Control of Leading-Edge Vortices on a Delta Wing" by C. Magness, O. Robinson, and D. Rockwell, AIAA Paper 89-0999, presented at AIAA Shear Flow Control Conference, March 13-16, Tempe, Arizona.*

The response of vortex breakdown on a pitching delta wing is examined for various classes of ramp motion, including pitch-up, pitch-down, continuous pitch-up and pitch-down, and combinations of ramp pitching rates. Depending upon which of these types of controlled motion is imposed, there can occur varying degrees of phase shift between the onset and development of vortex breakdown and the instantaneous angle of attack of the wing. These observations suggest that by properly tailoring the functional form of the pitching maneuver, the phase shift of the vortex breakdown can be exploited to optimize the loading on the wing. Analogous forcing and response of vortex breakdown on a stationary wing to localize suction and blowing is also addressed.

Detailed insight into the flow structure is acquired by direct particle tracking in conjunction with computer-aided construction techniques. This approach allows rapid approximations to the three-dimensional nature of the

leading-edge vortex from planar (laser sheet) slices through the flow. The phase shift between the instantaneous structure of the leading-edge vortex and the instantaneous position of the wing can also be characterized using this approach.

√ *"On Unsteady Flow Structure from Swept Edges Subjected to Controlled Motion" by D. Rockwell, R. Atta, C.-H. Kuo, C. Hefele, C. Magness and T. Utsch. Proceedings of Workshop II on Unsteady Separated Flow held at U. S. Air Force Academy, Colorado Springs, Colorado, July 26-30, 1987. Appearing as Frank J. Seiler Research Laboratory Report FJSRL-TR-80-0004, September, 1988, Project 2307-F1-38 Air Force Systems Command, United States Air Force, pp. 299-312.*

Recent developments in the direction of new experimental methods and insight into the mean and unsteady vortex structure are provided in synoptic form.

Development of an integrated active control and quantitative measurement system has aimed towards relating the instantaneous flow structure to the instantaneous wing motion. Active control of the flow structure of leading-edge vortices on a delta wing and delta wing segments through both small and large (displacement) amplitude pitching motion is attainable if the excitation frequency is properly selected. Such excitation should consider the following characteristic frequencies: the fundamental frequency (or its subharmonics) of the unstable shear layer separating from the edge of the wing; the frequency of vortex breakdown; and the characteristic frequency of the separation zone downstream of the onset of vortex breakdown.

√ *"Flow Visualization and Its Interpretation" by D. Rockwell, R. Atta, L. Kramer, R. Lawson, D. Lusseyran, C. Magness, D. Sohn, and T. Staubli. Proceedings of the AGARD Symposium on Aerodynamic and Related Hydrodynamic Studies Using Water Facilities, Monterey, California, 1986, AGARD CP-413, pp. 29-1 - 29-13.*

Unsteady two- and three-dimensional flow structure at leading- and trailing-edges of bodies can be characterized effectively using recently developed techniques for acquisition and interpretation of flow visualization. The techniques addressed herein include: flow image-surface pressure correlation; three-dimensional reconstruction of flow structure from flow images; and interactive interpretation of flow images with theoretical simulations. These techniques can be employed in conjunction with: visual correlation and ensemble averaging, both in a given image and between images; recognition of patterns of flow structure from images; and estimates of velocity eigenfunctions from images.

√ *"Control of the Leading-Edge Vortices on a Delta Wing" by C. Magness, O. Robinson, and D. Rockwell, Proceedings of the NASA/AFOSR/ARO Workshop on Physics of Forced Separation, NASA Ames Research Center, Moffett Field, California, April 17-19, 1990 (ed. L. W. Carr)*

The unsteady flow structure of leading-edge vortices on a delta wing has been investigated using new types of experimental techniques, in order to provide insight into the consequences of various forms of active control. These investigations involve global control of the entire wing and local control applied at crucial locations on or adjacent to the wing. Transient control having long and short time-scales, relative to the convective time-scale C/U_∞, allows substantial modification of the unsteady and time-mean flow structure.

Global control at long time-scale involves pitching the wing at rates an order of magnitude lower than the convective time-scale C/U_∞, by large amplitudes. The functional form of the pitching maneuver exerts a predominant influence on the trajectory of the feeding sheet, the instantaneous vorticity distribution and the instantaneous location of vortex breakdown.

Global control at short time-scales of the order of the inherent frequency of the shear layer separating the leading-edge and the natural frequency of vortex breakdown shows that "resident" response of the excited shear layer-vortex breakdown system is attainable. The spectral content of the induced disturbance is preserved not only across the entire core of the vortex, but also along the axis of the vortex into the region of vortex breakdown. This unsteady modification results in time-mean alteration of the axial and swirl velocity fields and the location of vortex breakdown.

Localized control at long and short time-scales involves application of various transient forms of suction and blowing using small probes upstream and downstream of the location of vortex breakdown, as well as distributed suction and blowing along the leading edge of the wing applied in a direction tangential to the feeding sheet. These local control techniques can result in substantial alteration of the location of vortex breakdown; in some cases, it is possible to accomplish this without net mass addition to the flow of the field.

XXI. PARTICIPANTS

During this program, graduate students, post-doctoral associates, and undergraduate students were associated with the project:

1. C. Magness (M.S. completed; Ph.D. Candidate)*
2. B. Fredricksson (M.S. Candidate)**
3. O. Robinson (Post-Doctoral Associate) +
4. C.-H. Kuo (Post-Doctoral Associate) +
5. S. Guzy (B.S. Candidate)
6. R. Atta (Ph.D. Candidate) +
7. I. Gursul (Ph.D. Candidate)
8. A. Klink (M.S. Candidate) +
9. C. Walsh (B.S. Candidate)
10. W. Gu (Visiting Scientist) +

* Entirely supported by AFOSR Grant.
** Supported partially by AFOSR Grant and Teaching.
\+ Supported on a part-time basis by AFOSR grant.

The titles and dates of completion of theses are as follows:

1. Atta, R. 1987, Ph.D. Thesis "Unsteady Structure of Flow Past a Pitching Delta Wing".

2. Klink, A. 1987, M. S. Thesis "Development of a High Speed Laser Scanning Visualization System".

3. Utsch, T. 1987, M.S. Thesis "Flow Structure Generated by Segmented Delta Wings Undergoing Controlled Rolling Oscillations".

4. Magness, C. 1988, M. S. Thesis "Flow Structure and Loading on a Delta Wing Subjected to Arbitrary Pitching Moment".

5. Fredriksson, B. 1990, M. S. Thesis "Measurement of Instantaneous Lift, Pitching Moment, and Drag on a Delta Wing Subjected to Arbitrary Motion".

6. Magness, C. 1990, Ph.D. Dissertation in progress.

AIAA '89

AIAA-89-0999

CONTROL OF LEADING-EDGE VORTICES ON A DELTA WING

C. MAGNESS, O. ROBINSON, AND D. ROCKWELL
DEPARTMENT OF MECHANICAL ENGINEERING
AND MECHANICS
LEHIGH UNIVERSITY, BETHLEHEM, PA

AIAA 2nd Shear Flow Conference
March 13–16, 1989 / Tempe, AZ

CONTROL OF LEADING-EDGE VORTICES ON A DELTA WING

by

C. Magness, O. Robinson, and D. Rockwell
Department of Mechanical Engineering and Mechanics
354 Packard Laboratory #19
Lehigh University
Bethlehem, Pennsylvania 18015

Abstract

The response of vortex breakdown on a pitching delta wing is examined for various classes of ramp motion including: pitch-up, pitch-down, continuous pitch-up and -down; and combinations of ramp pitching rates. Depending upon which of these types of controlled motion is imposed, there can occur varying degrees of phase shift between the onset and development of vortex breakdown and the instantaneous angle of attack of the wing. These observations suggest that by properly tailoring the functional form of the pitching maneuver, the phase shift of the vortex breakdown can be exploited to optimize the loading on the wing. The analogous forcing and response of vortex breakdown on a stationary wing to localized suction and blowing is also addressed.

Detailed insight into the flow structure is acquired by direct particle tracking in conjunction with computer-aided construction techniques. This approach allows rapid approximations to the three-dimensional nature of the leading-edge vortex from planar (laser sheet) slices through the flow. The phase shift between the instantaneous structure of the leading-edge vortex and the instantaneous position of the wing can also be characterized using this approach.

1. Introduction

Of critical importance in optimizing the maneuverability of delta wing aircraft is knowledge of the unsteady structure of the leading-edge vortices, including the occurrence of vortex breakdown. It is well known that this vortex breakdown process involves an abrupt transition from a jet-like to a wake-like core, accompanied by a marked increase in the level of turbulence. Vortex breakdown on stationary wings has been investigated extensively, and is assessed by Wedemeyer[1]. Woffelt[2] demonstrated that the phase lag, or hysteresis, of the vortex breakdown response relative to the wing motion could produce hysteresis of the forces acting upon the wing. For delta wings subjected to sinusoidal motion at high reduced frequency, Atta and Rockwell[3] found that the maximum length of the vortex core prior to breakdown could occur near the maximum angle of attack, as opposed to the minimum angle of attack expected from quasi-steady considerations. Moreover, at sufficiently high reduced frequency, the vortex core exists over only a portion of the oscillation cycle. The detailed nature of the vortex development as a function of reduced frequency is addressed by Atta and Rockwell[4]. At low reduced frequency, the vortex core develops in the upstream direction towards the apex, whereas at sufficiently high reduced frequency the leading-edge of the vortex core is ejected in the downstream direction. There is substantial phase shift of the evolution of the vortex core with respect to the instantaneous position of the wing, extending to very low reduced frequencies $K = \pi fC/U_\infty = 0.025$. Delta wings subjected to ramp motion in the pitching mode were investigated by Reynolds and Abtahi[5]. They found that, at sufficiently high angles of attack, the response of the vortex breakdown has a very long time scale. It is an order of magnitude larger than the convective time scale at low angles of attack, where breakdown occurs downstream of the trailing-edge. This long time scale is associated with a propagation speed of the position of vortex breakdown that is much smaller than the convective speed of the vortex core.

The location of vortex breakdown on a stationary wing can be subjected to analogous types of control in the form of suction (Parmenter and Rockwell[6]) or blowing (Visser et al[7]) applied locally along the axis of the vortex or along the leading-edge. Of particular interest in this investigation are responses of the vortex breakdown to abrupt, ramp-type suction and blowing.

An objective of this investigation is to: examine the overall response of the vortex breakdown to several classes of controlled ramp (linear)-type motions in the pitching mode, including pitch-up and pitch-down motions, continuous pitch-up and pitch-down maneuvers, and abrupt changes in the ramp rate of the pitching motion; and to study the response to analogous, transient suction and blowing of the vortex on a stationary wing. These observations will be complemented by detailed characterization of the structure of the vortex cross-section, relative to that on the corresponding stationary wing. Selected features of the instantaneous structure of the vortex cross-section during vortex breakdown will also be addressed.

2. Experimental Systems and Techniques

Experiments were carried out in a water channel having a cross-section 610 mm by 914 mm and a maximum freestream velocity of 335 mm/s. As represented in the schematic of Figure 1, delta wings having a sweep angle $\lambda = 75^\circ$ and chord lengths C = 241 and 508 mm and thickness t = 12 mm were employed. Each delta wing was flat on the upper (downstream) side and beveled at an angle of 40° on the lower (upstream) side. The wing was mounted via a 9.5 mm diameter sting to a custom-designed pitching mechanism that allows arbitrary pitching axis and functional form of the pitching maneuver. For the results given herein, the wing of C = 241 mm was employed at a freestream velocity of 51 mm/s, corresponding to a Reynolds number $Re = U_\infty C/\nu = 1.2 \times 10^4$. Experiments conducted over the Reynolds number range $1.2 \times 10^4 \leq Re \leq 3.6 \times 10^4$ showed undetectable effects of Reynolds number, supporting the concept that the onset and development of vortex breakdown is predominantly an inviscid process, in agreement with the survey of Atta[8] over a much wider range of Reynolds number.

The wing was pitched about mid-chord at dimensionless rates $\dot{A} = \dot{\alpha}C/2U_\infty$ having values $0.0125 \leq \dot{A} \leq 0.15$. Angles of attack α over the range $5^\circ \leq \alpha \leq 55^\circ$ were employed, the upper limit corresponding to the occurrence of vortex breakdown at the apex of the stationary wing.

Flow visualization involved interactive use of three techniques: dye visualization; hydrogen bubbles; and solid (Pliolite) particles. For dye injection, the dye marker was allowed to seep from 0.8 mm diameter holes located on the upper surface of the wing at a distance 11.6 mm along the leading-edge from the apex, and 1.5 mm inboard from the leading-edge. This location insured that there was a continuous supply of marker to the central portion of the developing vortex. In employing the hydrogen bubble technique, a periodically crimped wire of 25 micron diameter was located along the underside of the leading-edge, so as to allow continuous generation of streamlines/streaklines at a number of locations along the edge. Lighting for both the dye and hydrogen bubble techniques involved combinations of continuous and stroboscopic lighting. Images were recorded on the high speed (Videologic) video system at 120 frames per second, which was synchronized with the stroboscopic lighting; or, on a Nikon F-3, 35 mm camera. For the technique employing Pliolite particles, having typical diameters of 500 microns, desired cross-sections of the flow were illuminated using a scanning laser sheet. A two watt Argon-ion laser operating in the multi-line mode impinged upon a mirror oscillating at frequencies in the range of 30 to 40 c/s; the exact value of the scan rate depended upon the desired particle displacement on the image.

An overview of the laser scanning system is given in Figure 2. A system of mirrors was devised such that the scanning frequency and the orientation of the scanning sheet, involving translation in two orthogonal directions as well as rotation, could be accomplished without refocussing the optics or repositioning any of the mirrors. The image was reflected, by another system, to a camera located exterior to the water channel. The mirror system generating the laser scanning sheet, the instantaneous angle of attack of the wing, and the firing of the camera were controlled by an external frequency generator and a microcomputer system.

For the studies described herein, most of the laser scans were taken at the midplane, coincident with a line parallel to and between lines AB and DC in Figure 3. In order to construct three-dimensional images of the instantaneous flow structure, the additional laser sheet locations and orientations given in Figure 3 were employed. This concept is addressed in the subsequent section on image construction.

3. Global Control: Response of Vortex Breakdown to Type of Pitching Motion

Representative classes of ramp motion are illustrated in Figures 4a and 4b. In Figure 4a, the case of simple ramp-up, ramp-down, and ramp-up with an interrupted delay are illustrated for representative values of dimensionless pitching rate $\dot{A} = \dot{\alpha}C/2U_\infty$. Figure 4b shows continuous pitch-up and pitch-down motions for three typical values of $\dot{A}$ as well as for the hybrid ramp function characterized by an abrupt increase in pitch rate during the pitch-up motion.

For the types of maneuvers described in Figure 4, both dye and hydrogen bubble visualization were carried out in order to determine the instantaneous location of vortex breakdown $x_b(t)$ in relation to instantaneous angle of attack $\alpha(t)$.

The essential features of the response of the leading-edge vortex to the prescribed pitching motion are indicated in Figure 5 showing plan views of the leading-edge vortex development during a pitch-up maneuver from $\alpha = 15^\circ$ to 40° at a pitch rate $\dot{A} = 0.025$. The total time for the wing maneuver from $\alpha = 15^\circ$ to $\alpha = 40^\circ$ is $U_\infty \Delta t/C = 8.66$. The left photo corresponds to an angle of attack $\alpha = 15^\circ$ immediately before the onset of motion; the middle photo immediately upon completion of the wing motion at $\alpha = 40^\circ$; and the right photo corresponding to a dimensionless time $U_\infty t/C = 0.63$ after the motion is completed at $\alpha = 40^\circ$. In the left photo there is no indication of vortex breakdown; it occurs downstream of the trailing-edge. In the middle photo, the location of breakdown has moved just upstream of the trailing-edge, and in the right photo, it has reached its

equilibrium position well upstream of the trailing-edge. This time shift, or phase lag, is central to the characteristics of the vortex response described in the following.

Overviews of the vortex breakdown location x_b/C as a function of dimensionless time tU_∞/C are illustrated in Figure 6 for simple pitch-up, pitch-down and continuous pitch-up-down motions of the wing. For the simple pitch-up and -down maneuvers, the location of vortex breakdown is allowed to relax to its equilibrium position. On the other hand, for continuous pitch-up-down motion, the downward motion commences immediately after the upward motion ceases and there is no opportunity for relaxation of the vortex breakdown. The extreme values of reduced pitch rate are considered: $\dot{\alpha}C/2U_\infty = 0.025$ and 0.15. For the simple pitch-up motion, the slope $d(x_b/C)/d(tU_\infty/C)$ is large during the initial part of the motion, then substantially decreases. For the pitch-down motion, the converse occurs. Similar trends are evident from inspection of the plots of Reynolds and Abtahi[5] for simple pitch-up and pitch-down motion. *Irrespective of whether one considers pitch-up or -down motion, the axial velocity of the location of vortex breakdown (corresponding to the aforementioned slope) has its lowest value when the location of vortex breakdown is furthest upstream coinciding with the existence of large-scale breakdown over a substantial portion of the wing surface. Higher velocities tend to occur when the breakdown is on the downstream portion of the wing. When the continuous pitch-up-down motion of the wing is invoked, the breakdown location remains downstream of the midchord and low values of the axial velocity of the breakdown location are avoided.* (Exceptions occur when the breakdown location is near the trailing-edge.) A time scale T may be defined as the total time elapsed from upstream movement of the vortex breakdown location across the trailing-edge ($x_b/C = 1$) during the pitch-up motion to its downstream movement across the edge during the pitch-down motion. *The value of the time-scale T for the continuous pitch-up-down motion can be as small as one-fifth of that corresponding to successive pitch-up and pitch-down motions*, evident for the case $\dot{\alpha}C/2U_\infty = 0.15$ in Figure 6. Although the plots of Figure 6 provide insight into the speed $d(x_b/C)/d(tU_\infty/C)$ of the vortex breakdown location, the phase shift between the instantaneous breakdown location x_b/C and the angle of attack α must be addressed. For example, the occurrence of the minimum $d(x_b/C)/d(tU_\infty/C) = 0$ for the continuous ramp-up-down motion is expected to lag the minimum $d\alpha/dt = 0$ of the maneuver schedule. In the following, this and other related features are addressed.

Figure 7 shows the response curves of vortex breakdown location x_b/C vs. angle of attack α for the cases of simple pitch-up and pitch-down motion. For both the upward and downward motions, the vortex breakdown location is allowed to relax to its static value before the wing is set into motion. For all three values of reduced pitching rate $\dot{\alpha}C/2U_\infty = 0.025$, 0.05 and 0.15, there is substantial departure from the static characteristic for both the pitch-up and pitch-down motions. During the pitch-up maneuver, the instantaneous value of x_b/C substantially overshoots the corresponding static values at angles of attack α in excess of that value at which the breakdown location x_b crosses the trailing-edge of the wing, i.e. at $\alpha = 30°$. Upon completion of the pitch-up motion at $\alpha = 40°$, relaxation of the locations of breakdown x_b/C at constant angle of attack α occurs over the range $0.75 \leq x_b/C \leq 0.30$. For pitch-down motion, there is large undershoot of the values x_b/C relative to the static characteristic. Relaxation after cessation of the motion at angle of attack $\alpha = 15°$occurs only for the highest pitch rate; it extends approximately from $x_b/C = 0.45$ to a location downstream of the trailing-edge. Taking an overview of the x_b/C vs. α characteristics of Figure 7, it is evident that *the process of relaxation of the vortex breakdown location to its equilibrium state at constant (terminal) angle of attack occurs even for low pitch rates during pitch-up motion; this relaxation can extend over a streamwise distance of the order of one-half the chord of the wing. The same type of relaxation occurs during pitch-down motion only for sufficiently high pitch rate.*

A comparison of the cases of simple pitch-up, pitch-down, and continuous pitch-up and -down motion is illustrated in Figures 8a and 8b. For the pitch-up portion of the maneuver, the curves of x_b/C vs. α are, as expected, very similar at a given value of pitch rate. During the pitch-down motion, these curves have a similar shape only at sufficiently low values of angle of attack. For the initial portion of the pitch-down motion, there is an initial decrease of the x_b/C vs. α characteristic of the continuous pitch-up-pitch-down curve, relative to the simple pitch-down curve. This initial decrease extends over a larger range of α at $\dot{A} = 0.15$ (from $\alpha = 40°$ to $\alpha = 29°$) than at $\dot{A} = 0.025$. In other words, *the effect of not allowing the vortex breakdown to relax to its static state during the continuous maneuver is to produce a movement of the breakdown location x_b upstream towards the apex for the initial decrease in angle of attack α.*

The effect of a hybrid ramp pitch rate, relative to the constant rate described in the foregoing, is given in Figure 9. The hybrid function is defined in Figure 4b. During the motion of the wing, there is an abrupt increase in pitch rate from $\dot{A} = 0.025$ to 0.05; during the pitch-down motion, the rate is constant at $\dot{A} = 0.025$. The angle of attack varies between $5° \leq \alpha \leq 55°$. The hybrid fraction was chosen such that the lower ramp rate was in effect for $\alpha(t) < \alpha_{cr}$, when α_{cr} is the angle of attack of the stationary wing at which the vortex breakdown occurs at the trailing-edge ($\alpha_{cr} \simeq 30°$). This lower ramp rate produces less undershoot of the x_b/C vs. α characteristic relative to the static characteristic. Threafter, in the region $\alpha(t) > \alpha_{cr}$, the higher ramp rate produces more overshoot of the static characteristic than the lower ramp rate. During the pitch-up motion, it is possible to obtain substantially higher values of x_b/C relative to those attainable with either of the two values of pitch rate, $\dot{A} = 0.025$ and 0.05, that form the hybrid. This observation suggests that *employment of a hybrid pitch rate accounting for the critical angle of attack can produce significantly higher values of overshoot of the static characteristic x_b vs. α than those attainable with either of the continuously applied pitch rates forming the hybrid.*

4. Instantaneous Structure

4.1 Overview of technique

By employing the computer-controlled wing motion and camera-trigger system, in conjunction with the scanning laser sheet, it was possible to obtain instantaneous slices of the vortical structure during a defined maneuver of the wing. This structure could then be compared with that on the wing for successive static values of angle of attack α. The concept of particle tracking involved multiple, consecutive images of each particle per exposure time of the 35 mm camera, accomplished by proper selection of the laser scanning rate. This technique allowed rejection of any incomplete trajectory, i.e. one that started or ended outside of the laser sheet. The typical thickness of the laser sheet was 3 mm, and a nominal scan rate of 40 c/s was employed. The exposure time of the camera was nominally 0.25 seconds.

Digitized images of the tracked particles were obtained from enlarged views of the flow field on 203 mm x 254 mm photographs by use of a Tektronix 4957 digitizing tablet driven by Unigraphics II. This process of data acquisition and digitization is currently being refined in order to provide a finer resolution and complete automation. A technique using Young's fringe analysis will be employed. Display of the raw digitized data, interpolated forms of the data, and various two- and three-dimensional reconstructions of the images were displayed on a Hewlett Packard 9000-300 work station.

The velocity field represented by the raw data is generally defined at random locations within the plane defined by the laser sheet. *Two well-known* interpolation schemes for two-dimensional scattered data were employed to compute the velocity vectors throughout the planes of interest: the Adaptive Gaussian Window (AGW algorithm) and the Spline Thin Shell (STS) interpolant. The STS scheme reproduces exactly the original values of velocity corresponding to the locations of the raw data, avoids spurious oscillations of the interpolant, and is independent of the reference axis. Moreover, for the three-dimensional interpolation scheme (discussed subsequently), the STS scheme gives analytical derivatives for the third velocity component. On the other hand, a limitation of this technique is that it is generally restricted to cases where the number of data points is relatively low, of the order of two hundred. The AGW method is simpler than STS to implement and can handle easily a higher number of data points, in our case over five hundred points per plane. The derivatives required for the third component in the three-dimensional reconstruction can be stored during the interpolation process and the degree of smoothing can be controlled through selection of the proper value of the Gaussian window width.

A representative velocity field obtained directly from the particle tracking followed by interpolation is given in the image of Figure 10. In this case, there are approximately 450 particle tracks in the original data, obtained from overlay of four successive phase-referenced photos obtained during the motion of the wing. It should be noted that phase referencing is appropriate only when the flow structure is relatively invariant from cycle to cycle. Otherwise a phase-(ensemble-) averaging process is called for. In the case of the stationary wing at high angle of attack, the occurrence of pronounced vortex breakdown over substantial cross-section of the vortex core promoted a high degree of unsteadiness. In this situation, only instantaneous realizations of the flow structure, without superposing or averaging data from successive instants, are meaningful. As a consequence, the number of particle tracks was of the order of 200.

4.2 Relaxation of flow structure during wing motion

It is of interest to compare the relaxation of the flow structure to its steady state condition, as occurs on a stationary wing, immediately after the cessation of the motion of the wing. To illustrate this concept, the representative case of a simple pitch-down motion from $\alpha = 40^\circ$ to $\alpha = 15^\circ$ is addressed. Figure 11 shows the cross-section of the vortical flow structure at the midchord immediately after cessation of the pitch-down motion at $\alpha = 15^\circ$. Both raw and interpolated velocity fields are illustrated. In each series, the upper image corresponds to that at $t^* = tU_\infty/C = 0$ after cessation of the motion. Comparing this image with subsequent ones taken at time intervals of $\Delta t^* = 1.05$ shows that the flow structure in the middle and bottom images is essentially the same. In other words, *in absence of any breakdown within its core, the detailed structure of the vortex cross-section relaxes to its steady state value within approximately one convective time scale* C/U_∞ *after cessation of the wing motion*, an observation consistent with the qualitative observation of Lambourne et al[9]. Moreover, a distinguishing feature of the image at $t^* = 0$, relative to subsequent images, is the substantially higher elevation of the vortex center above the surface of the wing. Evaluation of corresponding values of circulation and vorticity concentration are currently underway. The rapid relaxation illustrated in Figure 11 is possible because there is no region of significant vortex breakdown in the central portion of the vortex core. The effect of occurrence of vortex breakdown at this cross-section of the flow on the relaxation time is addressed in the following.

The evolution of the flow structure prior to the cessation of the wing motion is depicted in Figure 12. Each pair of images directly compares the flow structure for the corresponding stationary wing (top image) with that of the instantaneous structure for the wing undergoing the pitch maneuver (bottom image). The upper left set of images at $\alpha = 35^\circ$ is taken shortly after the onset of the ramp-down motion of $\alpha = 40^\circ$. The lower left set is at $\alpha = 20^\circ$ and the upper right set at $\alpha = 15^\circ$, immediately upon cessation of the wing motion. The striking difference between the pairs of images at $\alpha = 35^\circ$ and 20° is the occurrence of a region of vortex breakdown over a substantial extent of the vortex cross-section for the moving wing and absence of such breakdown for the stationary wing. The boundary of the region of vortex breakdown was obtained from consideration of the raw photographs and the raw velocity fields. The interface between the randomly

disposed velocity vectors of the turbulent breakdown region and the organized velocity vector orientation in the exterior region of the vortex core was well-defined. Within the region of vortex breakdown, the interpolated velocity field is meaningless. It is necessary to employ a sufficiently narrow window in the Adaptive Gaussian Window Scheme in order to obtain a sufficiently close match of the interpolated velocity field with the raw velocity data in the domain immediately exterior to the vortex breakdown region.

Two features of the pattern shown in Figure 12 are noteworthy. First of all, for the ramp motion from $\alpha = 35^\circ$ to $\alpha = 20^\circ$, there has elapsed a total time of 1.95 C/U_∞. However, there is little change in the cross-sectional structure of the vortex core. Except for a slight decrease in the extent of the region of vortex breakdown, the structure of the vortex cross-section has changed very little and the distance of the apparent centers of the regions of vortex breakdown from the wing surface are essentially unaltered. In essence, *existence of vortex breakdown within the core of the vortex precludes significant relaxation of the detailed structure of the vortex cross-section within time scales of the order of* C/U_∞. All of the foregoing patterns are substantially different from their counterparts on the stationary wing. No vortex breakdown is evident, and the centers of the vortices move closer to the wing surface as angle of attack decreases. The second point to be made is that *when the region of vortex breakdown moves downstream of the plane of observation*, as indicated in the set of images at the upper right of Figure 12, *it leaves a vortical flow structure that is significantly elevated above the wing relative to its counterpart on the stationary wing.* These features, in relation to the angle and shape of the separation streamline from the leading-edge of the wing, the overall circulation, and the distribution of vorticity are currently being evaluated.

4.3 Competition of leading-edge vortices

Difficulties in evaluating the instantaneous flow structure are particularly apparent on a stationary wing at high angle of attack, or a wing moving at sufficiently low pitch rate. Figure 13 shows the instantaneous flow structure at two successive times on a stationary wing at angle of attack 40°. *Not only are there significant asymmetries of the regions of vortex breakdown occurring in the vortices from the left and right leading-edges of the wing, but the cross-sectional shape and vertical distance of the breakdown region above the wing surface vary with time.* For example, in the left image, the center of the region of vortex breakdown is approximately at the same level as on the right side of the wing. On the other hand, it is significantly lower than that on the right side in the second image. Preliminary considerations indicate that the fluctuations and instantaneous value of circulation are substantial, which would produce corresponding fluctuations in the rolling moment upon the wing.

5. Local Control

Whereas global control involves forcing of the leading-edge vortex along its entire extent, local control takes the form of suction or blowing applied at a specified location within the vortex. In the following, preliminary findings are addressed to transiently applied suction and blowing.

5.1 Suction

Localized suction applied downstream of the region of vortex breakdown can result in restabilization of the vortex core, accompanied by downstream movement of the onset of vortex breakdown, as indicated in Figure 14. Parmenter and Rockwell[6] address the effectiveness of abruptly applied suction, accounting for the effects of amplitude of the suction coefficient, and location of the suction probe on the time required for restabilization of the vortex core. Figure 15 shows an excerpt from this investigation. The angle of attack was $\alpha = 35^\circ$ and the Reynolds number $Re = 3.1 \times 10^4$. In this case, the dimensionless suction coefficient $C_\mu = [V_p/U_\infty]^2(A_p/A_w) = 0.57$, in which U_∞ = freestream velocity, V_p = velocity of suction probe inlet, A_p = area of probe inlet, and A_w = surface area of wing. Restabilization of the vortex core over a distance of about a half chord of the wing is attainable at lower values of suction coefficient, down to $C_\mu = 0.035$, the lower limit of the pumping system. It is anticipated that much smaller values of suction coefficient can be employed when the distance between the suction probe inlet and onset of vortex breakdown is less than the half chord of the wing.

The flow visualization of Figure 15 shows the structural response of the vortex with time t^*, where $t^* = tU_\infty/C$, which ranges from $t^* = 0.10$ (shortly after the application of suction of $t^* = 0$) to $t^* = 2.76$ marking complete stabilization of the core flow. This stabilization exhibits four distinct stages: (a) downstream movement of the onset of vortex breakdown and an imperceptible change of the radius of the breakdown spiral (compare $t^* = 0.10$ with $t^* = 1.55$); (b) continued downstream movement of the spiral pattern, accompanied by a decrease in the radius of the spiral (compare $t^* = 1.55$ with $t^* = 1.95$); (c) rapid decrease in radius of the spiral, eventually becoming indiscernible and leaving a breakdown bubble upstream of a turbulent wake (compare $t^* = 1.95$ with 2.29); and (d) stabilization of the turbulent breakdown region as it is drawn into the probe (compare $t^* = 2.29$ with 2.56).

Further consideration of the effects of localized suction involve abrupt cessation of the suction after the vortex core has been stabilized. There results substantial hysteresis, relative to that occurring for abrupt onset of suction. The magnitude and direction of this hysteresis depends on the amplitude of the suction coefficient C_μ (Parmenter and Rockwell[6]).

5.2 Blowing

Application of localized blowing along the leading-edge has been shown to extend the streamwise length of the vortex core prior to onset of breakdown, reviewed and demonstrated by Visser et al[7]. The purpose of this phase of the investigation is to examine the time-dependent restabilization of the vortex core after the abrupt onset of blowing. The concept of local blowing along the edge is illustrated in Figure 17. For a

half delta wing at angle of attack $\alpha = 40^\circ$, the location of vortex breakdown prior to the onset of blowing is at $x/C = 0.40$. A laser sheet cuts across the leading-edge vortex location $x/C = 0.52$. In the case addressed here, the amplitude of the blowing coefficient C_μ is of the order of unity; much lower values should be attainable by optimizing the location and orientation of the blowing or nozzle. It should be kept in mind that the ratio of the length of the vortex core prior to breakdown to the diameter of the core for jet blowing was of the order of 200. As a consequence, there is substantial decay in the centerline velocity of the jet, accompanied by widening of the jet. Consideration should be given to a blowing coefficient, based on the effective jet velocity and width at the location of vortex breakdown.

The photos of Figure 17 show raw particle images of the vortex breakdown prior to the onset of blowing and the restabilized cross-section of the vortex after blowing has been employed. The left photo corresponds to time $t^* = 0$ and the right photo to $t^* = 1.36$. In other words, the leading-edge vortex is, at the streamwise location shown, effectively restabilized in about one convective time scale C/U_∞.

6. Three-Dimensional Image Construction

6.1 Inverse technique using theoretical simulation

A major objective of this program is to construct the instantaneous (or phase-referenced), three-dimensional velocity field from minimum information on selected planes throughout the three-dimensional space of interest. Figure 3 shows a plan view of the laser sheet orientation that allows reconstruction of the three-dimensional velocity field. In principle, the acquisition of data on planes parallel to and between planes AB and CD in conjunction with data on planes DE and FB allows reconstruction of the three-dimensional field. Of course, there are many considerations with regard to the uncertainties arising from data density within each of the planes and the spacing and orientation of the planes which are related to the local gradients of the three-dimensional velocity field. All of these aspects are currently under investigation using an inverse technique, which starts with known theoretical solutions of three-dimensional flows such as a simple columnar vortex and a toroidal vortex. Streamlines corresponding to Hill's[10] spherical vortex are illustrated in Figure 18. This flow structure has many of the elements existing in complex leading-edge flows, including a well-defined distribution of vorticity. By slicing the three-dimensional vortex at selected locations and orientations, determining the velocity field in each plane, then randomizing the locations of the velocity vectors, it is possible to simulate the velocity field deduced from randomly placed particle tracks that would be generated in the laboratory using the laser-scanning technique. This concept is illustrated in Figure 19, showing side, top, and isometric views of the streamline pattern superposed upon the randomized velocity field in a plane oriented at 45° with respect to the axis of the vortex. With a number of planes of the randomized velocity field at hand, it is possible to reconstruct the three-dimensional image and determine the effect of the local velocity gradients and laser plane orientation and spacing on the accuracy of the reconstruction. This process is currently underway.

Irrespective of whether laboratory- or theoretically-generated data are employed, the technique for determination of the out-of-plane velocity component is the same. Applying the continuity equation at each node of the three-dimensional grid, the derivatives in the x and y directions of the in-plane (xy plane) velocity components u and v are fitted by a finite cosine series. The integrated form of this continuity equation is approximated by a modified finite sine series. Applying inverse discrete cosine and sine transforms, using a Fast Fourier Transform technique, the values of the out-of-plane velocity component w at each node can be computed. With the three-dimensional velocity field at hand, a tricubic spline interpolation can be employed to obtain the three-dimensional streamline pattern.

6.2 Construction of leading-edge vortex from experimental data

The three-dimensional image construction technique, described in the foregoing, was applied to the leading-edge vortex on the stationary wing at an angle of attack $\alpha = 20^\circ$, for which vortex breakdown occurs downstream of the trailing-edge. It should be noted that, in concept, the same technique illustrated here for a steady flow field can easily be applied to an unsteady flow by using phase-referencing or ensemble-averaging techniques.

Data were acquired in seven planes, oriented parallel to the span of the wing and passing vertically through the wing surface, as depicted in Figure 20. With reference to Figure 3, these planes can be viewed as lying parallel to lines AB and CD. To construct the three-dimensional image, it is necessary to provide initial conditions for the out-of-plane component by acquiring data in a plane oriented at an angle with respect to those of Figure 20. As illustrated in Figure 21, the plane cuts vertically through the wing at an angle of 42° with respect to its midplane. An approximation of the three-dimensional streamline pattern is illustrated in Figure 22. A solid model representation of the same leading-edge vortex from a different perspective is given in Figure 23. It should be emphasized that the spacing between the data planes illustrated in Figure 20 is not small relative to the streamwise distance over which one complete revolution of a typical three-dimensional streamline occurs. Consequently, the results displayed in Figures 22 and 23 are approximate and useful only for global representations of the flow structure. Improvements in the reconstruction scheme and in the density of data acquisition are currently underway.

7. Concluding Remarks

Global control, whereby the motion of the entire wing influences the structure of the leading-edge vortex along its entire extent and local control, involving application of suction or blowing at a defined location within the vortex, have been addressed herein.

Emphasis has been given to the unsteady response of the vortex to transient, ramp-type forcing.

A common feature of all of these types of control is a time delay, or phase shift, between the onset of the control and the eventual response of this vortex. Depending upon the type of control, the amplitude of the control forcing function, and whether or not vortex breakdown occurs, this time delay may range from a value less than C/U_∞ to a value several times C/U_∞. This time delay has been characterized with respect to: the streamwise development of the vortex core, emphasizing the changes in location of the onset of vortex breakdown; and the development in the cross-stream plane of the vortical structure.

For global motion of the entire wing, examination of the instantaneous location of the vortex breakdown, relative to the instantaneous position of the wing, reveals that:

(a) For simple pitch-up and pitch-down motions of the wing, the speed of propagation of the vortex breakdown has its minimum value when the location of vortex breakdown is furthest upstream and it tends to its largest value as the location of breakdown moves towards the trailing-edge. Exceptions occur near the trailing-edge of the wing, where the discontinuity of boundary conditions is associated with low propagation speeds.

(b) Variation of the location of vortex breakdown with angle of attack α shows large departures from the static characteristic even for low reduced pitch rates $\dot{\alpha}C/2U_\infty = 0.025$. The breakdown location can relax to its equilibrium position over a distance of as much as a half chord after cessation of the wing motion.

(c) Continuous pitch-up-down motions of the wing preclude low propagation speeds of the vortex breakdown (except near the trailing-edge) by not allowing the breakdown to move to upstream portions of the wing. For the continuous ramp-up-down motion of the wing, the total time scale for the breakdown location to cross the trailing-edge during the upstroke, then again during the downstroke, can be about one-fifth that for the corresponding cases of simple pitch-up and pitch-down motions where full relaxation of the breakdown is allowed to occur between the motions.

(d) For continuous pitch-up-down motions of the wing, the effect of not allowing the vortex breakdown to relax to its static state during the maneuver is to produce *upstream* movement of the breakdown location towards the apex for initial *decreases* in angle of attack α.

(e) Combinations of simple, ramp-type motions to form a hybrid pitching motion can produce overshoots of the static x_b vs α characteristic beyond that attainable with any of the simple ramp motions alone.

These features of the streamwise movement of the vortex breakdown during global control are associated with variations in the cross-sectional structure of the vortex. The time scales involved in relaxation of the vortex cross-section are strongly dependent upon existence of breakdown within the core.

(a) In absence of breakdown, the detailed structure of the vortex rapidly relaxes to its static state within about one convective time scale C/U_∞.

(b) Existence of breakdown within the core can produce long delays in the relaxation; insignificant changes were observed over as long as two convective time scales C/U_∞ while the wing is in motion.

For local control in the form of suction or blowing, substantial streamwise movement of the vortex breakdown and corresponding restabilization of the cross-section of the vortex can be achieved with a time delay of one to two convective time scales. However, minimization of the energy input to effect the alteration of the vortex is likely to result in longer time scales. Optimization of these control concepts and establishment of analogies with the vortex response to global control are currently underway.

8. Acknowledgements

The authors are grateful to the Air Force Office of Scientific Research for financial support of this research program.

9. List of References

1. Wedemeyer, E., 1982 "Vortex Breakdown", AGARD Lecture Series No. 121, High Angle of Attack Aerodynamics, December, pp. 9-1 to 9-17.

2. Wolfelt, K. W. 1986 "Investigation on the Movement of Vortex Burst Position with Dynamically Changing Angle of Attack for a Schematic Delta Wing in a Water Tunnel with Correlation to Similar Studies in Wind Tunnel", AGARD Conference Proceedings #413, Aerodynamic and Related Hydrodynamic Studies Using Water Facilities, Symposium of the Fluid Dynamics Panel in Monterey, California, 20-23 October, 1986.

3. Atta, R. and Rockwell, D. 1987 "Hysteresis of Vortex Development and Breakdown on an Oscillating Delta Wing", *AIAA Journal*, Vol. 25, No. 11, pp. 1512-1513.

4. Atta, R. and Rockwell, D. 1989 "Leading-Edge of Vortices due to Low Reynolds Number Flow Past a Pitching Delta Wing", *AIAA Journal* (in press).

5. Reynolds, G. A. and Abtahi, A. A. 1987 "Instabilities in Leading-Edge Vortex Development", AIAA Paper No. 87-2424, AIAA Applied Aerodynamics and Atmospheric Flight Mechanics Conference, August 17-19, Monterey, California.

6. Parmenter, K. and Rockwell, D. (1989) "Transient Response of Leading-Edge Vortices to Localized Suction", *AIAA Journal* (in press).

7. Visser, K., Iwanski, K. T., Nelson, R. C. and Ng, T. T. 1988 "Control of Leading-Edge Vortex Breakdown by Blowing", AIAA Paper 88-0504, AIAA 26th Aerospace Sciences Meeting, January, 1988, Reno, Nevada.

8. Atta, R. 1987 "Unsteady Structure of Flow Past a Pitching Delta Wing", Ph.D. Thesis, Department of Mechanical Engineering and Mechanics, Lehigh University, Bethlehem, Pennsylvania.

9. Lambourne, N. C., Bryer, D. W., and Maybrey, J. F. M. 1969 "The Behavior of Leading-Edge Vortices following a Sudden Change in Incidence", NPL Aero. R and M 3645.

10. Hill, M. J. M. 1894 Phil. Trans. Roy. Soc. A 185 (in Batchelor, G. 1970 An Introduction to Fluid Mechanics, Cambridge University Press).

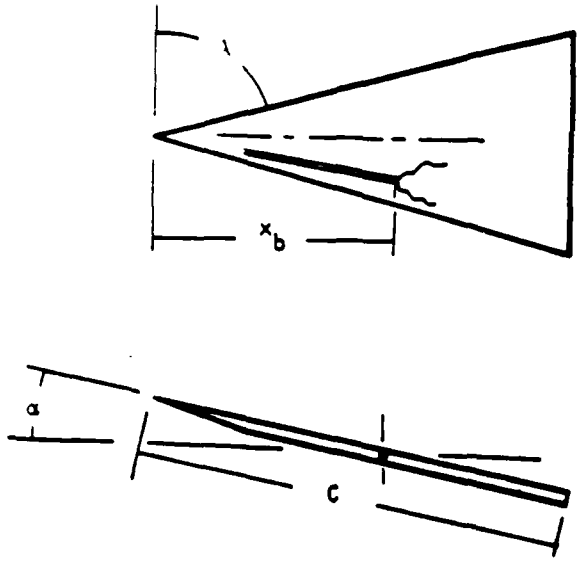

Figure 1: Schematic of delta wing.

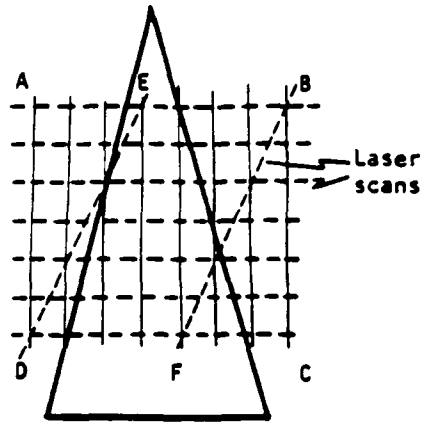

Figure 3: Location and orientation of planes of laser scanning technique.

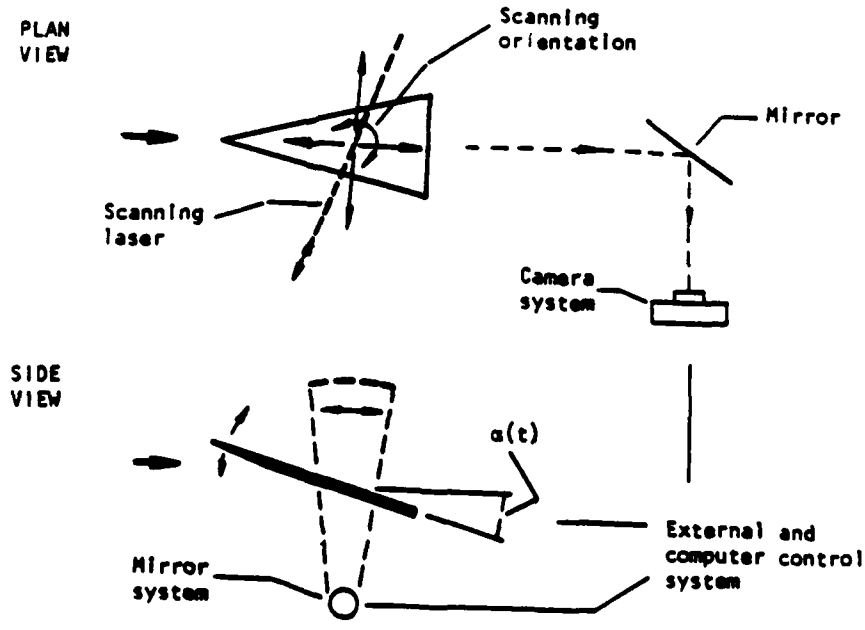

Figure 2: Illustration of integrated flow visualization-active control system employing computer-controlled wing motion and camera unit in conjunction with laser scanning technique.

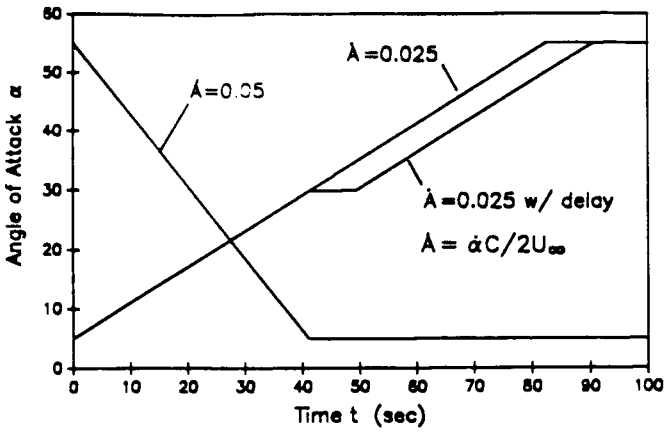

Figure 4a: Representative pitching schedules for simple pitch-up and pitch-down motion of wing, allowing for relaxation of leading-edge vortices after cessation of wing motion.

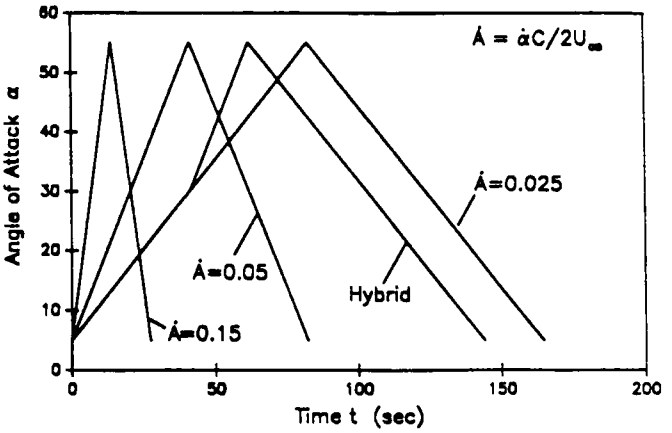

Figure 4b: Representative pitching schedules for continuous pitch-up-down motion of wing.

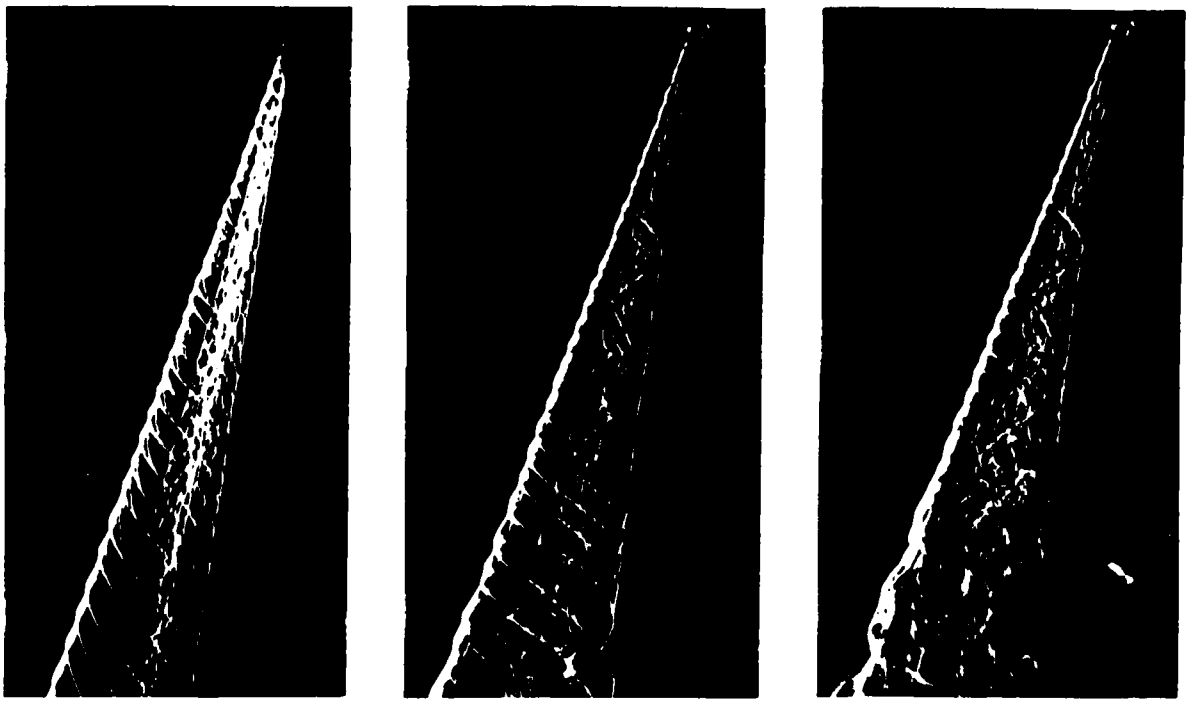

Figure 5: Visualization of development of leading-edge vortices via the hydrogen bubble technique for pitch-up motion from $\alpha = 15^\circ$ to $\alpha = 40^\circ$ at pitch rate $\dot{\alpha}C/2U_\infty = 0.025$. Left photo corresponds to $\alpha = 15^\circ$ immediately prior to the onset of wing motion; middle photo taken at $\alpha = 40^\circ$ immediately after cessation of motion; and right photo represents time $tU_\infty/C = 0.63$ after cessation of motion.

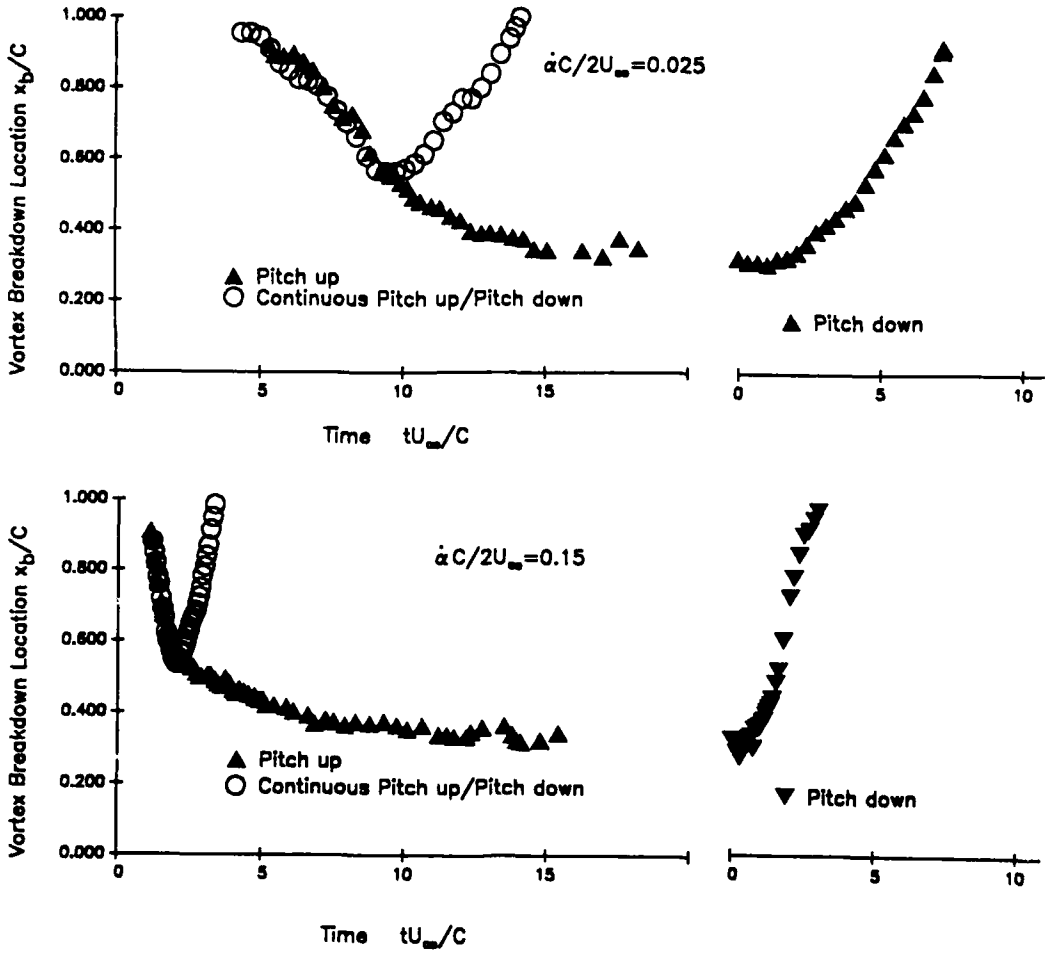

Figure 6: Time history of location of vortex breakdown for simple pitch-up, simple pitch-down, and continuous pitch-up-down motions of wing. Cases of relative low (top graph) and high (bottom graph) pitching rates are illustrated.

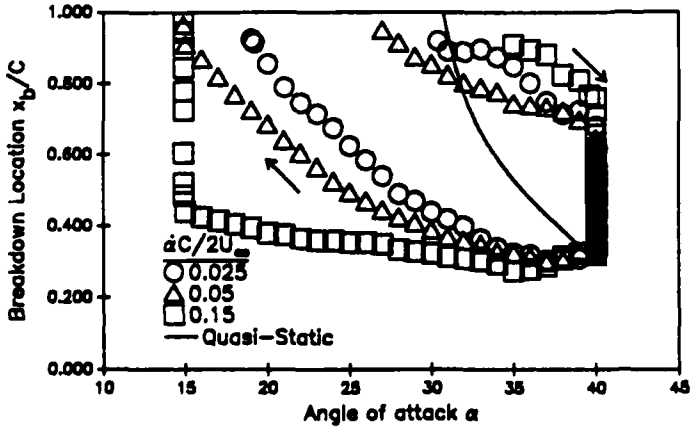

Figure 7: Location of vortex breakdown as function of angle of attack for three representative values of pitching rate for simple pitch-up and pitch-down motions, where flow structure is allowed to relax to static condition of wing motion.

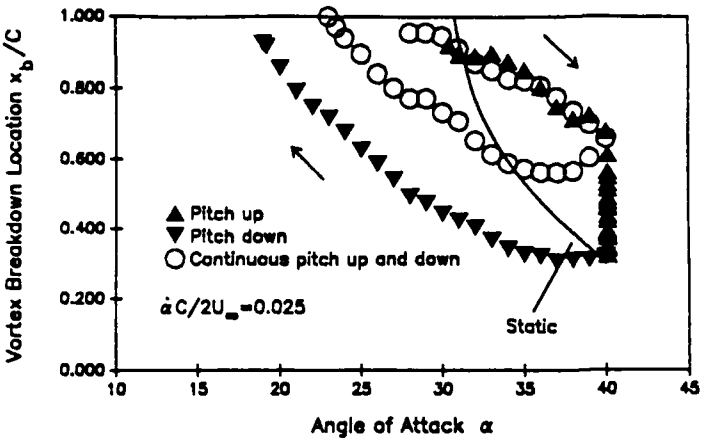

Figure 8: Location of vortex breakdown as function of angle of attack for various types of pitching motion at relatively low (top graph) and high (bottom graph) pitching rates.

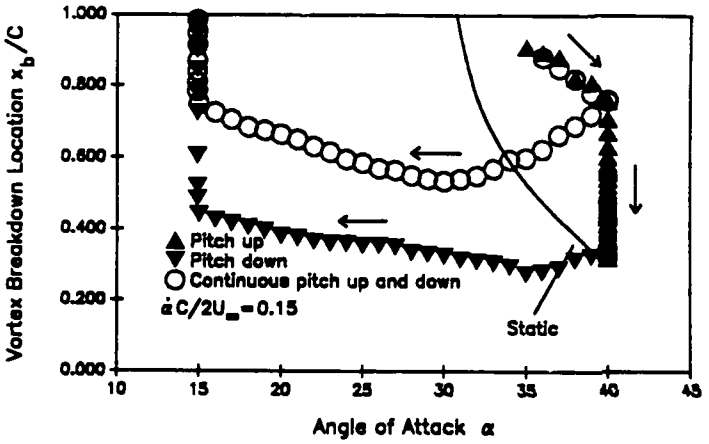

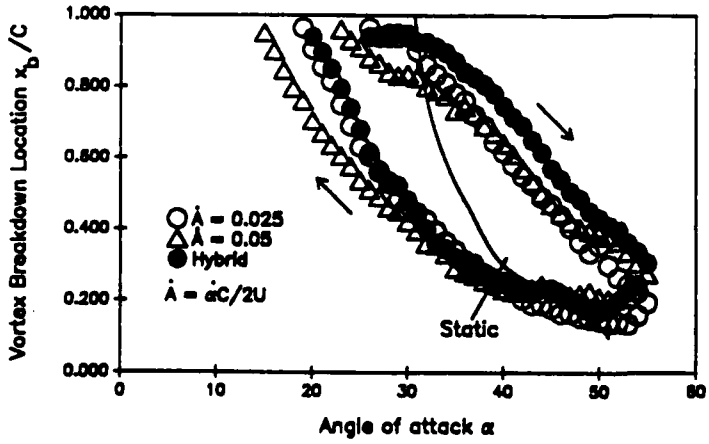

Figure 9: Location of vortex breakdown as function of angle of attack for continuous pitch-up-down motions of wing. Hybrid pitching schedule is defined in Figure 4b.

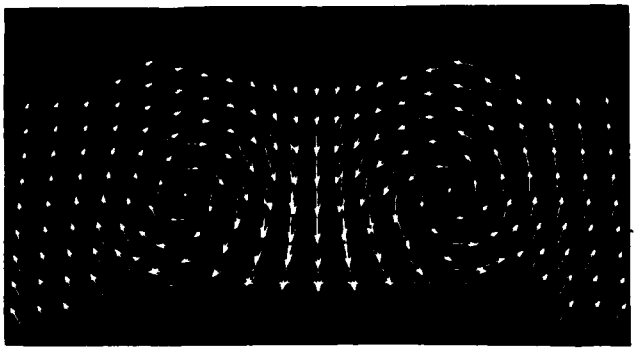

Figure 10: Representative velocity field obtained directly from particle images followed by interpolation. Images acquired at midchord and at $\alpha = 15^{\circ}$ immediately after cessation of pitch-down motion from $\alpha = 40^{\circ}$. Pitch rate $\dot{\alpha}C/2U_{\infty} = 0.15$.

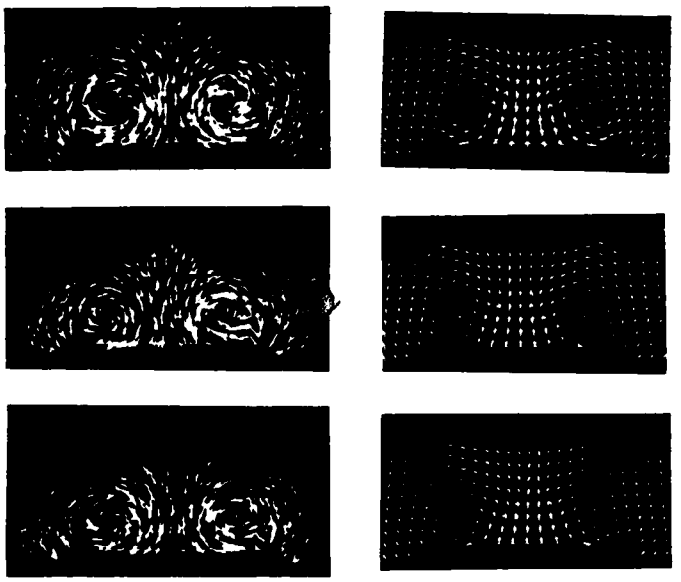

Figure 11: Raw and interpolated data showing relaxation of instantaneous vortical flow structure at midchord immediately after cessation of pitch-down motion from $\alpha = 40^{\circ}$ to $\alpha = 15^{\circ}$ at pitch rate $\dot{\alpha}C/2U_{\infty} = 0.15$. Upper image corresponds to $t^{*} = tU_{\infty}/C = 0$ after cessation of motion; middle image to $t^{*} = 1.05$; lower image to $t^{*} = 2.10$.

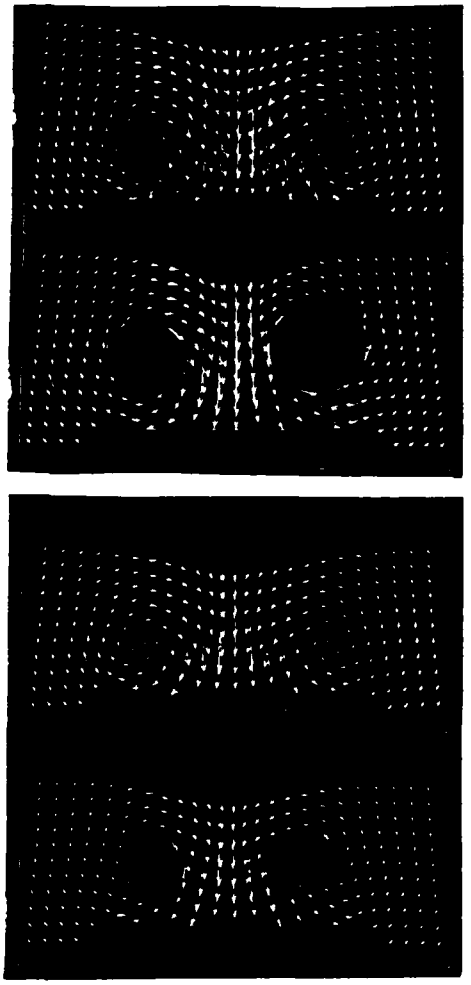

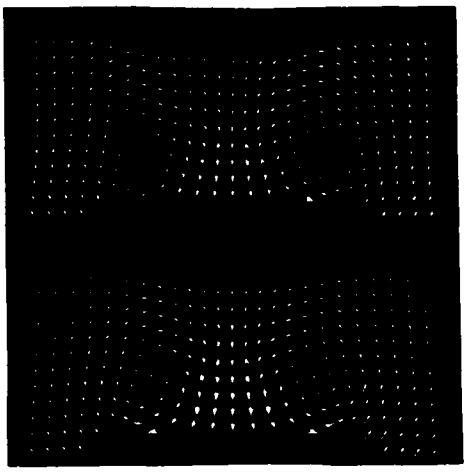

Figure 12: Instantaneous vortical flow structure at midchord at successive instants of time during pitch down maneuver (bottom image in each set) relative to structure for stationary wing (top image in each set). Upper left set of images corresponds to $\alpha = 35^{\circ}$; lower left set to $\alpha = 20^{\circ}$; and upper right set to $\alpha = 15^{\circ}$. Closed contours represent boundaries of region of vortex breakdown. Pitch rate $\dot{\alpha}C/2U_{\infty} = 0.15$.

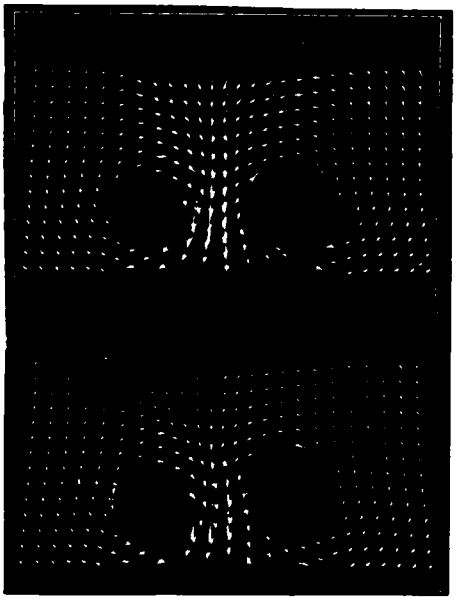

Figure 13: Instantaneous flow structure at two successive times near midchord ($x/C = 0.51$) of stationary wing at $\alpha = 40^{\circ}$. Extent and location of region of vortex breakdown oscillates with time.

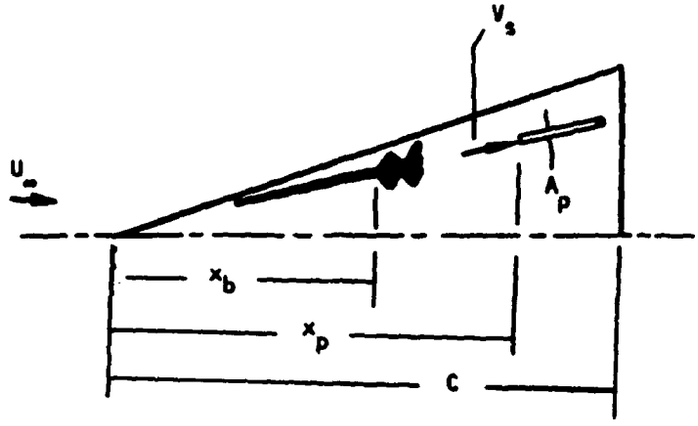

Figure 14: Schematic illustrating concept of suction applied to vortex in region downstream of onset of vortex breakdown.

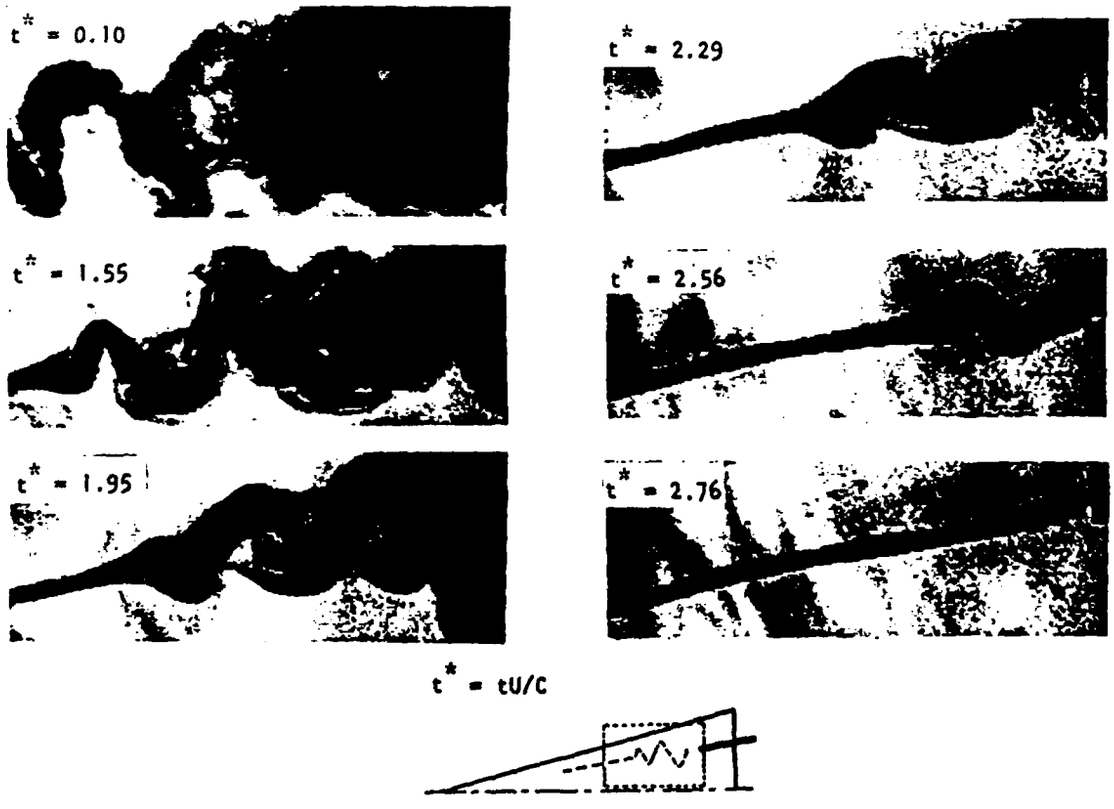

Figure 15: Visualization of process of stabilization of vortex core after abrupt onset of localized suction at $t^* = 0$. Left boundary of photo is at $x/C = 0.55$. Vortex breakdown in absence of suction occurs at $x_b/C = 0.45$. Suction probe is located at $x_p/C = 0.95$. Amplitude of suction coefficient $C_\mu = 0.57$. $Re = 3.1 \times 10^4$.

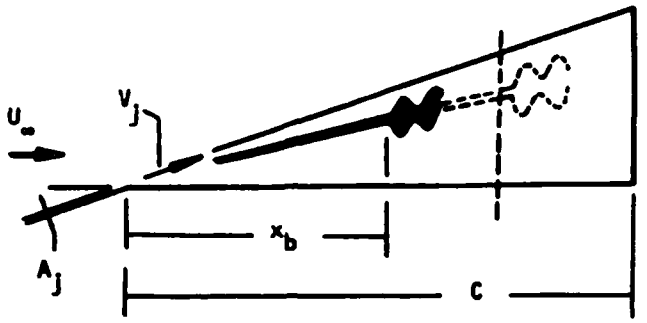

Figure 16: Schematic illustrating downstream movement of vortex breakdown due to blowing along leading-edge of wing applied at its apex.

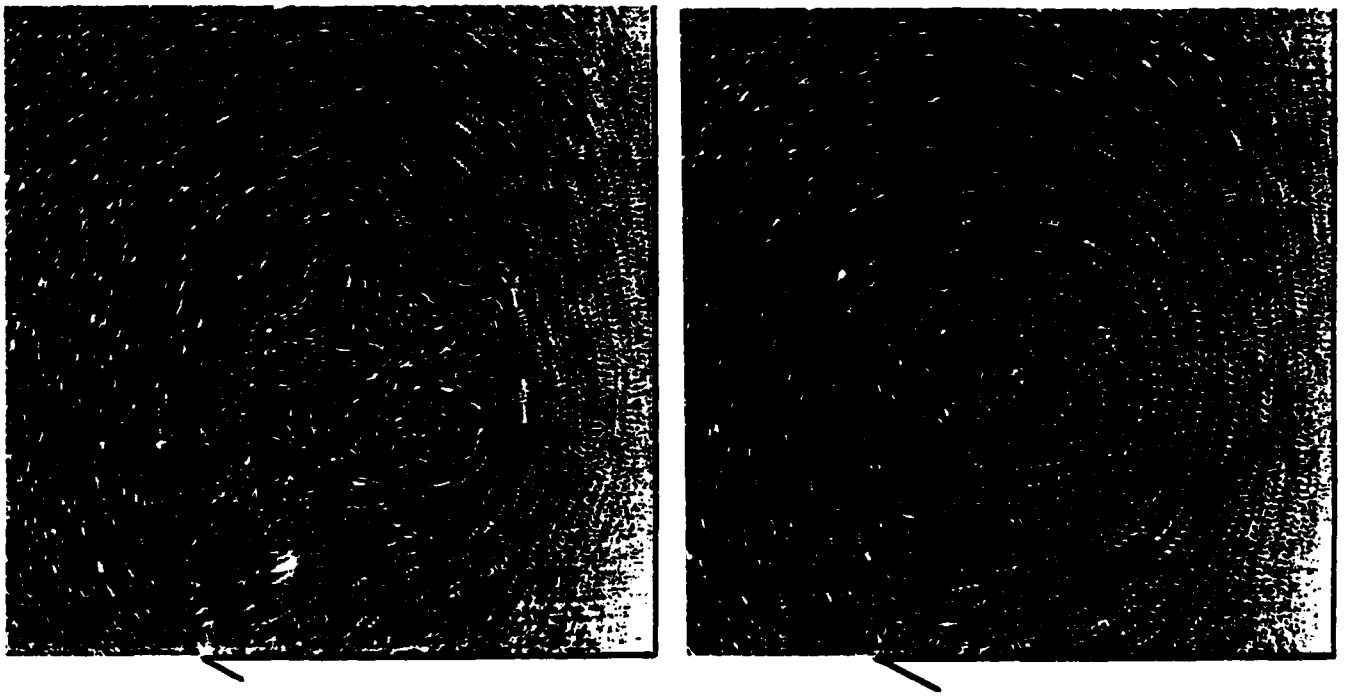

Figure 17: Particle images across cross-section of leading-edge vortex at laser sheet location x/C = 0.52 before ($t^* = tU_\infty/C = 0$) and after ($t^* = 1.36$) abrupt onset of blowing applied along leading- edge of wing at its apex. In absence of blowing, vortex breakdown occurs at $x_b/C = 0.40$. Re = 18.8 x 10^4. (Photos by C.-H. Kuo and S. Guzy).

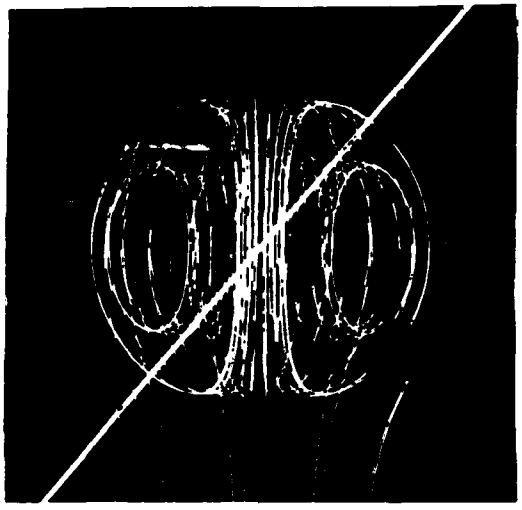

Figure 18: Representation of streamlines of Hill's spherical vortex employed for simulation of three-dimensional construction.

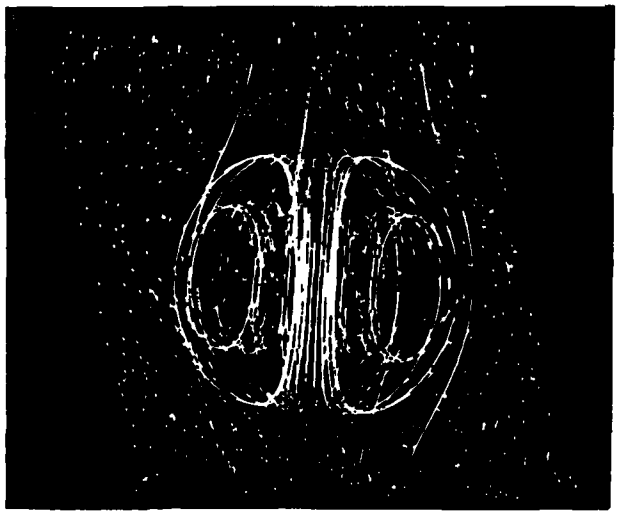

Figure 19: Superposition of streamlines of Hill's spherical vortex and randomized velocity field in plane cutting at an angle of 45° through the center of vortex.

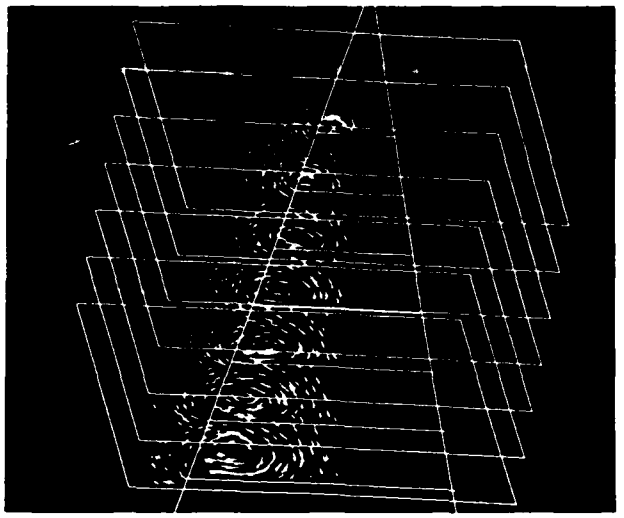

Figure 20: Velocity fields obtained directly from particle images in planes cutting vertically through wing which is stationary and at angle of attack $\alpha = 20^{\circ}$.

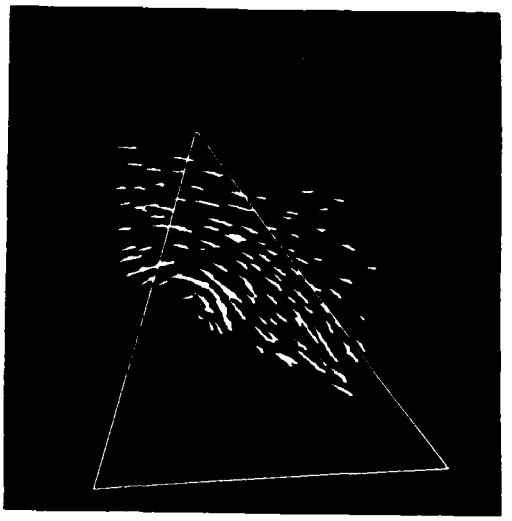

Figure 21: Velocity field in plane cutting vertically through wing at angle of 42° with respect to midplane of wing.

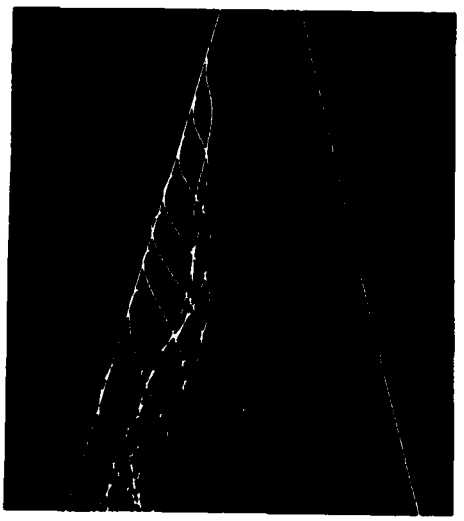

Figure 22: Approximation of three-dimensional streamline pattern of leading-edge vortex obtained from information in images of Figures 21 and 22.

Figure 23: Solids model representation of leading-edge vortex of Figure 22.

ON UNSTEADY FLOW STRUCTURE FROM SWEPT EDGES SUBJECTED TO CONTROLLED MOTION*

D. Rockwell, R. Atta, C.-H. Kuo, C. Hefele,
C. Magness and T. Utsch
Department of Mechanical Engineering and Mechanics
354 Packard Laboratory #19
Lehigh University
Bethlehem, Pennsylvania 18015

ABSTRACT

This investigation addresses active control of the leading-edge vortices formed from delta wings and wing segments. A variety of modifications of the flow structure are characterized with quantitative, global flow visualization in conjunction with LDA techniques.

INTRODUCTION

The structure of flow past a stationary delta wing has been studied extensively over the past few decades. Early investigations established that flow separation from the leading-edge of the wing gives rise to a spiral-vortex sheet on the upper surface of the wing; the consequence of this vortex pattern is an increase in lift, above that which would occur without leading-edge separation (e.g., Lee[1]; Ornberg[2]; Elle[3]). The study of Kuechemann[4], which involves a nonlinear lifting-surface theory, describes this effect. More recent studies (Kuechemann[5]; Hoeijmakers[6]; Rizzi et al[7]; Woodson and DeJarnette[8]) delineate details of the primary-secondary vortex system adjacent to the leading-edge and the corresponding separation and reattachment lines.

The unsteady flow structure on a delta wing subjected to controlled motion has received less attention. The investigation of Lambourne et al[9] demonstrated the concept of phase shift between development of the vortex pattern and the stepwise motion of the wing in the plunging mode. For the case of simple harmonic motion in the pitching mode, Gad-el-Hak and Ho[10] observed an analogous phase shift of the growth-decay cycle of the leading-edge vortices. This phase shift, or hysteresis, during the course of the wing oscillation cycle was characterized in terms of height or thickness of the dye blob marking the vortex; the degree of hysteresis was found to be a strong function of reduced frequency. Further aspects of the unsteady three-dimensional structure on various wings are addressed in the subsequent investigations of Gad-el-Hak and Ho[11,12]. They emphasize the importance of mutual induction between leading- and trailing-edge vortices in determining the overall flow structure.

Central to the unsteady structure of the leading-edge vortices is the time-dependent development of the vortex core along its streamwise extent and its eventual breakdown. This breakdown is characterized by abrupt transition from a jet-like to a wake-like core of the vortex, accompanied by a substantial increase in turbulence activity. Such vortex breakdown has been investigated for flow past a variety of stationary wing configurations, as reviewed by Wedemeyer[13]. For nonstationary (sinusoidal) wing motion, Atta and Rockwell[14] observed: occurrence of the maximum breakdown position of the core near the maximum angle of attack, rather than near the minimum value; substantial overshoot of the core breakdown length relative to its steady counterpart; and existence of the vortex core only over a fraction of the oscillation cycle. There have been extensive and insightful studies of vortex breakdown in various types of axisymmetric tube arrangements as, for example, described by Garg and Leibovich[15], Escudier[16] and Sarpkaya[17]. These, as well as other experimental studies and a wide range of theoretical approaches beyond the scope of this introduction are incisively assessed by Leibovich[18,19]. In essence, the investigations of vortex breakdown addressed therein focussed on steady inflow conditions. Exceptions include the investigations of Lambourne[20] and Sarpkaya[21] who reveal interesting aspects of transient vortex development and overshoot of the vortex breakdown position.

There are a number of unexplored features of unsteady vortex flows on oscillating delta wing and flap arrangements. These issues include: flow structure of the vortex development and breakdown; evolution of the mean and unsteady velocity fields of the vortex in the pre- and post-breakdown regions, including alteration of the velocity eigenfunctions and spectral energy transfer; and the effects of mutual interference between flap/wing combinations. Particularly helpful for investigating these aspects are quantitative flow visualization techniques which, when employed in conjunction with laser-Doppler and pressure measurement techniques, can provide both local and global views of the evolving flow structure.

EXPERIMENTAL SYSTEM AND TECHNIQUES

All experiments were carried out in one of the three water channel systems custom-designed for unsteady, separated flows. The cross-sectional areas of the test sections of these channels ranged from 1.5 ft^2 to 6 ft^2. In order to allow observation of the flow from an arbitrary

---

* Based on presentation at AFOSR Workshop on Unsteady and Separated Flows, U. S. Air Force Academy, Colorado Springs, Colorado, July 26 - 30, 1987.

perspective, all channels of the test section were made entirely of glass or Plexiglas. Furthermore, in the case of the largest channel, the entire system upstream and downstream of the test section is made of PVC and bronze, in order to preclude problems with corrosion. The chord C length of the delta wings ranged from C = 50.8 mm to C = 508 mm and the corresponding Reynolds number range extended over $5.8 \times 10^3 \leq U_\infty C/\nu \leq 3.9 \times 10^4$. Values of Re up to Re = 4.5×10^5 are attainable in the large-scale water facility, while still allowing reasonably low absolute frequencies (~0.5 Hz) to be employed to attain high values of reduced frequency. This concept simplifies the mechanical forcing of the wing, as well as data acquisition. In all cases, the viewing surface was the flat machined surface of the wing; the opposite side of the wing was machined at an angle of $\alpha = 10^\circ$ to 20°, depending upon the wing under consideration. All wings were of Plexiglas. For the technique of illumination by laser-induced reflection, the wing surface was machined to a one micron finish. In cases where diffuse stroboscopic lighting was employed, the wing was spray-painted flat black for employment of the hydrogen bubble technique and flat white for use of the dye injection method of visualization.

The experimental objectives require employment of laser-Doppler anemometry techniques in conjunction with quantitative flow visualization in order to characterize flow structure. Eventual measurements of the unsteady surface pressure will allow establishment of a direct relationship between the instantaneous loading and the instantaneous flow structure. The first stage of laser-Doppler measurements described herein were made with a single channel two watt Argon-ion system with a beam expander to optimize signal to noise ratio. Quantitative flow visualization involved tracking of hydrogen bubble markers. The intention of these tracking techniques is to circumvent the many fallacies associated with interpretation of traditional dye and smoke injection techniques (Lusseyran et al[22]; Hama[23]). Preliminary pressure measurements have been carried out with a high sensitivity Kulite transducer coated with a Paralene film to inhibit corrosion; alternately, a PCB transducer operating on the piezo electric principle was also employed. Further details of these techniques are described by Rockwell et al[24,25].

A primary objective of this program is to develop an integrated active control system that allows forcing of wings and wing segments with arbitrary functions and simultaneously accommodates acquisition of instantaneous quantitative flow visualization, laser-Doppler, and pressure information. The first version of this system has been completed. Forcing is provided by Superior Electric stepping motors with appropriate gear reduction; or with Compumotors running at ten to twenty thousand steps per revolution. These motors are interfaced with a Zenith-241 computer. Also interfaced with the computer are: the output of the LDA system; the marker pulse generator and switch system for producing grids of visualization marker at a desired phase of the wing motion; and the microprocessor linked to the servomotor drive system that will eventually translate the laser scanning system (in the direction of the flow) in order to allow three-dimensional sweeps of the flow structure.

Illumination of the flow structure is achieved by a two-watt Argon-ion laser (with a multi-line mirror holder) impinging upon a system of mirrors. This system allows a rotating mirror to sweep the laser at an arbitrary angle with respect to the freestream while the entire optical train is translated in the freestream direction. Alternately, diffuse illumination can be employed; it involves stroboscopic lights having a power of 90 watts, a flash duration of ten microseconds, and a repetition frequency of 120 Hertz. Or, a higher powered strobe having an intensity of 8.3 Joules at 120 cycles per second was employed. Recording of the visualization images was achieved with either one or two video cameras having a zoom lens capability. Each of the two video cameras could be connected to the mainframe of the video system and the corresponding images displayed simultaneously using the split-screen capability of the mainframe.

Figures 1a and 1b show simplified overviews of the two basic types of image acquisition: a dual-view method (Figure 1a); and a single-view method (Figure 1b). In concept, each of these techniques provides the capability for tracking visualization markers in three-dimensional space.

For the dual image method of Figure 1a, stroboscopic lighting is employed. The lights are angled with respect to the surface of the bubble markers in order to provide optimum reflection when viewed through the cameras. Mirror arrangements located external to the test section, as well as sufficiently far downstream of the region of interest so as to preclude interference, were employed to facilitate viewing the flow structure from various perspectives. Various locations and orientations of 25 micron platinum wires allow generation of hydrogen bubbles. In the arrangement shown in Figure 1a, the wire flies at the same velocity as the apex of the wing; this is accomplished by mounting the wire between two probe supports that are rigidly attached to the pitching axis of the wing. The orientation of the wire is adjusted to allow examination of either: the core flow, by ensuring continuous injection of marker at or near the apex of the wing; or, the exterior flow, by injecting markers from a wire in the plane of the wing at the apex (Rockwell et al[24,25]).

For the single image method of Figure 1b, the principle is to employ the localized injection of bubble markers of defined width and length in conjunction with a laser sheet (or sheets) of finite thickness in order to determine the velocity field. As opposed to the previous technique, only a single video camera is employed with various mirror arrangements in order to obtain the desired cross-sectional view of the flow image. This image is produced by laser-induced reflection from the hydrogen bubble markers. By use of an optically transparent wing, it is possible to view both sides of the wing simultaneously. Bubble markers are generated upstream of the wing from a single segmented wire, arrangements of them, or a wire grid as schematically portrayed in Figure 1b. The basic concept of this technique is that by generating bubble markers of defined frequency and duration and employing a laser sheet of finite thickness, estimates of the velocity field can be made from a single view.

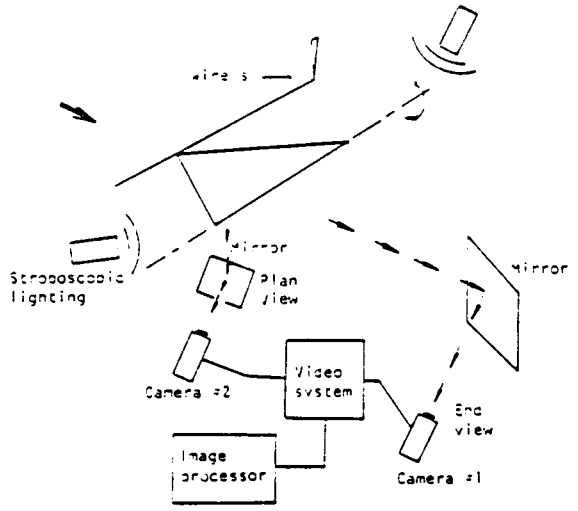

Figure 1a: Dual image technique for tracking three-dimensional flow structure.

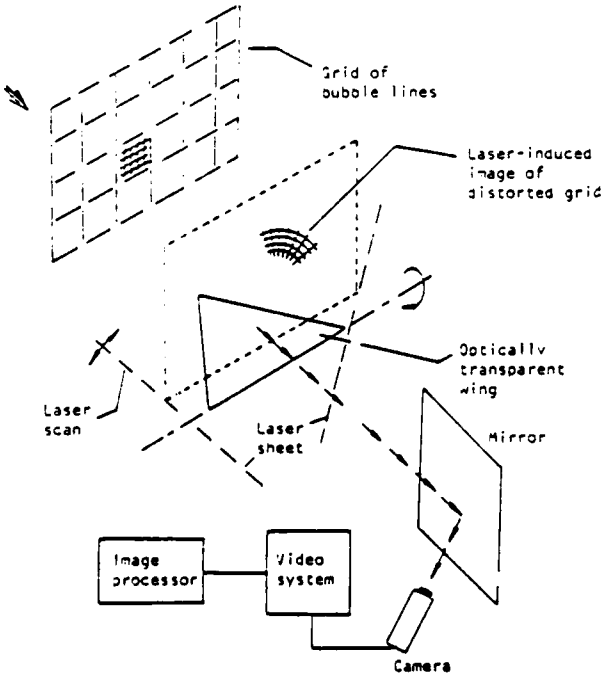

Figure 1b: Single image technique for determining two- and three-dimensional flow structure.

In order to facilitate quantitative interpretation of flow visualization images, a variety of image processing techniques have been developed. For overviews of these, the reader is referred to Rockwell et al[24,25] and Smith[26]. In short, quantitative techniques for characterizing the unsteady process of bursting in a turbulent boundary layer (Lu and Smith[27]) and vorticity in an unstable wake flow (Lusseyran and Rockwell[28]) have been employed. In addition, efforts have been focussed on the following techniques: reconstruction of three-dimensional flow structure using a phase-reference technique (Ongoren et al[29]); ensemble-averaging between images and correlation within or between images (Kerstens and Rockwell[30]); and Fourier discriptor techniques for pattern recognition (Gumas and Rockwell[31]).

QUANTITATIVE FLOW VISUALIZATION

Flow past a stationary delta wing having a sweep angle $\lambda = 45^{o}$ and inclined at an angle of attack $\alpha = 15^{o}$ with respect to the freestream produces the flow structure given in Figure 2a; the photos show only a portion of the flow field. In this case, the wing is made of brass, requiring modification of the single image technique of Figure 1b; use of an appropriate mirror arrangement allowed simultaneous views of the upper and lower sides of the wing. Bubbles were generated continuously from the grid located upstream of the wing, and the laser was translated to various distances x from the apex in order to provide the desired images. It should be emphasized here, and in subsequent photos of this type, that the thickness of the bubble sheets forming the grid pattern is of the order of 25 microns. Use of high gain on the video system, for purposes of illustration, greatly exaggerates the actual thickness. In this sequence of photos, the direction of circulation about the wing is readily apparent. Moreover, it clearly increases in the streamwise direction.

By tracking each of these nodes of the bubble grid in three-dimensional space, and making use of photos in addition to those of Figure 2a, it is possible to determine the three-dimensional streamline pattern of the flow. This is accomplished by digitizing the node locations, then using CROSS THREE-D of the Unigraphics CAD software system. The three-dimensional pattern is displayed on a McAuto D-100 C color terminal allowing rotation of the three-dimensional image in real time. Figures 2b through 2d show selected results. In Figure 2b, an end view of the streamline pattern is illustrated. Figure 2c shows an end view of stream surfaces, formed by connecting streamlines whose upstream positions are located in defined vertical planes prior to encounter with the wing. Figure 2d shows the same stream surfaces from a different perspective. Various combinations of horizontal surfaces, not shown here, were also constructed. With this type of streamline information, it is possible, in concept, to proceed with calculation of the corresponding velocity field and circulation. Occurrence of flow separation along the upper surface of the wing (see photo corresponding to x/C = 0.8 in Figure 2a) produces inaccuracies of the streamline pattern in and immediately around that region. Moreover, there is inadequate spatial resolution there that

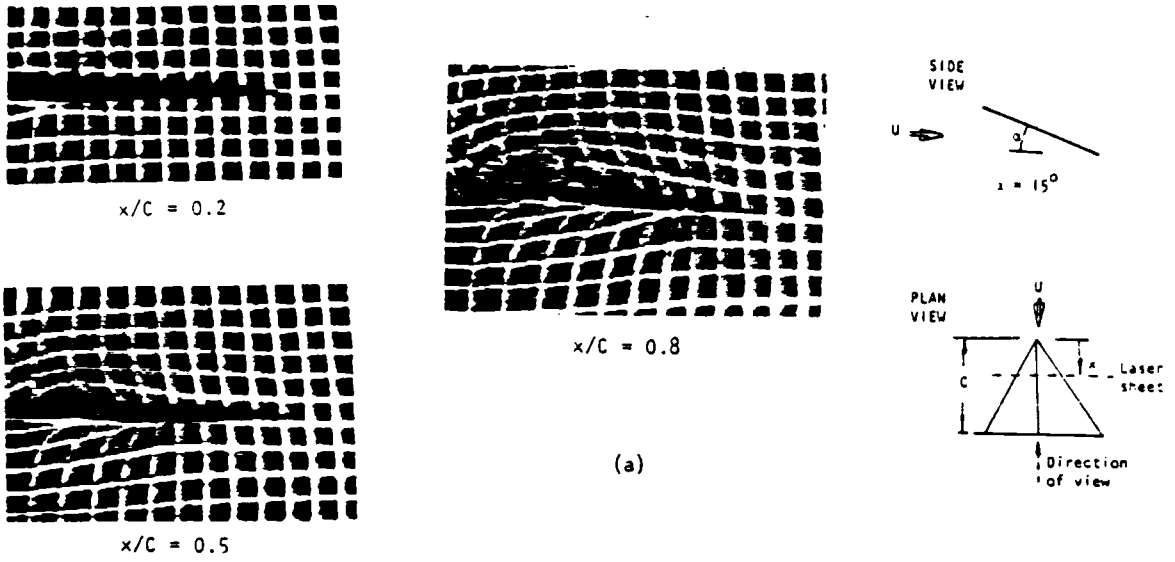

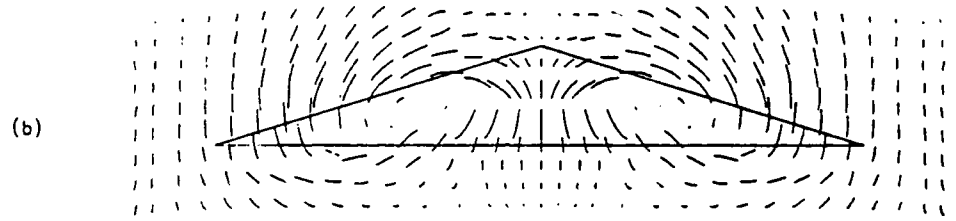

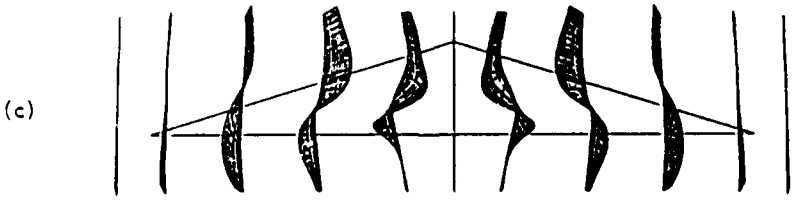

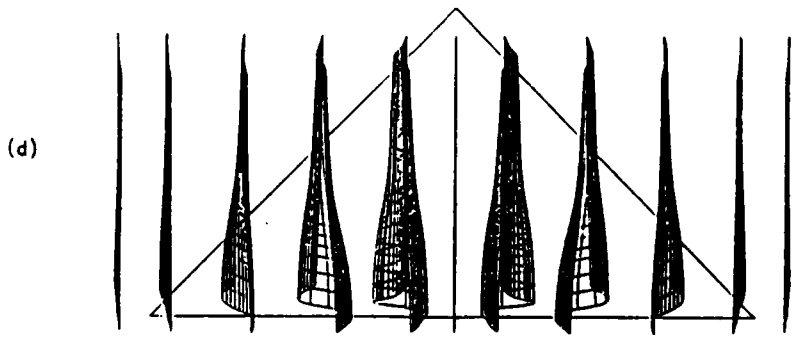

Figure 2: (a) End view of distorted grid of hydrogen bubble lines (actual thickness of 25 microns greatly exaggerated by high video gain); (b) end view of streamline pattern obtained by tracking nodes of distorted grid in three-dimensional space and connecting them with CROSS-3-D CAD technique; (c) end view of stream surfaces obtained from connecting streamlines in initially vertical plane before encounter with the wing; and (d) an additional view of (c) from an elevated perspective.

precludes calculation of the velocity and vorticity distributions. This technique for determining the flow structure exterior to the vortex core is currently being extended to unsteady flows past oscillating delta wings.

In order to determine the streamline pattern and velocity field of the vortex core, it is most effective to generate markers locally from a single wire or an arrangement of wires located within the core itself. The photo of Figure 3a shows representative markers from a single, segmented bubble wire located in the core of a vortex on a delta wing having a sweep angle $\Lambda = 75^{o}$, an angle of attack $\alpha = 20^{o}$, and at a streamwise location $x/C = 0.87$. In the case of steady flow, translation of the laser sheet in the streamwise direction provides a family of marker locations in three-dimensional space which, in turn, can be connected to give the streamline pattern of the flow. Note the distortion in the marker pattern on the left-side of the photo as well as to the right of the apparent center of the vortex. These distortions are caused by the shear layer that originally separated from the edge of the wing. Averaging provides the streamline pattern shown in Figures 3b through 3d. In Figure 3b, the view is in the upstream direction along the axis of the center of the vortex. Figures 3c and 3d show this streamline pattern at different orientations; in both of these cases, both the streamlines and lines corresponding to constant streamwise coordinate are displayed.

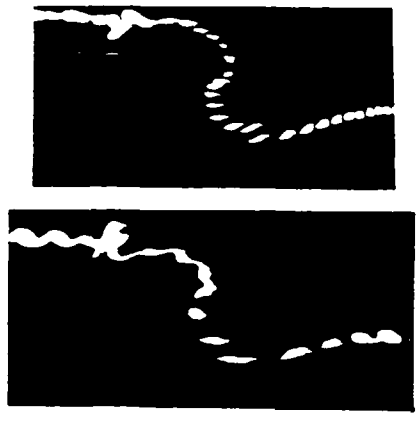

(a)

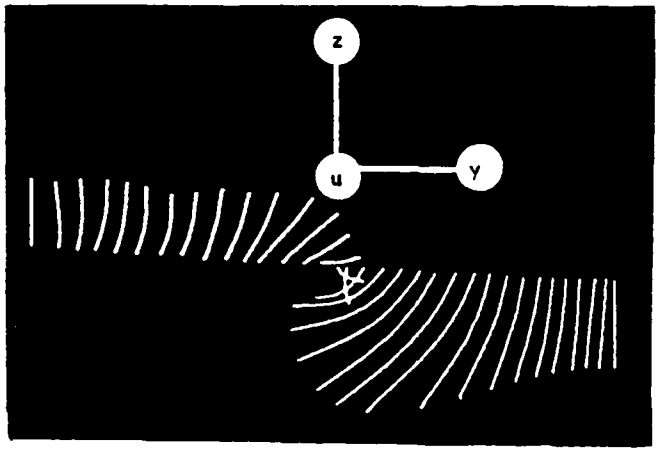

(b)

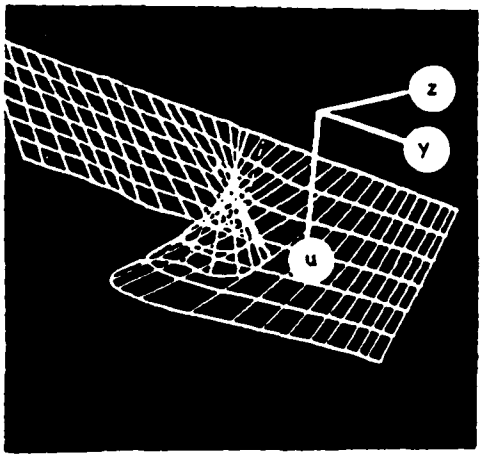

(c)

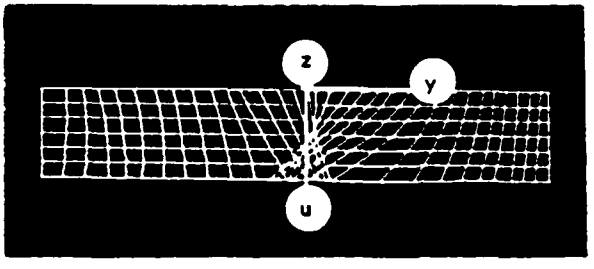

(d)

Figure 3: (a) Elements of bubbles generated from two different segmented wires located in vortex core; (b) end view of streamlines obtained by translating laser sheet in streamwise direction and tracking bubble elements in three-dimensional space; (c) pattern of (b) from another perspective including lines representing constant values of streamwise coordinate; and (d) view of (c) from another perspective.

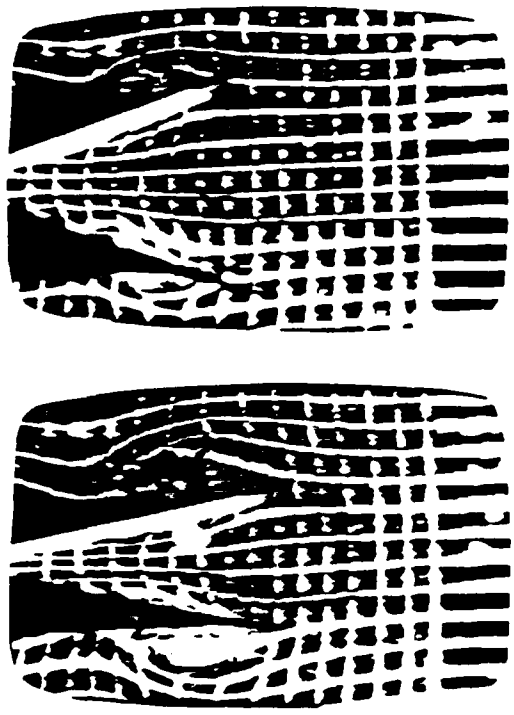

(a)

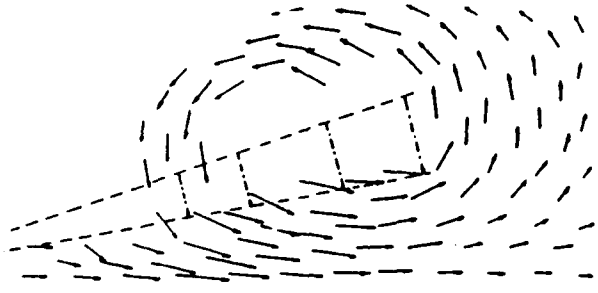

(b)

Figure 4: (a) End view of delta wing segments oscillating about a common axis in harmonic version of clap and fling maneuver, with top photo taken at x/C = 0.7 and bottom photo x/C = 0.8 and a time delay between photos corresponding to the transit time of the freestream between two stations (bubble sheets have a thickness of 25 microns, greatly exaggerated here due to video gain); (b) excerpt of upper half of velocity field.

Using the general types of techniques shown in conjunction with Figures 2 and 3, it is possible to determine directly the velocity field by pulsing the voltage applied to the bubble wires, such that discrete markers are generated. Such methods can be applied to both steady and unsteady flows, and efforts are continuing in this direction in our laboratory. In fact, distributions of axial and swirl velocity components obtained for the conditions described in conjunction with Figure 3a show a reasonable approximation to the expected distributions.

Determination of the instantaneous velocity field in the cross-stream plane is of obvious importance in determining the circulation for various wing-flap or flap-flap arrangements. The photos in Figure 4a correspond to a simple harmonic version of the clap and fling motion of two delta wing segments (or "flaps") oscillating about a common axis, corresponding to the center of the corresponding stationary delta wing. The top photo was taken at x/C = 0.7 and the bottom one at x/C = 0.8. The wing segments are in the process of closing, and the time shift between the two photos was calculated to correspond to the time required for a defined bubble segment to travel between x/C = 0.7 to 0.8 in the freestream region. The axial velocity component at any location in the cross-section can be estimated by pulsing the front of the bubble grid and calculating the "glow time" corresponding to passage of this pulsed front of bubbles through the laser sheet of finite thickness. Outside the vortex core, the axial velocity deviates relatively little from the freestream value, simplifying the tracking process. For the present purposes, it is the circulation about the vortex core that is of primary interest. The velocity field corresponding to the upper half of the flow is shown in Figure 4b. It was obtained by averaging the node displacements about the plane of symmetry of the wing segments, then carrying out a linear interpolation. Circulation calculated using two different circuits differed by less than 3%, thereby suggesting that the circuit for determining the circulation was exterior to the vortex core. The dimensionless circulation corresponding to the pattern of Figure 4a is about one-half that generated in a ramp-type fling of a two-dimensional wing system (Spedding and Maxworthy[32]) with no mean flow in the axial direction.

PHASE SHIFT AND HYSTERESIS OF VORTEX CORE DEVELOPMENT AND BREAKDOWN

When a delta wing is pitched about its trailing-edge in sinusoidal motion, examination of the flow structure over the range of reduced frequency $0.025 \leq K \leq 1.7$, and mean angle of attack $5^{\circ} \leq \alpha \leq 20$ shows that there are two fundamental types of vortex development during the course of an oscillation cycle. At low reduced frequencies, the core development is of the form shown in the left column of photos of Figure 5, while at higher reduced frequency, the form is as shown in the right column. Considering first the case of low reduced frequency at $\alpha = 9^{\circ}\uparrow$, the dye has been swept from the mid-portion of the wing to a region along its leading-edge. At $\alpha = 15^{\circ}\uparrow$, onset of vortex core development is evident in the right portion of the photo, and at $\alpha = 18^{\circ}\uparrow$ and $19^{\circ}\uparrow$, this core development progresses in the upstream direction towards the apex.

On the other hand, at higher reduced frequency, as shown in the right column of Figure 5, the scenario is as follows. At $\alpha = 15^{o}\uparrow$, the dye still flows along the mid-portion of the wing. At $\alpha = 18^{o}\uparrow$, it has been abruptly swept to the leading-edge and at $\alpha = 19.5^{o}\uparrow$, there is onset of vortex core formation characterized by ejection of the leading-edge of the dye marker from the pocket of dye. At $\alpha = 20^{o}$, this ejected leading-edge of the core has moved to the right-edge of the photo. There are many additional features of this vortex core development and breakdown, which have been visualized using various dye marker and flying wire (see Figure 1a) techniques. They will be

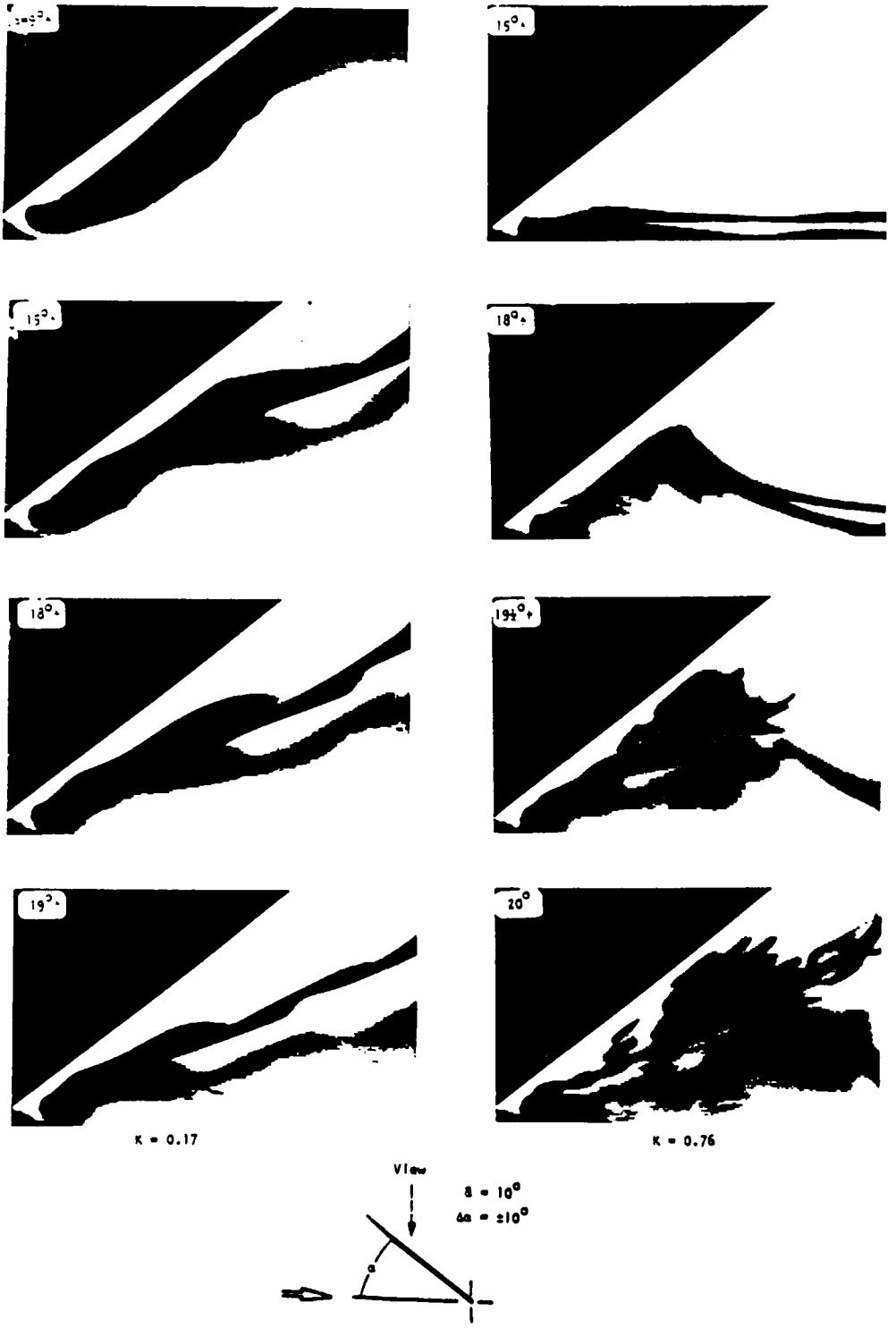

Figure 5: Comparison of development of vortex core on an oscillating delta wing. Left column of photos shows development representative of low frequencies of wing oscillation and right column that of higher frequencies.

delineated in forthcoming writeups. Among them is the fact that the process of vortex breakdown shows new types of structure beyond that of the traditional spiral mode observed on stationary wings. These breakdown mechanisms include abrupt onset of a very large-scale spiral mode; or a column-type instability that can supercede the classical, small-scale spiral mode.

It is evident from the photos of Figure 5 that there is substantial phase shift between the process of vortex development and the instantaneous position of the wing. For the stationary wing, the vortex core is completely broken down at the apex for $\alpha = 20^{\circ}$. In contrast, the photo of Figure 5 shows that at the maximum instantaneous angles of attack shown therein, the core maintains its integrity well downstream of the immediate vicinity of the apex. A particulary dramatic illustration of this phase shift occurs at a mean angle of attack $\bar{\alpha} = 20^{\circ}$ for K = 0.13 (not shown here). In this case, the maximum streamwise length of the vortex core occurs at $\alpha = 29^{\circ}+$. The issue arises as to whether this sort of drastic phase shift can be effectively employed in phased motions of control surfaces during a typical maneuver.

These phase shifts are manifested in hysteresis loops when the instantaneous position of the vortex breakdown x_b is plotted as a function

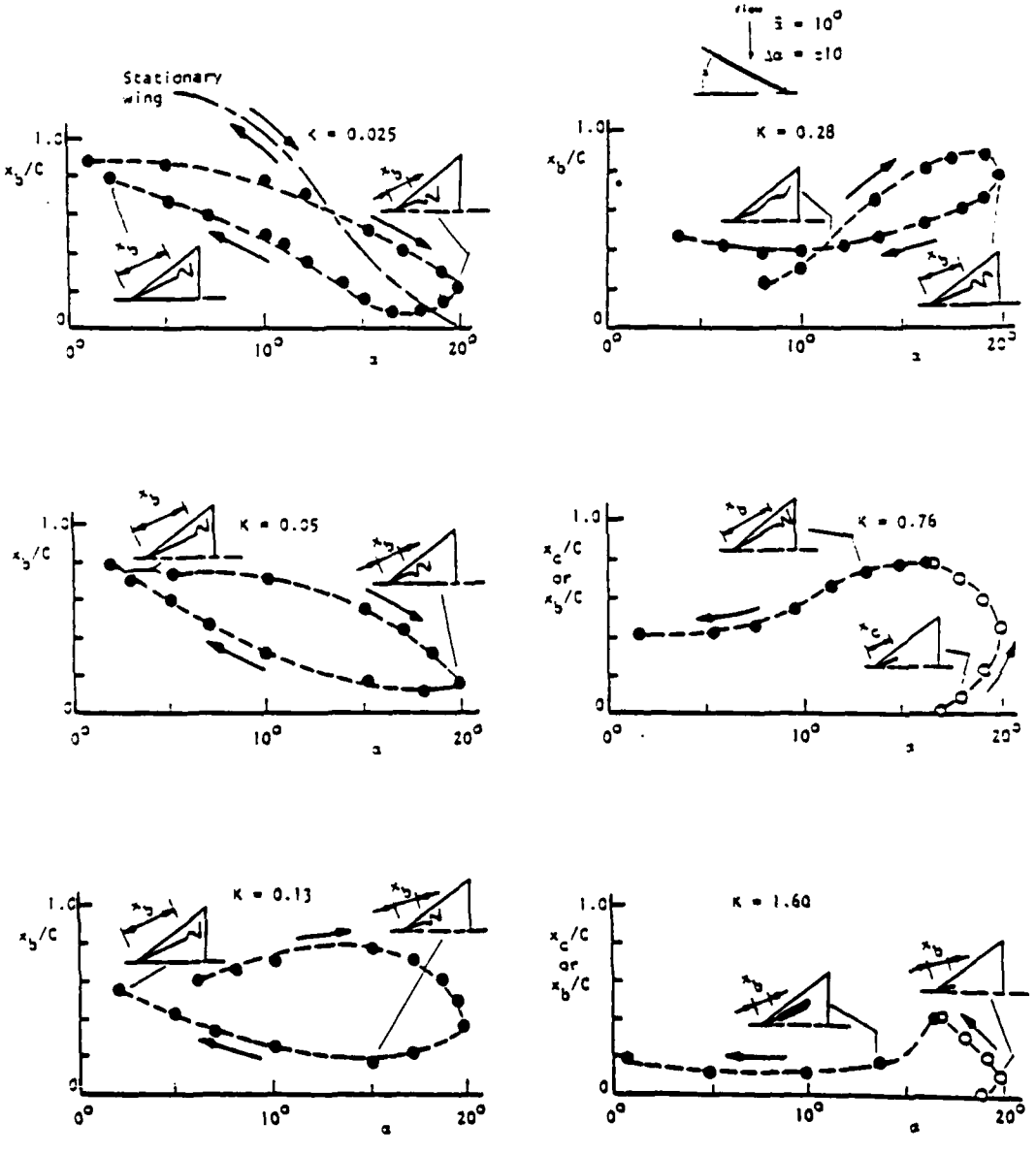

Figure 6: Hysteresis loops characterizing instantaneous position of vortex core and vortex breakdown as a function of instantaneous angle of attack.

of instantaneous angle of attack α. It is essential to verify the character of such loops by considering various types of dye injection and hydrogen bubble flying wire methods in order to preclude fallacious interpretation. Figure 6 shows that even at a reduced frequency as low as K = 0.025, there is substantial hysteresis relative to the characteristic of the stationary wing. The form and sense of the hysteresis loop is generally the same for higher values of K until K = 0.28 is attained. At K = 0.28, the form of the hysteresis loop takes on a figure eight form, and at K = 0.76 and higher values of K, the form and the sense of the hysteresis loop change drastically. Whereas the hysteresis loops corresponding to lower values of K are in the clockwise direction, the sense of higher frequency loops is in the counterclockwise direction. These differences in form and sense of the hysteresis loops are directly related to the manner in which the vortex core develops, as discussed in conjunction with Figure 5. At K = 0.025, it is of the low frequency type, at K = 0.76 of the high frequency type, and at K = 1.28 there is transition between these two extremes.

In addition to the primary vortex described in the foregoing, there also exists an unsteady secondary (counterrotating) vortex between the primary vortex and the leading-edge of the wing. Typical hysteresis loops of the secondary vortex, in relation to their primary counterparts, are given in Figure 7. Over the range of reduced frequencies considered, the following trends, exemplified in Figure 7, are evident for the secondary vortex: the same form (shape) of hysteresis loop as for the primary vortex; a smaller value of maximum breakdown length than that of the primary vortex; and a phase shift with respect to the primary vortex, i.e. lag of breakdown of the primary vortex relative to that of the secondary vortex.

To characterize the time-dependent evolution of the vortex core, characteristic axial and swirl velocities are required. Figure 8 shows the variation of the axial velocity component u_c along the core centerline as a function of distance x from the apex. For reference, the case K = 0 is also shown. Remarkable is the essentially constant value of u_c during the initial stage of the core development followed by an abrupt decrease to zero, corresponding to the instantaneous stagnation condition at the onset of vortex breakdown. Not shown here are normalized velocity variations within the deceleration region over a range of mean angle of attack $\bar{\alpha}$ and reduced frequency K. Such normalization suggests a universal velocity variation for the unsteady core that is essentially coincident with that corresponding to the stationary wing.

Under current consideration is a comparison of various functional forms of the wing forcing, e.g., sinusoidal vs. ramp forcing. This comparison will allow further insight into the mechanisms of phase shift of vortex development and breakdown with respect to the wing history.

PERTURBATIONS OF VORTEX CORE

Perturbations applied to a swept leading-edge can provide further insight into the possibility of vortex control by various means of alteration of boundary conditions at the leading-edge in the form of very small flaps, pulsed blowing, etc. In determining the appropriate excitation frequency f_e, consideration should be given to: the frequency of vortex breakdown (Leibovich[18]); and the inherent instability frequency of the shear layer separating from the edge (Pierce[34]; Payne and Nelson[35]; Gad-el-Hak and Blackwelder[36]). Here, the case of a delta wing having a sweep angle $\lambda = 75^\circ$, at an angle of attack $\alpha = 35^\circ \pm 10^\circ$, will be addressed. Oscillations were in the pitching mode about the trailing-edge; the amplitude of the apex motion was 0.0175 C and the dimensionless frequency of oscillation was $f_e r_c/u_c = 0.027$, which corresponds to the natural breakdown frequency of the core on the stationary wing. These parameters apply to Figures 9 through 14. In Figures 9 through 13, data was acquired at x/C = 0.38, upstream of vortex breakdown. In Figure 14, the station x/C = 0.883 was considered.

The mean distributions of the axial and swirl

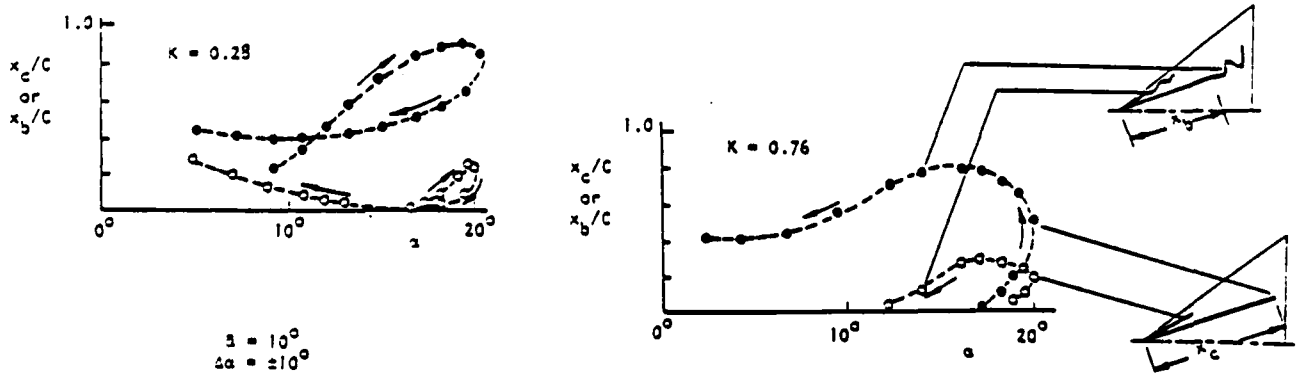

Figure 7: Representative hysteresis loops of secondary (counter-rotating) vortex in comparison with its corresponding primary vortex.

velocity, designated by $\tilde{u}$ and $\tilde{w}$ are given in Figure 9. The forms of these distributions are similar to those corresponding to the stationary wing ($f_e = 0$). Particularly important is the asymmetry of these velocity distributions with respect to the center of the vortex core. Asymmetry arises from mutual induction by the vortices from both of the leading-edges of the wing, as well as from distortion of the unsteady shear layer shed from the edges of the wing. Clearly, theoretical formulations that assume symmetry of the velocity and vorticity field of the vortex core must be interpreted with care. Calculation of criticality conditions and instability criteria for the vortex core should account for the nonaxisymmetric mean vorticity field. Further studies of the mean velocity field

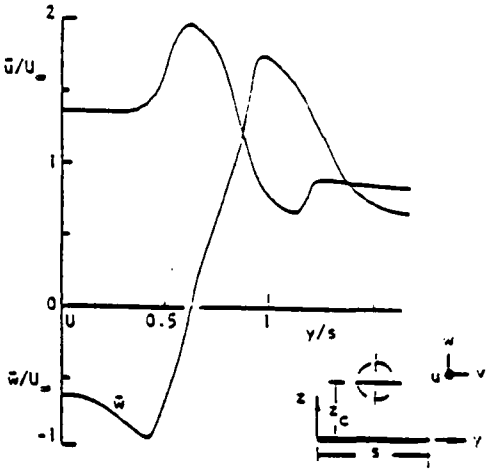

Figure 9: Mean axial and swirl velocity components on a delta wing (sweep angle $\lambda = 75^o$) at a mean angle of attack $\bar{\alpha} = 35^o$ undergoing oscillations of magnitude $\Delta\alpha = 1^o$ at a frequency $f_e r_c/u_c = 0.027$. Velocities determined at $x/C = 0.38$.

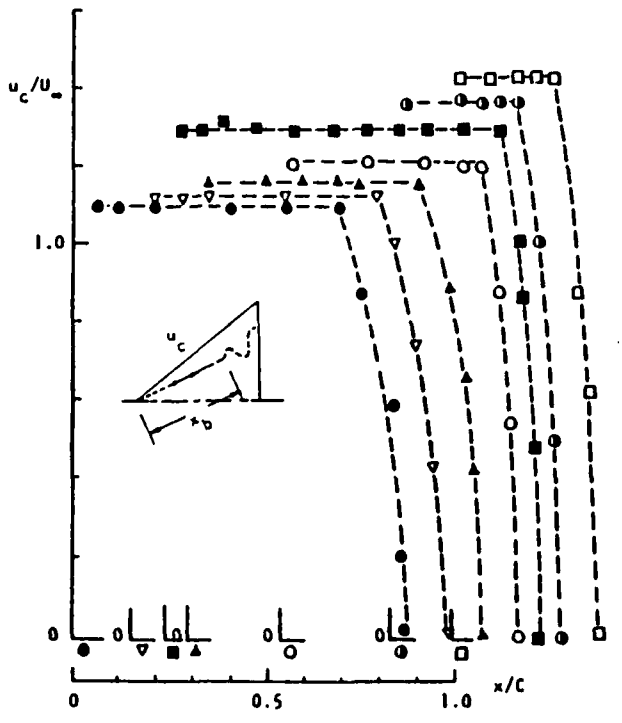

Figure 8: Variation of instantaneous axial velocity along centerline of vortex core as a function of distance from the apex of wing for a range of reduced frequency.

are focussing on determination of the $\tilde{u}$ and $\tilde{w}$ distributions for forcing at fundamental, as well as sub- and superharmonics of the inherent instability of the shear layer separating from the edge and the vortex breakdown frequency.

Rigorously speaking, one should consider the entire cross-section of the flow, and not simply the velocity distribution through the center of the vortex core, as suggested in Figure 9. As illustrated in Figures 10 and 10b, the distribution of the axial velocity component $\tilde{u}$ across the flow shows further features of the asymmetry. These three-dimensional plots extend over elevations from the wall of $z/s = 0.1$ to $z/s = 1.1$, in which z is normal to the wing surface and s is the local semi-span.

The amplitude and phase distributions of the axial fluctuation component $\tilde{u}$ at the forcing frequency f_e are given in Figure 11. These distributions were taken at the same elevation $z = z_c$ as for the mean velocities of Figure 9. The distributions of amplitude and phase at a spanwise location near the edge of the wing are characteristic of those observed in unstable shear flows: two adjacent peaks of unequal amplitude with a phase shift of about π across them. Further inboard, near the apparent center of the vortex, there occur two additional peaks with a gradual phase shift of about π across them. These amplitude and phase distributions extending across the vortex through the separating shear layer form what might be termed a composite eigenfunction; it embodies both the eigenfunction of the separating shear layer as well as that of the integrated history of the vortex of the core. A clear picture of this composite eigenfunction requires similar

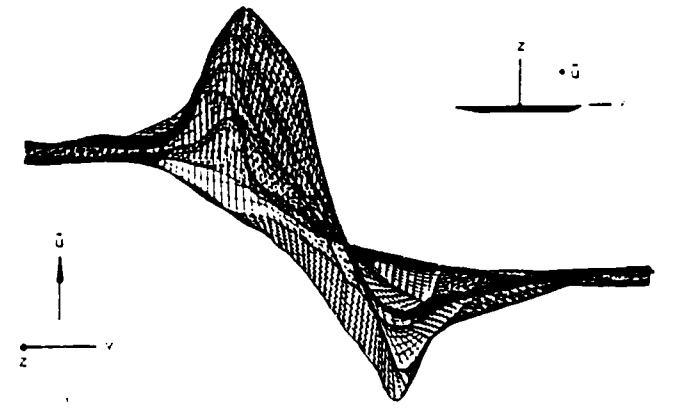

(a)

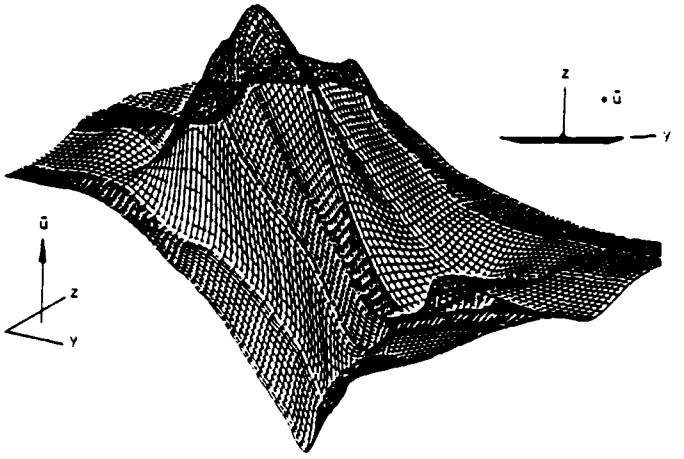

(b)

Figure 10: (a) Three-dimensional representation of the distribution of the mean velocity component ũ over the cross-section of the flow. (b) Same as (a) but viewed from different perspective.

information for the swirl component of velocity; it is currently being acquired.

Contours of constant magnitude of the fluctuating velocity ũ over the flow cross-section are given in Figure 12. The location of the star * corresponds approximately to the apparent center of the mean vortex. The region of high intensity near the wall just inboard of the edge is tentatively attributed to the secondary (counter-rotating) vortex in that region. Above the edge, the elongated regions of high intensity are clearly due to the separated shear layer. As the shear layer evolves in the direction of the mean swirl, there is a region of large fluctuation amplitude, located above the vortex center, whose leading portion is distorted in the direction of the swirl. Just below the apparent center of the

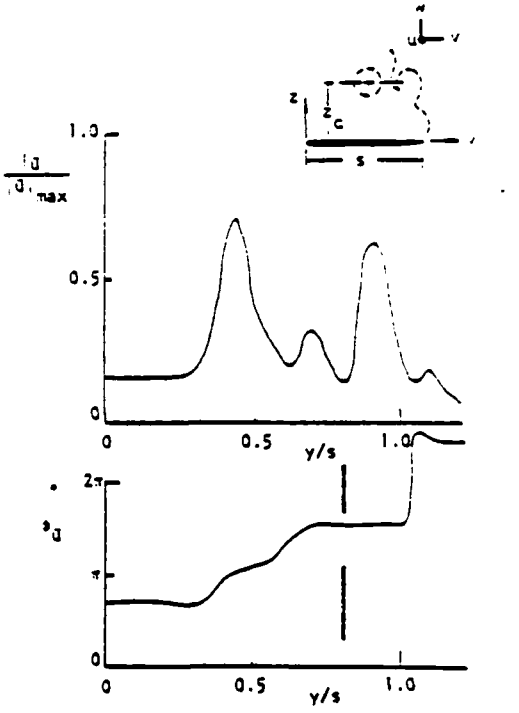

Figure 11: Distribution of axial component of fluctuating velocity ũ and its phase $\phi_{\tilde{u}}$ through the center of the mean vortex.

vortex, there is yet another peak of ũ. The structure suggested by the contours of Figure 12, namely that of an unstable three-dimensional shear layer, continuously feeding into the inner portion of the vortex, is in accord with flow visualization (not shown here).

Up to this point we have addressed amplitude and phase variations only at the excitation component f_e. However, due to nonlinearity of the flow structure, other spectral components will be present. Detailed spectra have been acquired for a range of excitation conditions, and representative ones are shown in Figure 12. In Figure 13a, the spectra were taken at the location of the large amplitude peak at y/s = 0.90 in Figure 11 and in Figure 13b at the location of the peak at y/s = 0.45. As evidenced in Figures 13a,b and in other spectra not shown here, the organized, multiple-peaked spectral content persists across the entire extent of the vortex core including the separating shear layer. Remarkable is the highly ordered nature of these spectra showing as many as nine well-defined peaks over the frequency range. Each of these peaks corresponds to a multiple of the fundamental spectral component, representing the forcing frequency f_e. The possible interpretation of these ordered spectra in terms of concepts of nonlinear interaction is underway. There are, of course, many issues related to the spectral evolution of the flow in the streamwise direction.

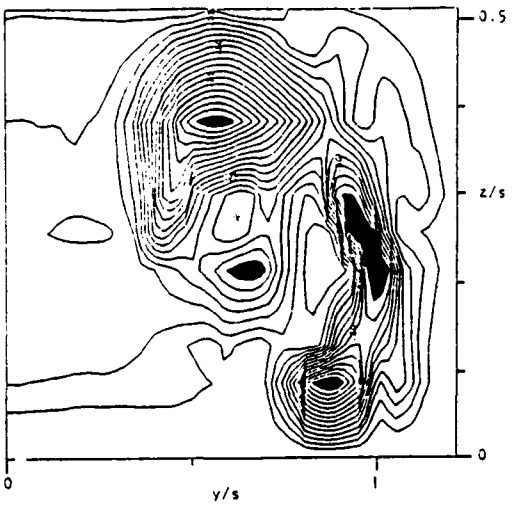

Figure 12: Contours of constant magnitude of $\tilde{u}$ over the flow cross-section.

In particular, the nature of the spectral energy transfer as the vortex enters and passes through the breakdown region is of particular importance.

External forcing can alter the mean flow character and thereby the vortex breakdown location in several interesting fashions, as will be addressed in forthcoming writeups. We address here one such observation. The vortex on the opposite side of the wing (relative to the one under consideration) is stabilized such that its breakdown occurs beyond the trailing-edge. For excitation at frequency f_e equal to that of the natural breakdown frequency f_o^*, Figure 14 compares representative mean and fluctuating velocity distributions without and with forcing at the same streamwise location x/C = 0.883. Without forcing, there is clearly vortex breakdown: the mean velocity distribution $\bar{u}$ shows a wake-like profile and the velocity goes through zero to a negative value as the vortex centerline is approached. The $\tilde{u}$ distribution of the organized component at the breakdown frequency f_o^* is also illustrated. On the other hand, in the case of forcing at the natural frequency of vortex breakdown, i.e. at $f_e = f_o^*$, vortex breakdown does not occur. The distance that the breakdown of the forced vortex is delayed, relative to the unforced vortex, corresponds to about twenty percent of the chord C. The mean velocity $\bar{u}$ of the forced vortex shows the same general form as that of Figure 9. The magnitudes of the spectral components $\tilde{u}(f_e)$ and $\tilde{u}(2f_e)$ are comparable. Determination of the possibility of a simultaneous or intermittent presence of symmetric and spiral modes of instability requires corresponding phase distributions; this issue is currently under consideration.

CONCLUDING REMARKS

Active control of the flow structure of leading-edge vortices on a delta wing and delta

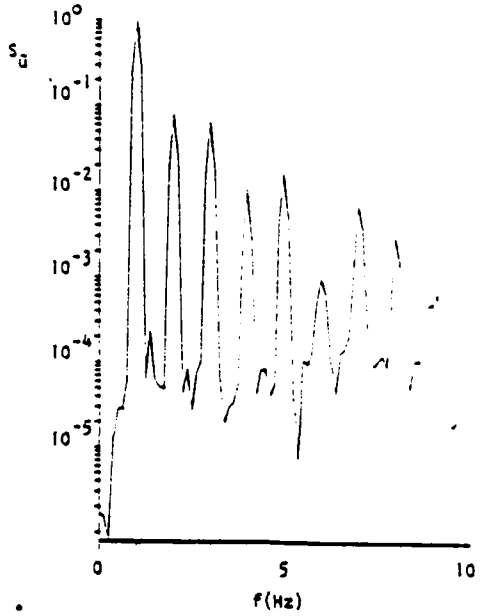

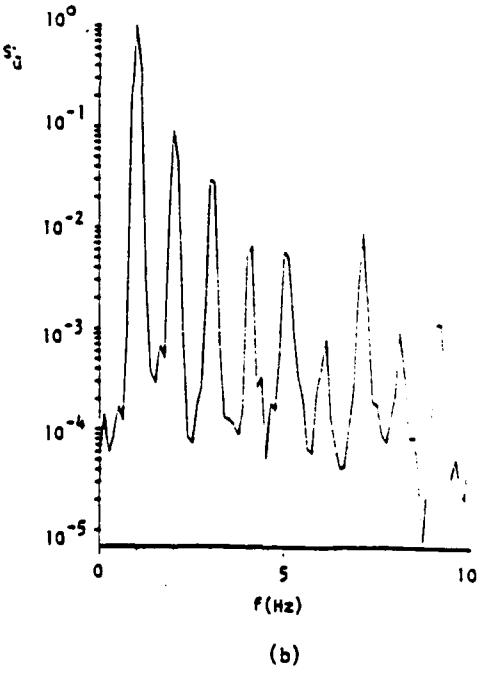

Figure 13: Representative spectra of the velocity fluctuation $\tilde{u}$.

wing segments through both small and large (displacement) amplitude pitching motion is attainable if the excitation frequency is properly selected. Such excitation should consider the following characteristic frequencies: the fundamental frequency (or its subharmonics) of the unstable shear layer separating from the edge of the wing; the frequency of vortex breakdown; and

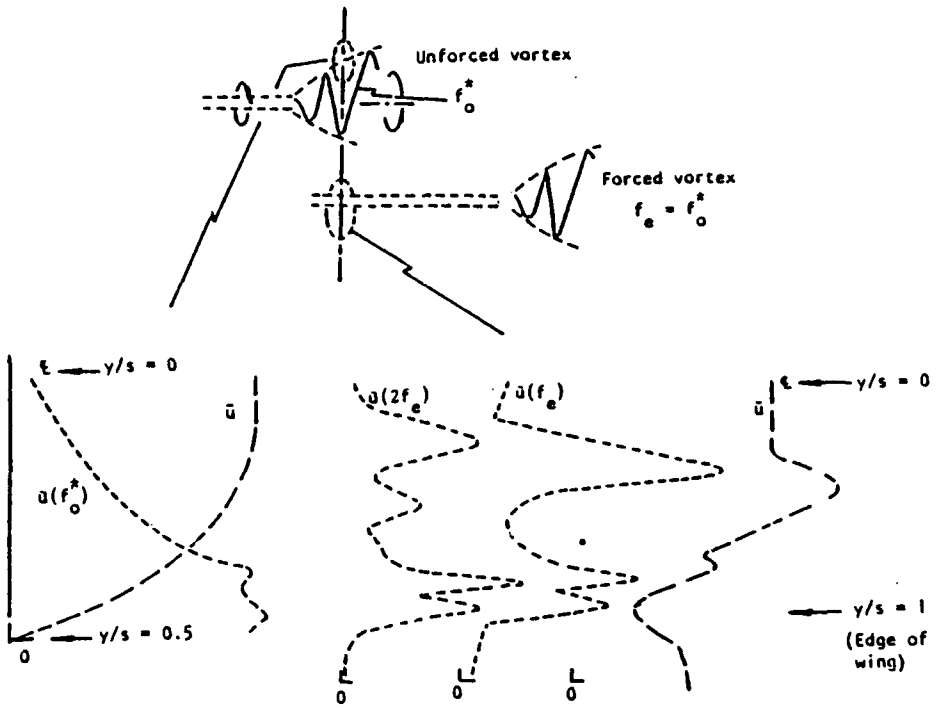

Figure 14: Comparison of representative mean and fluctuating velocity distributions of the unforced and forced vortices at the same streamwise location x/C = 0.883.

the characteristic frequency of the separation zone downstream of the onset of vortex breakdown. Depending upon the frequency selected, there can occur a variety of interesting modifications of the leading-edge vortices. Among them are alteration of: the mean velocity field of the vortex; the mechanism of vortex breakdown; and the phase shift of the instantaneous vortex breakdown position relative to the instantaneous angle of attack.

Development of an integrated active control and quantitative measurement system is aimed towards relating the instantaneous flow structure to the instantaneous wing motion. Both global and local characterization, exterior to and within the vortex core, are insightful and constitute the thrust of further efforts in this direction.

ACKNOWLEDGEMENTS

The authors are pleased to acknowledge financial support of AFOSR Grant 86-0177 and insightful feedback during the course of this program from Dr. L. Carr, Captain H. Helin, and Dr. J. McMichael.

REFERENCES

1. Lee, G. H., "Note on the Flow Past Delta Wing with Sharp Leading-Edges", Aeronautical Research Council, Report & Memorandum 3070, September.

2. Ornberg, H., "A Note on the Flow Around Delta Wings", Swedish Technical Note K. T. H. Aero. T. N. 38, 1954.

3. Elle, B. J., "An Investigation at Low Speed of the Flow Near the Apex of Delta Wings with Sharp Leading-Edges", Aeronautical Research Council, Report & Memorandum 3176, 1958.

4. Kuechemann, D., "On Nonlinear Lifting-Surface Theory for Wings of Small Aspect Ratio with Separation", Aeronautical Research Council, Reprt 17769, April, 1959.

5. Kuechemann, D., "The Aerodynamic Design of Aircraft - An Introduction. Part V", RAE Tech. Memo. Aero. 1622, 1975.

6. Hoeijmakers, H. W. M., "Computational Vortex Flow Aerodynamics", Aerodynamics of Vortical Type Flows in Three Dimensions, AGARD Conference Proceedings No. 342, 1983, pp. 18-1 to 18-35.

7. Rizzi, A., Eriksson, L.-E., Schmidt, W., and Hitzel, S., "Numerical Solutions of the Euler Equations Simulating Vortex Flows Around Wings", Aerodynamics of Vortical Type Flows in Three Dimensions, AGARD Conference Proceedings No. 342, 1983, pp. 21-1 to 21-14.

3. Woodson, S. H. and DeJarnette, S. R., "A Direct and Inverse Boundary Layer Method for Subsonic Flow Over Delta Wings", Vortex Flow Aerodynamics, NASA Conference Publication 2416, Vol. I (edited by J. F. Campbell, R. S. Osborn and J. T. Fougnner), 1986, pp. 115-133.

9. Lambourne, N. C., Bryer, D. W., and Maybrey, J. F. N., "The Behavior of the Leading-Edge Vortices Over a Delta Wing Following Sudden Change of Incidence", Aeronautical Research Council Technical Report, Report & Memorandum 3645, 1969.

10. Gad-el-Hak, M. and Ho, C.-M., "The Pitching Delta Wing", AIAA Journal, Vol. 23, No. 11, 1985, pp. 1660-1665.

11. Gad-el-Hak, M. and Ho, C.-M., "Three-Dimensional Effects on a Pitching Lifting Surface", AIAA Paper No. 85-0041 presented at AIAA 23rd Aerospace Sciences Meeting, January 14-17, 1985, Reno, Nevada.

12. Gad-el-Hak, M. and Ho, C.-M., "Unsteady Vortical Flow Around Three-Dimensional Lifting Surfaces", AIAA Journal, Vol. 24, No. 5, May, 1986, pp. 713-721.

13. Wedemeyer, E., "Vortex Breakdown", AGARD Lecture Series No. 121, High Angle of Attack Aerodynamics, December, 1982, pp. 9-1 to 9-17.

14. Atta, R. and Rockwell, D., "Hysteresis of Vortex Development and Breakdown on an Oscillating Delta Wing", AIAA Journal (in press), 1987.

15. Garg, A. K. and Leibovich, S., "Spectral Characteristics of Vortex Breakdown Flow Fields", Physics of Fluids, Vol. 22, No. 11, 1979, pp. 2053-2064.

16. Escudier, N. P., "Confined Vortices in Flow Machinery", Annual Review of Fluid Mechanics, Vol. 19, 1987, pp. 27-52.

17. Sarpkaya, T., "Effect of Adverse Pressure Gradient on Vortex Breakdown", AIAA Journal, Vol. 12, No. 5, 1974, pp. 602-607.

18. Leibovich, S., "Vortex Stability and Breakdown: Survey and Extension", AIAA Journal, Vol. 22, No. 9, 1984, pp. 1192-1206.

19. Leibovich, S., "Structure of Vortex Breakdown", Annual Review of Fluid Mechanics, Vol. 10, 1978, pp. 221-246.

20. Lambourne, N. C., "The Breakdown of Certain Types of Vortex", Aeronautical Research Council Current Paper No. 915, 1965.

21. Sarpkaya, T., "On Stationary and Travelling Vortex Breakdown", Journal of Fluid Mechanics, Vol. 45, Part 3, 1971, pp. 549-559.

22. Lusseyran, D., Rockwell, D., and Gursul, I., "On Interpretation of Flow Visualization of Unsteady Shear Flows", in preparation for publication, 1987.

23. Hama, S. R., "Streaklines in a Perturbed Shear Flow", Physics of Fluids, Vol. 5, No. 6, June, 1962, pp. 644-650.

24. Rockwell, D., Atta, R., Kramer, L., Lawson, R., Lusseyran, D., Magness, C., Sohn, D., and Staubli, T., "Structure of Unsteady Flows at Leading- and Trailing-Edges: Flow Visualization and Its Interpretation", Aerodynamic and Related Hydrodynamic Studies Using Water Facilities, AGARD Conference Preprint No. 413 based on Symposium of the Fluid Dynamics Panel, Monterey, California, 20-25 October, 1986.

25. Rockwell, D., Gumas, C., Kerstens, P., Backenstose, J., Ongoren, A., Chen, J., and Lusseyran, D., "Computer-Aided Flow Visualization", Proceedings of Sixteenth Symposium on Naval Hydordynamics (ed. W. C. Webster), National Academy Press, 1986.

26. Smith, C. R.,"Computer-Aided Flow Visualization", Handbook of Flow Visualization (ed. W. J. Yang), Hemisphere Publishing Corporation, New York, 1987.

27. Lu, L. J. and Smith, C. R. "Image Processing of Hydrogen Bubble FLow Visualization for Determination of Turbulence Statistics and Bursting Characteristics", Experiments in Fluids, Vol. 3, 1985, pp. 349-356.

28. Lusseyran, D. and Rockwell, D., "Estimation of Velocity Eigenfunction and Vorticity Distributions from the Timeline Visualization Technique", Experiments in Fluids, Vol. 6, 1988 (in press).

29. Ongoren, A., Chen, J., and Rockwell, D., "Multiple Time-Surface Characteristics of Time-Dependent, Three-Dimensional Flows", Experiments in Fluids, Vol. 5, 1987, pp. 418-422.

30. Kerstens, P. and Rockwell, D., "Ensemble-Averaging and Correlation Techniques for Flow Visualization Images", Experiments in Fluids, 1988 (in press).

31. Gumas, C. and Rockwell, D., "The Fourier Descriptor Technique: Means of Pattern Description and Recognition in Fluid Mechanics", in preparation for publication, 1988.

32. Spedding, G. R. and Maxworthy, T., "The Generation of Circulation and Lift in a Rigid Two-Dimensional Fling", Journal of Fluid Mechanics, Vol. 165, 1986, pp. 247-272.

33. Pierce, D., "Photographic Evidence of the Formation and Growth of Vorticity Behind Plates Accelerated from Rest in Still Air", Journal of Fluid Mechanics, Vol. 11, 1961, pp. 460-464.

34. Payne, S. M. and Nelson, R. C., "An Experimental Investigation of Vortex Breakdown on a Delta Wing", Vortex Flow Aerodynamics, Vol. I, NASA Conference Publication 2416, 1985, pp. 135-162.

35. Gad-el-Hak, M. and Blackwelder, R., "The Discrete Vortices from a Delta Wing", AIAA Journal, Vol. 23, June, 1985, pp. 961-962.

AGARD

ADVISORY GROUP FOR AEROSPACE RESEARCH & DEVELOPMENT

7 RUE ANCELLE 92200 NEUILLY SUR SEINE FRANCE

Paper reprinted from
Conference Proceedings No.413

AERODYNAMIC AND RELATED HYDRODYNAMIC STUDIES USING WATER FACILITIES

NORTH ATLANTIC TREATY ORGANIZATION

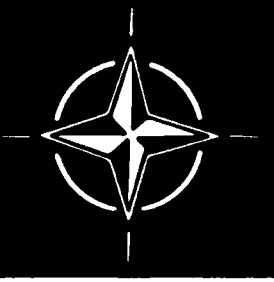

STRUCTURE OF UNSTEADY FLOWS AT LEADING- AND TRAILING-EDGES:

FLOW VISUALIZATION AND ITS INTERPRETATION

by

D. Rockwell, R. Atta, L. Kramer, R. Lawson,
D. Lusseyran, C. Magness, D. Sohn, T. Staubli
Department of Mechanical Engineering and Mechanics
354 Packard Laboratory, Building #19
Lehigh University
Bethlehem, Pennsylvania 18015

SUMMARY

Unsteady two- and three-dimensional flow structure at leading- and trailing-edges of bodies can be characterized effectively using recently developed techniques for acquisition and interpretation of flow visualization. The techniques addressed herein include: flow image-surface pressure correlations; three-dimensional reconstruction of flow structure from flow images; and interactive interpretation of flow images with theoretical simulations. These techniques can be employed in conjunction with: visual correlation and ensemble-averaging, both within a given image and between images; recognition of patterns of flow structure from images; and estimates of velocity eigenfunctions from images.

1. INTRODUCTION

There are a wide variety of methods for visualizing and interpreting flow phenomena. The overviews of Emrich[1] and Merzkirch et al[2] assess a range of techniques including, for example: smoke and dye injection; laser-induced fluorescence; and density gradients induced in mixing of dissimilar fluids. These methods have provided valuable insight into a number of features of the flow structure.

Flow visualization using water as a working fluid has several advantages. Perhaps the foremost is the ease of marking and tracking fluid elements at relatively long time scales, i.e. low frequencies, in comparison with the corresponding scales in a gaseous medium. If instantaneous, as opposed to time-averaged, surface pressure, lift, etc. in conjunction with the visualized flow structure is desired, then the time and length scales offered by a water facility are highly advantageous. Although concurrent, quantitative measurement of unsteady velocity and pressure may be more delicate and laborious, judicious choice of the most physically meaningful locations for measurement of the flow field, identified with the aid of flow visualization, can reduce the amount of effort in this direction.

Interpretation of visualized steady flows is relatively straightforward; however this is not the case for unsteady flows, especially for perturbed shear flows. It is well known from linear stability theory that there exist drastic gradients of amplitude and phase of fluctuating velocity and pressure across an unsteady shear flow. As a consequence, the apparent, visualized flow structure may not be compatible with the actual, underlying vorticity field (Hama[3]; Lusseyran and Rockwell[4]). Clearly, considerable care must be exercised in interpreting unsteady phenomena. By proper choice of visualization technique, and employment of simple theoretical simulations, fallacies of interpretation can be precluded.

In the series of investigations described herein, we address techniques for implementing and interpreting a particular class of flow visualization methods: generation and tracking of lines of elements marked at specified times, i.e. timelines. Emphasis is on: correlating the instantaneous, visualized flow structure with instantaneous surface pressure; reconstruction of three-dimensional flow structure from dual views of the flow field; and interpretation of the flow visualization in conjunction with basic classes of theoretical simulation. In addition, possibilities are addressed for: visual correlation and ensemble-averaging of visualization images; pattern recognition of flow structure using images; and evaluation of images for determination of velocity eigenfunction and vorticity.

2. EXPERIMENTAL TECHNIQUES

All experiments were carried out in one of three water channel systems, custom designed for study of unsteady, separated flows. The cross-sectional areas of the test sections of these channels ranged from 1.5 ft^2 to 6 ft^2. In all cases, the test sections were made entirely of plexiglas or glass to facilitate multi-dimensional views of the flow structure. Moreover, all components of the largest channel, including the test section contraction, inlet and outlet tanks, and all attendant piping are made of plexiglas or PVC in order to preclude difficulties arising from system corrosion.

Figure 1 shows an experimental arrangement that is generic to the variety of techniques employed in the fluid mechanics laboratory at Lehigh University. A platinum wire, or an arrangement of wires, generates hydrogen bubble timelines. The bubble lines or sheets are then tracked, recorded, and processed by employing: video cameras synchronized with the mainframe of the video system; a digitizing system; and an image processing system located in the computer-aided design (CAD) laboratory.

Using a custom-designed function generator, it is possible to generate hydrogen bubble timelines of desired frequency and width. Two stroboscopic (90 watt) lights, interfaced with the mainframe of the video system, illuminate these bubble timelines.

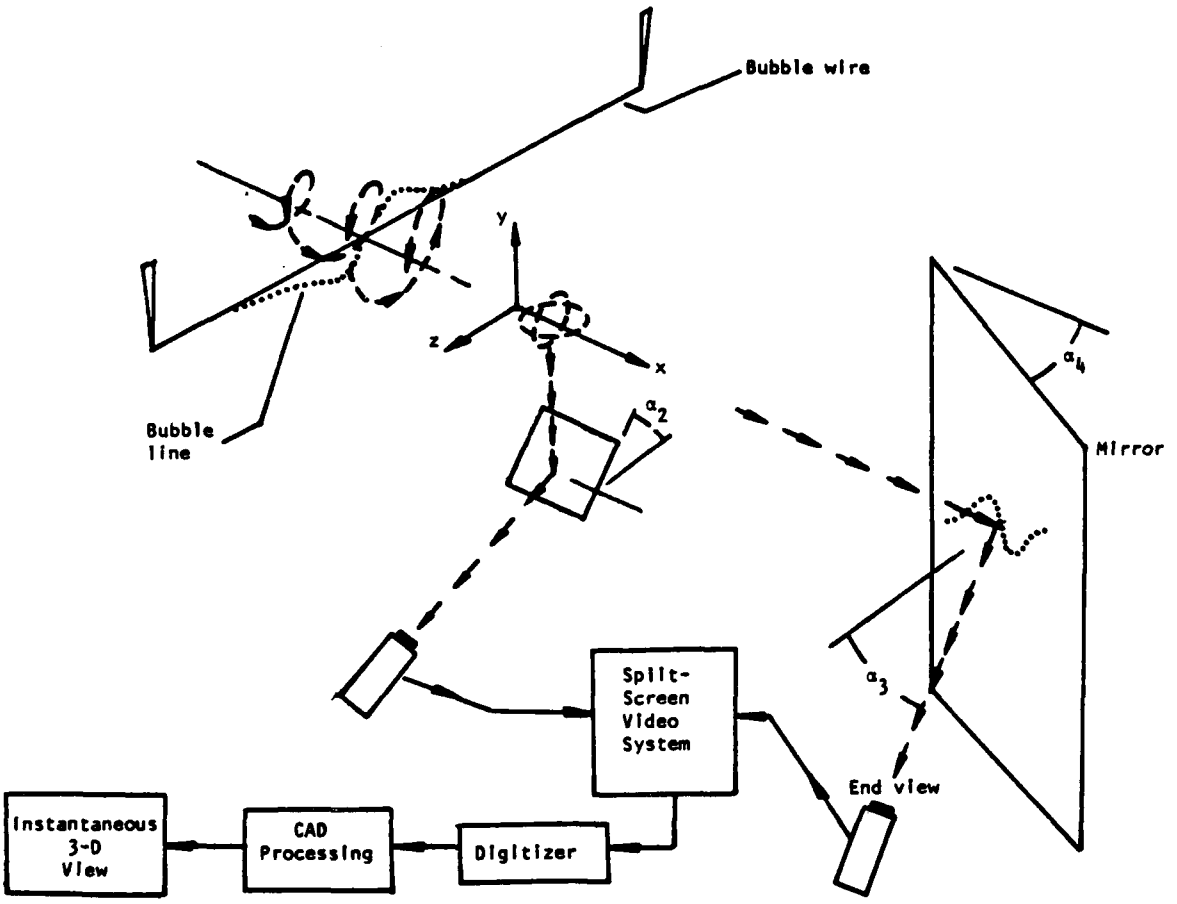

Figure 1: Schematic of technique for acquiring and processing flow visualization using two-camera, split-screen video system, digitizer, and computer-aided design system. Technique shown is generic to the variety of arrangements employed in the Lehigh University fluid mechanics laboratories.

Two simultaneous images, corresponding to two arbitrary views of the flow field, can be displayed on the split-screen video system. A variety of mirror arrangements provides views of the flow field from a number of perspectives. These mirrors are located either external to the transparent test section, or within the flow field at a location sufficiently far downstream of the region of interest.

Video images can be digitized using a Colorado video (model 270A) digitizer or a digitizing tablet. Images obtained from the digitizer are put on file in the CAD laboratory, allowing application of a range of image pre-processing and processing techniques.

Pre-processing of digitized images enhances the definition of the bubble timeline patterns. These processing operations include: a "band-pass" spatial filter; a thresholding operation; a thinning algorithm; a two-dimensional, low-pass filter; and other related techniques, which are described in detail by Gumas and Rockwell[5]. As a follow-on to this image pre-processing, it is possible to employ a curve-tracking technique which, in essence, transforms timelines having multiple grey levels to continuous well-defined timelines in binary form. Gumas[6] describes the curve-tracking algorithm, which is based on the concept of linear predictive coding.

3. QUANTITATIVE INTERPRETATION OF VISUALIZATION IMAGES

Figure 2 shows a typical timeline visualization photo, corresponding to antisymmetrical vortex shedding from a cylinder oscillating in the streamwise direction (Ongoren and Rockwell[7]). Also illustrated is a representation of the digitized timelines, providing a basis for quantitative interpretation of the flow structure. A timeline is, by definition, made up of all fluid elements originally marked at the same time at the upstream location of the bubble wire. Taking these timelines as representative, we address possibilities for: visual correlation and ensemble-averaging of images; pattern recognition using visualization images; and image evaluation for velocity eigenfunction and vorticity.

Figure 2: Typical flow visualization photograph representing vortex shedding in antisymmetrical mode arising from streamwise perturbations of cylinder. Also shown is digitized representation of upper half of timeline pattern (Ongoren and Rockwell[7]; Kerstens and Rockwell[8]).

Visual correlation and ensemble-averaging of images

Although correlations of velocity and pressure at a point, or between two points, in a flow field have received considerable attention over the past few decades, relatively little effort has been devoted to defining a more globally-oriented correlation based on flow visualization. In doing so, it is necessary to define quantitatively the elemental portions of a visualization image. One possibility is to define the local tangent of each of the individual timelines as a function of position along the timeline. This local tangent is termed the tangent angle function $\phi(x,y)$. If we know the function ϕ along all the timelines in an image, we have, in effect, defined the image on a physically meaningful basis.

The obvious approach to defining a correlation between two points A-1 and B-1 on two different timelines A and B is to consider the product of the respective tangent angle functions $\phi_{A-1}\phi_{B-1}$. However, as shown by Kerstens and Rockwell[8], this definition is inadequate, as it cannot distinguish certain features of two curves oriented arbitrarily with respect to each other. Rather, it is useful to employ a correlation function based on the difference between tangent angle functions $\phi_{A-1}-\phi_{B-1}$. Employing such a definition, it is then possible to define a global, visual correlation between two timelines by integrating over the spatial extent of the normalized timelines. This approach can lead to various types of auto- and cross-correlations between defined regions of the flow field. Ideally, it would be desirable to carry out these correlations for segmented timelines, where a timeline is broken into discrete segments through use of a segmented bubble wire; then, by tracking these segments and carrying out the aforementioned visual correlation, a comparison can be made with the measured vorticity field.

The visual average of several successive images follows from the spatial averages of respective timelines in a number of successive images (Kerstens and Rockwell[8]). In selecting the images to be averaged, a physically meaningful criterion must be applied. If each of the selected images corresponds to a defined phase of an unsteady event within the flow, such as an extreme displacement of a body, then the averaging is of the ensemble-averaging type. In principle, a variety of sensors, including pressure and velocity transducers, can be employed as a phase reference for the ensemble averages; moreover, an interesting possibility involves use of a repetitive, coherent portion of the image itself in order to trigger the ensemble-averaging.

Pattern recognition using images

In the event that the flow is non-periodic, it is useful to determine how often certain large-scale features of the flow-structure occur. Consequently, it is necessary to formulate a technique for rapidly identifying these structures from flow images. If a library of basic types of flow patterns can be described, then comparison of visualized flow patterns with this library provides a basis for characterizing the frequency of appearance of elemental types of flow structure. This approach represents a type of pattern recognition.

A technique employed for identification of machine parts (Persoon and Fu[9]), handprint character recognition (Granlund[10]), and recognition of aircraft silhouettes (Wallace and Mitchell[11]) involves definition of a library of Fourier descriptors for basic types of patterns. The Fourier descriptor is simply the Fourier transform of the tangent angle function ϕ, as previously defined. The advantage of the Fourier descriptor technique is that the curve description is essentially independent of orientation, position, and scale of the curve. Whereas the traditional use of the Fourier descriptor technique is for closed curves, flow images are typically made up of open curves in the form of streaklines, pathlines, or timelines. Gumas and Rockwell[5] describe implementation of the Fourier descriptor technique for open curves of the timeline type.

Image evaluation for velocity eigenfunction and vorticity

The displacement of a timeline over a given interval of time is related to the flow velocity.

Consequently, it is possible to relate the time of flight of timelines to the velocity distribution across the flow. In fact, Lu and Smith[12] have shown that the higher order statistics of a turbulent boundary layer can be determined using this concept; this approach can lead to insight beyond that attainable with traditional point measurements.

A primary advantage of the timeline technique is that it gives instantaneous information across the entire flow; it therefore leads to the instantaneous streamwise velocity component across the flow. Consequently, this method is well-suited to characterizing flows for which there are substantial gradients of velocity amplitude and phase in the cross-stream direction. That is, the local deflection of a timeline will be in accord with the local fluctuation amplitude and its relative phase. Lusseyran and Rockwell[13] have demonstrated that this technique can provide a reasonable estimate of the eigenfunction of the streamwise velocity component. Through application of the continuity equation, it leads to approximation of contours of constant vorticity in an unstable wake flow.

4. FLOW IMAGE - SURFACE PRESSURE CORRELATION

In order to determine the underlying mechanisms that produce unsteady pressure fluctuations along a surface, it is desirable to correlate the instantaneous, visualized flow structure with the instantaneous surface pressure. One possibility is to record simultaneously the visualized flow and the time-dependent surface pressure from a large array of surface-mounted transducers. If the flow structure is highly organized then, in principle, it is possible to employ a single transducer switched to successive locations along the surface. By keeping track of pressure amplitude and phase, the instantaneous pressure field can be reconstructed.

In acquiring these pressure measurements, it is necessary to have an appropriate phase reference, which can take the form of a second pressure transducer signal, or a hot film or laser signal, appropriately located at the outer edge of the mean shear layer. Proper location of this reference is necessary to avoid phase gradients associated with the fluctuating field, as well as high frequency noise from the flow. In linking the unsteady surface pressure measurements to the visualized flow field, it is necessary to determine, at a given instant, the phase shift between the visualized flow structure and the instantaneous pressure. One possible technique for accomplishing this is to record simultaneously the flow structure and the oscilloscope trace of the reference signal on a split-screen video system. Obviously, there are other methods of indirectly determining this phase link.

Aside from the advantages of visualization, use of water as a working medium allows use of remote transducer locations, as opposed to the classical surface-mounting of transducers. The characteristic frequencies of the pressure fluctuations in water are typically very low - on the order of 1 Hz. At these low frequencies, the amplitude and phase distortion arising from locating the transducer away from the surface are insignificant, provided the connecting line between the surface tap and the transducer is properly designed.

A means of visually displaying the instantaneous flow structure and surface pressure has been developed in our CAD laboratory. First, the flow images are digitized and processed. Then each of these images is, in turn, displayed with the instantaneous surface pressure field. This field is obtained from cross-spectral analysis between the surface pressure at a given location and an appropriate phase reference. In the following, we discuss cases where the raw, instantaneous visualization images, without any processing or enhancement, are shown in conjunction with the instantaneous surface pressure.

Figure 3 shows the interaction of an incident vortex with an elliptical leading-edge. In this case, the vortex is generated in a mixing-layer flow arising from the inherent instability of the shear layer. As a consequence, the process of vortex-edge interaction is harmonic. Full details of this experiment, including the circulation and degree of concentration of vorticity of the incident vortex, are given by Sohn and Rockwell[14]. In the left column of Figure 3, the vertical hatched lines represent the amplitude envelope, and the closely-spaced hatched lines represent the instantaneous surface pressure fluctuations. Considering the visualization in the right column of photos in Figure 3, it is evident that the incident vortex undergoes substantial distortion as it encounters the leading-edge region. Concurrently, there is local flow separation from the leading portion of the edge, giving rise to a small-scale secondary vortex that becomes nested within the incident primary vortex. The third row of pressure-visualization shows that onset of flow separation induces a local negative pressure; the fourth and fifth rows show that this negative pressure region moves downstream as the formation of the secondary vortex evolves. It is clear, especially from the fourth row of Figure 3, that there are very large gradients of instantaneous pressure in the vicinity of the tip. In fact, maximum positive pressure occurs at the tip itself, and a short distance downstream of that location, there is a maximum of negative pressure.

Figure 4 shows the instantaneous loading and corresponding flow structure for the case of a fully turbulent boundary layer separating from an actively-controlled trailing-edge. In this case, the displacement perturbations of the trailing-edge are about two orders of magnitude smaller than its thickness Nevertheless, the surface pressure fluctuations arising from the edge perturbations overshadow those of the background turbulent flow. Since the first harmonic component of these pressure fluctuations is very small, we can represent the fluctuating surface pressure as approximately sinusoidal, and employ the edge displacement as a phase reference in relating the instantaneous pressure to the flow structure. The top row of pressure-visualization shows the case of excitation at a frequency f_e just below the natural shedding frequency f_o^*, and the middle row at a frequency just above it. From the visualization, we note that the initially shed vortex switches from the bottom to the top corner of the trailing-edge as the excitation frequency increases. The bottom row of pressure-visualization represents the case of excitation at a frequency well above the natural shedding frequency. It is apparent that the initial vortex is still shed from the upper surface. In fact, only when the edge is excited at a frequency near that of the natural shedding is a switch in phasing of the initially-shed vortex possible.

In the corresponding pressure plots, the solid line and the cross-hatched regions represent respectively the amplitude envelope and the instantaneous value of the pressure amplitude at the forcing

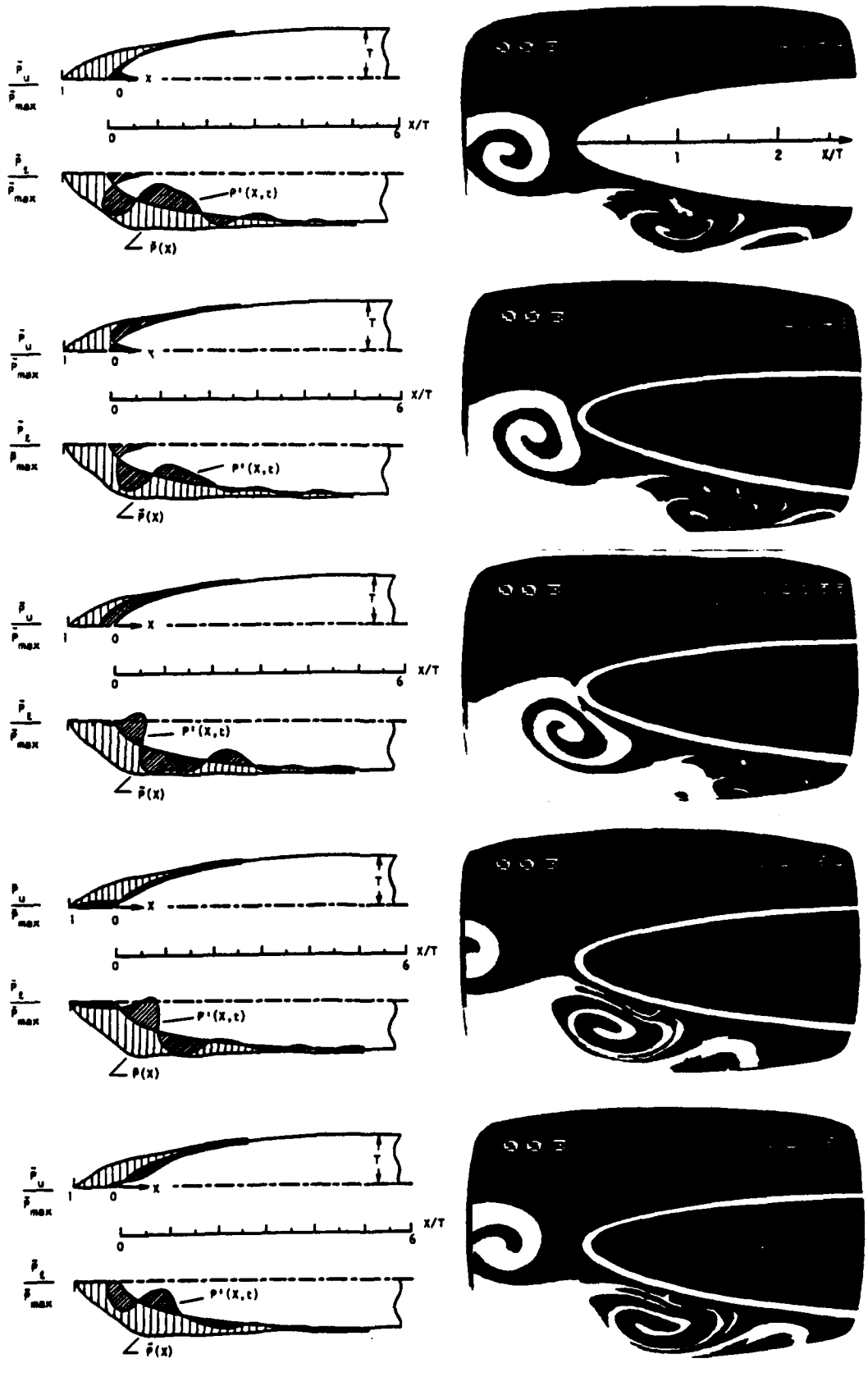

Figure 3: Interaction of vortex generated in mixing layer with elliptical leading-edge (Sohn and Rockwell[14]).

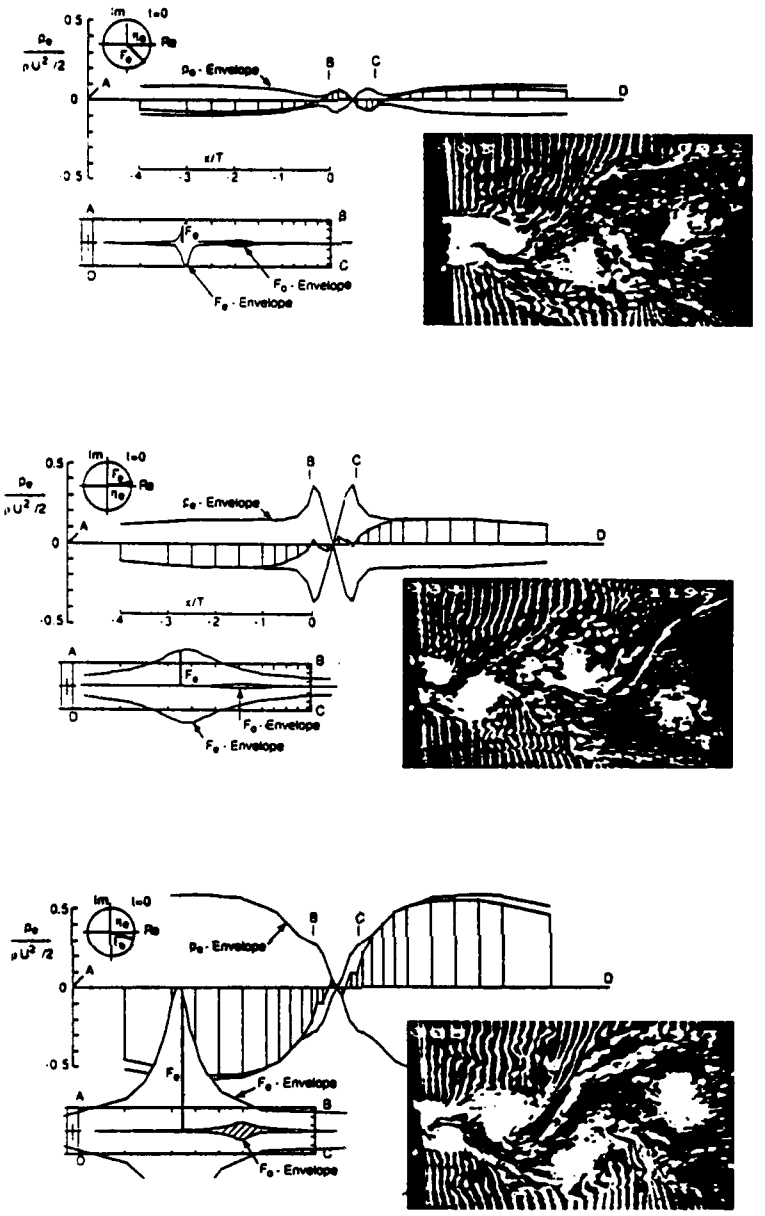

Figure 4: Flow structure and instantaneous surface pressure induced by oscillating trailing-edge. Approach boundary layer is fully turbulent and pressure field is that resulting from motion of edge. Frequency f_e of excitation relative to frequency f_o^* of shedding from stationary edge is: $f_e/f_o^* = 0.87$ (top row); 1.02 (middle row); and 2.0 (bottom row) (Staubli and Rockwell[15]).

frequency. Moreover, within the schematic of the edge are shown the amplitude envelopes of the fluctuating force F_e at the excitation frequency f_e and the force F_o at the self-excited frequency component f_o. The vertical bar represents the instantaneous location of the force F_e. Finally, the phase clock in the upper left of each schematic shows that the force F_e lags the edge displacement η_e at the excitation frequency below the natural shedding frequency (top diagram), while it leads at a frequency above natural frequency (middle diagram) and again lags at high excitation frequency (bottom diagram). For the conditions of the top and middle diagrams, the amplitude of the fluctuating pressure rapidly increases as the corner (B) of the edge is approached; it goes to zero at the middle of the vertical base (BC). In the bottom diagram this is no longer the case; due to the high excitation frequency, the noncirculatory ("added-mass") contribution to the surface pressure dominates that associated with shedding of vorticity, except in the base region BC.

These types of flow structure - pressure correlations have the potential for providing insight into the source of unsteady lift and drag acting on bodies; they are currently being interpreted in this context.

5. THREE-DIMENSIONAL RECONSTRUCTION FROM FLOW IMAGES

Determination of the instantaneous structure of time-dependent, three-dimensional flows poses a particular challenge. By use of a timeline marking technique, it is possible to reconstruct the three-dimensional evolution from two-dimensional images using computer-aided design methods. There are basically two types of approaches: a dual-view method, where the three-dimensional structure is determined from two arbitrary views of the flow field; and a single-view method, involving acquisition of phase-locked images from a single view of the flow field.

Smith and Paxson[16] have constructed a single three-dimensional surface by generating timelines from a single wire oriented in the spanwise direction, and using a two-camera system with two simultaneous views. Their study provides new insight into the character of a turbulent boundary layer. Ongoren and Rockwell[17] have generated a family of three-dimensional surfaces representing the wake from a three-dimensional body by employing phase-locked images of timelines from a single view. In this technique, the body was subjected to controlled oscillations. Its displacement served as a phase reference, thereby allowing definition of phase-locked images at successive spanwise planes. In the following, we demonstrate the dual-view method for obtaining three-dimensional surfaces representing separated flows from stationary and oscillating bodies.

Figure 5 shows time sequences of end and plan views of a tip vortex. In generating these images, a one mil, kinked platinum wire was employed. By pulsing the wire at a desired time, and over a defined interval, it is possible to reveal the principal features of the flow structure. In the end view of Figure 5, the pulse width is relatively long, being initiated just prior to the first photo and terminated prior to the last photo. The plan view of Figure 5 shows that the free-stream is moving in the downward direction. The vortex core has a significantly lower axial velocity than that of the free-stream. In these end and plan views, it is, in principle, possible to estimate the unsteady velocity field. In addition, as depicted at the bottom of Figure 5, three-dimensional surfaces can be constructed using the CAD system. The various views shown therein are from arbitrary perspectives. Real time, three-dimensional simulation of the structure of this tip vortex can be carried out either on the Unigraphics UG-2 terminal or the Evans and Sutherland PS-300 terminal in the Lehigh University CAD laboratory.

Another class of three-dimensional flows that can be characterized effectively by the dual view technique is that generated by an oscillating delta wing. To illustrate the complexity of the flow, we first consider a plan view of a delta wing oscillating in pitch about its trailing-edge (Figure 6). Since the tip of the delta wing undergoes large excursions during an oscillation cycle, only limited information can be obtained by examining timeline patterns from a fixed wire. A "flying wire" technique has been developed (Atta and Rockwell[18]); the platinum wire is aligned in the spanwise (z) direction, stretched between two supports located well away from the wing, and fixed to the mechanism that controls the wing motion. Consequently, the wire "flies" at the same angular velocity as the wing, and provides an indication of the degree to which the flow entering a plane parallel to the wing passes below, as opposed to above, the wing surface. For the photos of Figure 6, the wire is at the tip. Moreover, the reduced frequency $K = 2\pi fC/U_\infty = 4.0$, the mean angle of attack $\alpha = 35^o$ and fluctuating angle of attack $\Delta\alpha = 10^o$. From quasi-steady considerations, one expects the pattern of vortex formation to be the same at a given value of angle of attack α, irrespective of whether the tip of the wing is moving in the upward or downward direction. Comparison of photos C and E, taken at nearly the same value of α, shows that the flow structure is markedly dissimilar. Evidently, there is strong hysteresis of the vortex rollup relative to the wing motion.

With bottom views of the sort shown in Figure 6, taken simultaneously with corresponding end views, it is possible to reconstruct the three-dimensional character of the flow on the CAD system. Figure 7 shows three-dimensional surfaces obtained using the flying wire technique for a similar experimental situation as that of Figure 7, i.e. a delta wing pitching about its trailing-edge. (Note that the hidden lines therein appear as solid lines). The top set of photos shows three basic views at relatively high reduced frequency. In this set, the bottom (plan) view shows that pronounced rollup of the sheet commences at about one-third chord and extends to about two-thirds chord. This rollup is particularly evident in the end view. Upstream of this region of rollup, there appear bulges of opposite curvature. In the bottom sets of plots, plan and end views are compared at the same instantaneous angle of attack. Within each set, from top to bottom, cases of static, moderate frequency, and high frequency are compared. Efforts are underway to relate basic patterns of three-dimensional distortion to the concepts of hysterisis and vortex breakdown.

6. FLOW STRUCTURE INTERPRETATION FROM IMAGES: INTERACTIVE VISUALIZATION AND SIMULATION

In any type of flow visualization technique, the visualized flow at any location represents the integrated history of the marked fluid elements. This history extends from the upstream location where the flow is marked to the downstream location where the flow structure is viewed. This concept can be used in conjunction with simple theoretical simulations of the flow structure in order to identify basic classes of vorticity concentration and circulation, as shown by Lusseyran and Rockwell[4]. In essence, they employ the velocity eigenfunctions from linear stability theory, in conjunction with the mean flow, to provide simulation of the vorticity field of an unstable wake. Since, in practice, we can often estimate a priori certain features of the mean flow, it should be possible to estimate the local circulation of the vorticity field when flow visualization is interpreted in conjunction with such a theoretical simulation.

Figure 8 shows simulation of the timeline patterns for a fixed- (upper diagram) and moving- (lower diagram) timeline marker (e.g., hydrogen bubble wire) for the case of a vorticity field having successively increasing values of dimensionless circulation $\Gamma^* = 1$, 2, 3, and 4. As illustrated in the middle schematic of Figure 8, the vorticity field, defined by the concentric contours is spatially periodic. Moreover, these contours of constant vorticity represent a neutral disturbance, i.e. the vorticity is neither amplifying or decaying. The amplitudes of the vorticity contours are related to the overall circulation; however, the shapes of the contours are relatively independent of the circulation.

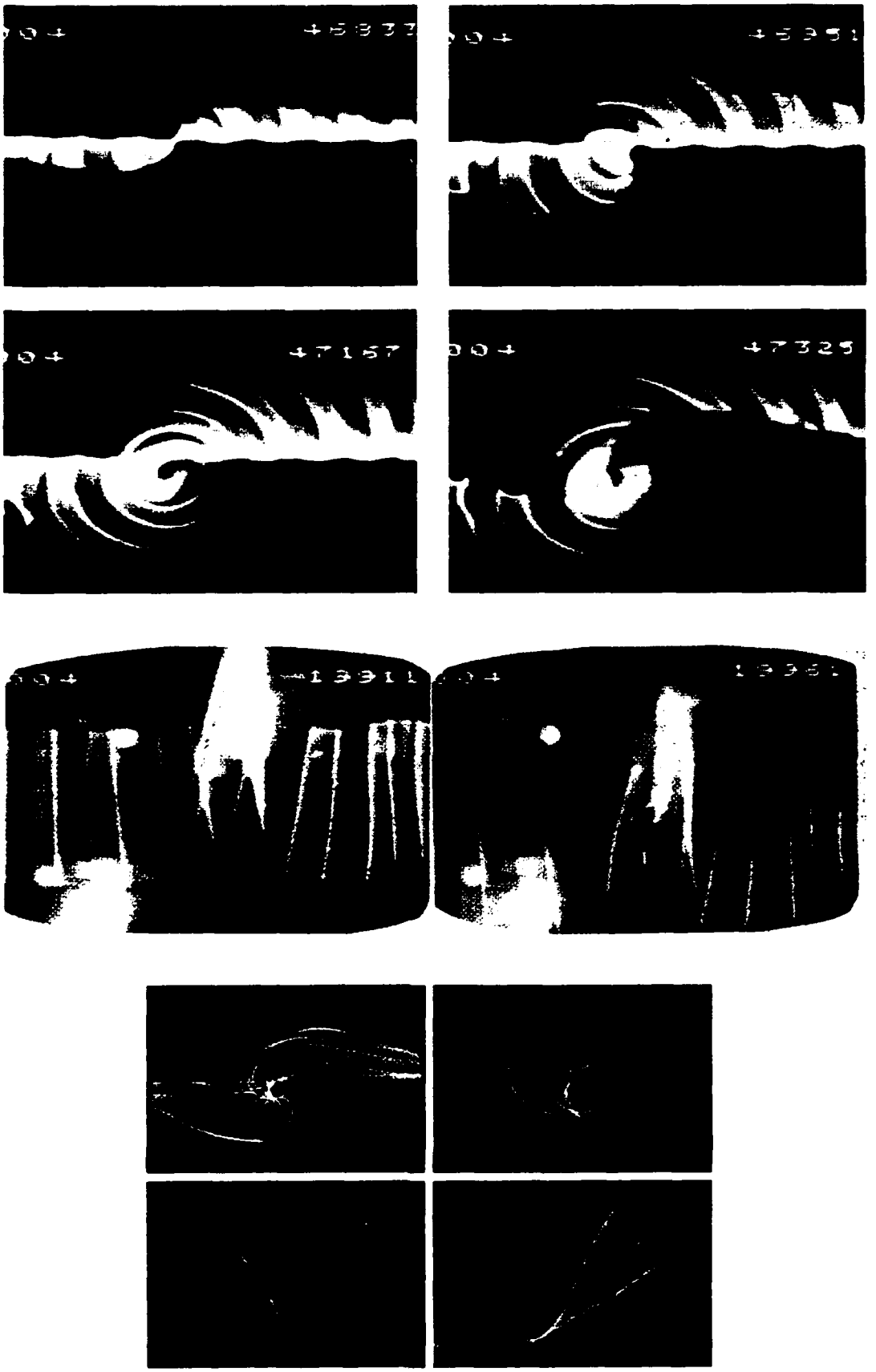

Figure 5: Visualization of tip vortex showing end and plan views of evolution in time, as well as three-dimensional representation of vortex development obtained from CAD simulation (Kramer and Rockwell[19]).

Figure 6: Flow structure at leading-edge of an oscillating delta wing obtained by "flying wire" technique. (Atta and Rockwell[18]).

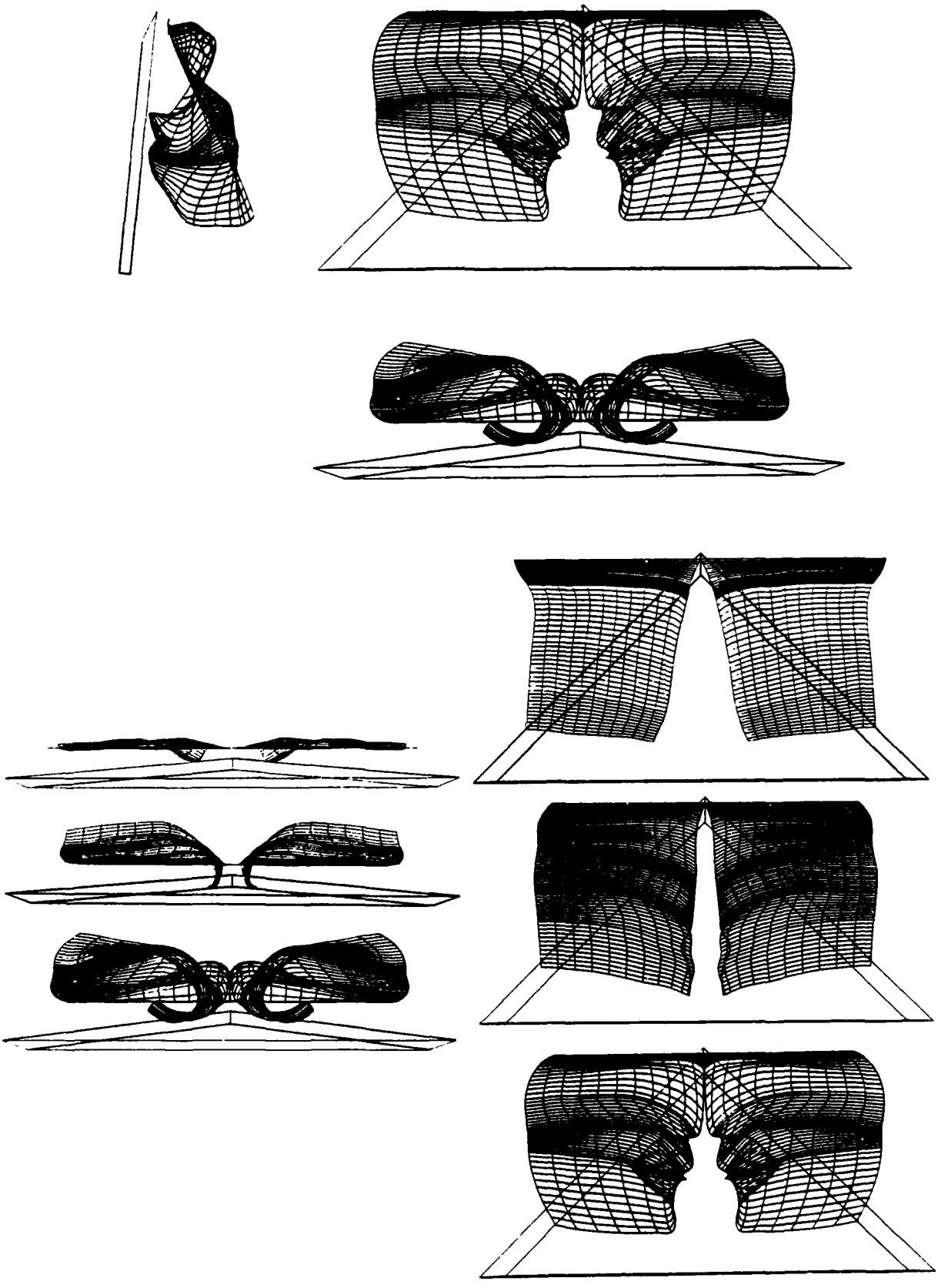

Figure 7: Various views of three-dimensional surface constructed from dual views of oscillating delta wing using CAD techniques. Original visualization data obtained from "flying wire" technique applied to wing pitching about its trailing-edge. Top set of views corresponds to relatively high reduced frequency. Bottom sets of views (from top to bottom) represents static, moderate, and high reduced frequencies. All views in this figure are at the same angle of attack (Magness, Lawson, and Rockwell[20]).

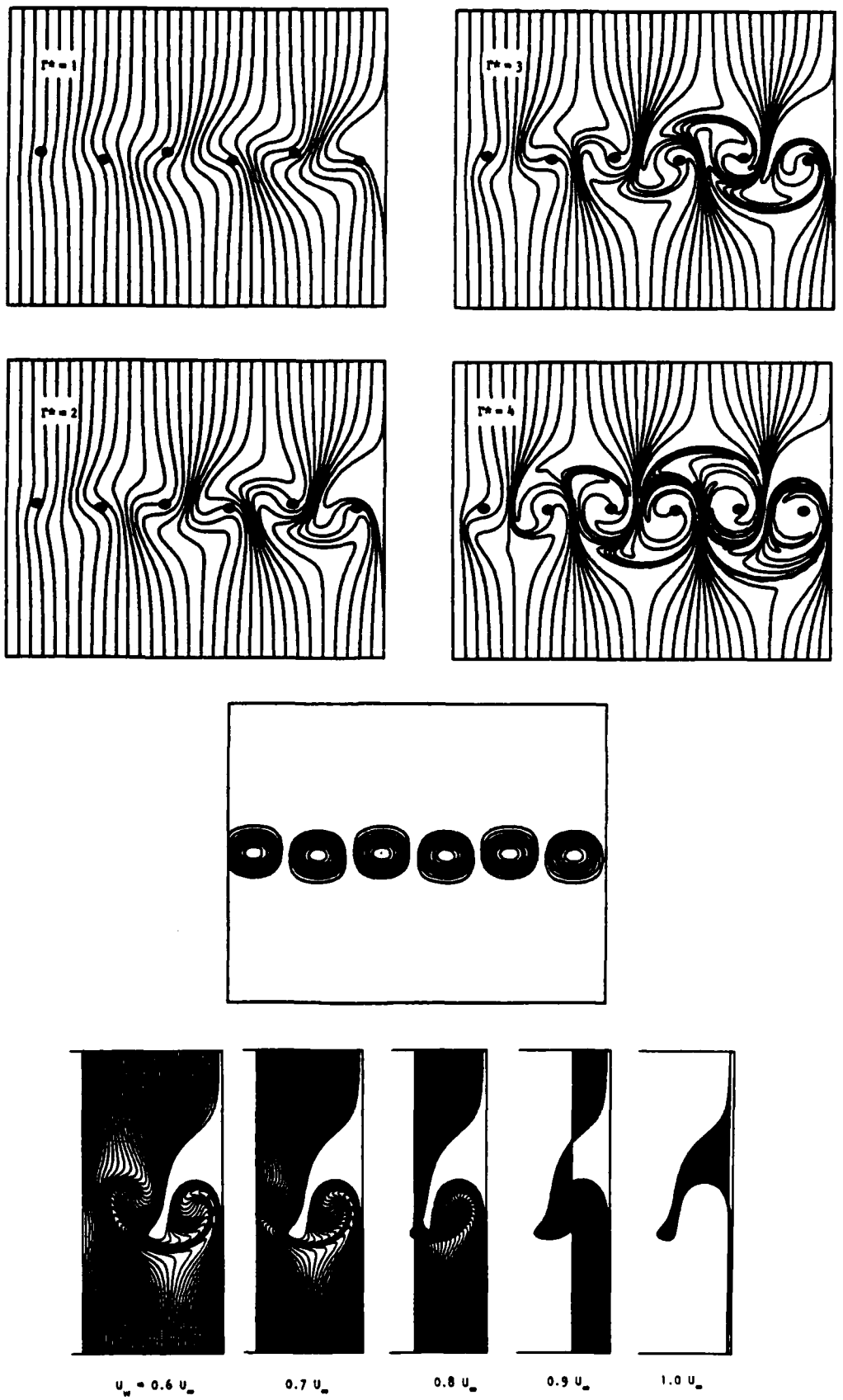

Figure 8: Simulation of flow visualization of a periodic wake using concepts of inviscid stability theory. Top series of diagrams represents timeline generation from a fixed wire located at lefthand side of each diagram; middle schematic shows the neutral, spatially-periodic vorticity field; and bottom diagram shows timeline generation from a wire moving at velocity U_w relative to the free-stream U_∞ (Lusseyran and Rockwell[4]).

In each of the four timeline plots, indicated in the upper part of Figure 8, the fixed timeline generator is located at the left side of each plot. Comparing these four timeline patterns, it is evident that the rate of "roll-up" of the timelines into a "vortex" appears to occur relatively slowly or rapidly depending upon the circulation Γ^*. The dots in these diagrams represent locations of vorticity extrema of the vorticity field illustrated in the middle diagram of Figure 8. The delay in deformation of the timeline pattern, from an initially vertical line, is related quantitatively to the circulation. By knowing the distance from the timeline generator required to turn an initially vertical timeline to an angle of, say 45°, a direct estimate of the circulation follows.

Further interpretation of the flow structure follows from use of a moving timeline generator as indicated in the bottom series of plots in Figure 8. The wire velocity U_w in the downstream section is a given fraction of the streamwise velocity U_∞. In all diagrams, the vorticity field is the neutral one given in the middle plot of Figure 8; the corresponding circulation is $\Gamma^* = 3$. It is apparent that the apparent rate of roll-up of the timeline pattern changes with the value of U_w, even though the vorticity field has the same circulation in all cases. This concept can be used to our advantage to indirectly determine the circulation in conjunction with the aforementioned flow simulation. For each value of Γ^*, there is a unique, threshold value of U_∞ for which a timeline marker moves upstream of the wire. For the parameters here, it occurs at $U_w = 0.8\ U_\infty$.

CONCLUDING REMARKS

From the foregoing, it is evident that there are a wide variety of possibilities for quantitatively interpreting flow visualization in conjunction with computer-aided image processing and simultaneous acquisition of pressure, lift, etc. Central to this approach, however, is a physically meaningful basis for defining the image. In fact, if portions of an image or portions of successive images are to be correlated with one another, then it is essential to have a means of identifying these domains. In a general sense, it is possible to generate an array of streaklines, pathlines, or timelines in order to accomplish this identification. However, one must be aware of the limitations inherent to flow visualization methods, namely that the visualized flow structure may not necessarily be an accurate representation of the underlying, unsteady vorticity field. Insofar as possible, it is desirable to implement techniques that employ a time of flight concept. That is, even though the velocity or vorticity may not be directly evident from the image, the marked fluid elements in the image should provide a basis for determining these central quantitative parameters.

ACKNOWLEDGEMENTS

The financial support of the Office of Naval Research, the Air Force Office of Scientific Research, the National Aeronautics and Space Administration, the National Science Foundation, and the Volkswagen Foundation is gratefully acknowledged.

LIST OF REFERENCES

1. Emrich, R. J., Methods of Experimental Physics: Fluid Dynamics, Vol. 18, Part A, Academic Press, New York, 1981.

2. Merzkirch, W., Chassery, J. M., Hesselink, L., Schon, J. P., Lourenco, L. and Monti, R., "Flow Visualization and Digital Image Processing" in von Karman Institute for Fluid Dynamics Lecture Series Monographs (1985-1986). Based on June 9-13, 1986, Lecture Series, Designated as 1986-09 Monograph.

3. Hama, F. R., "Streaklines in a Perturbed Shear Flow", Physics of Fluids, Vol. 5, No. 6, June 1962, pp. 644-650.

4. Lusseyran, D. and Rockwell, D. "On Interpretation of the Visualization in Unsteady Shear Layers", 1986, in preparation for publication.

5. Gumas, C. and Rockwell, D. "The Fourier Descriptor Technique: A Means of Pattern Description and Recognition in Fluid Mechanics", 1986, to be submitted for publication.

6. Gumas, C. "A General Pattern Recognition Technique for Open Curves", M.S. Thesis, Department of Computer Science and Electrical Engineering, Lehigh University, 1985.

7. Ongoren, A. and Rockwell, D., "Flow Structure from an Oscillating Cylinder. Part 1: Mechanisms of Phase Shift in the Near-Wake", 1986, submitted for publication.

8. Kerstens, P. and Rockwell, D., "Ensemble-Averaging on Correlation Techniques for Flow Visualization Images", 1986, to be submitted for publication.

9. Persoon, E. and Fu, K.-S., "Shape Discrimination Using Fourier Descriptors", IEEE Transactions on Systems, Man, and Cybernetics, Vol. SMC-7, No. 3, March 1977, pp. 170-179.

10. Granlund, G. H. "Fourier Processing for Hand Print Character Recognition", IEEE Transactions on Computers, Vol. C-21, February 1972, pp. 195-201.

11. Wallace, T. P. and Mitchell, O. R., "Analysis of Three-Dimensional Movement Using Fourier Descriptors", IEEE Transactions on Pattern Analysis and Machine Intelligence, Vol. PAME, No. 2 - No. 6, November, 1980, pp. 583-588.

12. Lu, L. J. and Smith, C. R. "Image Processing of Hydrogen Bubble Flow Visualization for Determination of Turbulence Statistics and Bursting Characteristics", Experiments in Fluids, Vol. 3, 1985, pp. 349-356.

13. Lusseyran, D. and Rockwell, D. "Estimation of Velocity Eigenfunction and Vorticity Distributions from the Timeline Visualization Technique", 1986, to be submitted to Experiments in Fluids.

14. Sohn, D. and Rockwell, D. "Vortex-Elliptical Edge Interactions", 1986, in preparation for publication.

15. Staubli, T. and Rockwell, D., "Pressure Fluctuations on an Oscillating Trailing-Edge", 1986, in preparation for publication.

16. Smith, C. R. and Paxson, R. D., "A Technique for Evaluation of Three-Dimensional Behavior in Turbulent Boundary Layers Using Computer Augmented Hydrogen Bubble-Wire Flow Visualization", Experiments in Fluids, Vol. 1, 1983, pp. 43-49.

17. Ongoren, A. and Rockwell, D., "Multiple Time-Surface Characterization of Time-Dependent, Three-Dimensional Flows", 1986, submitted for publication.

18. Atta, R. and Rockwell, D. 1986, in preparation for publication.

19. Kramer, L. and Rockwell, D. "Visualization of the Three-Dimensional, Time-Dependent Flow Structure of a Tip Vortex", Department of Mechanical Engineering and Mechanics, Lehigh University, 1986, unpublished.

20. Magness, C., Lawson, R., and Rockwell, D., 1986, in preparation for publication.

PROCEEDINGS OF THE

NASA/AFOSR/ARO WORKSHOP

PHYSICS OF FORCED UNSTEADY SEPARATION

NASA Ames Research Center
Moffett Field, CA
April 17-19, 1990

Edited by L.W. Carr

CONTROL OF LEADING-EDGE VORTICES ON A DELTA WING[1]

by

C. Magness, O. Robinson, and D. Rockwell

I. INTRODUCTION

The unsteady flow structure of leading-edge vortices on a delta wing has been investigated using new types of experimental techniques, in order to provide insight into the consequences of various forms of active control. These investigations involve global control of the entire wing and local control applied at crucial locations on or adjacent to the wing. Transient control having long and short time-scales, relative to the convective time-scale C/U_∞, allows substantial modification of the unsteady and time-mean flow structure.

Global control at long time-scale involves pitching the wing at rates an order of magnitude lower than the convective time-scale C/U_∞, but at large amplitudes. The functional form of the pitching maneuver exerts a predominant influence on the trajectory of the feeding sheet, the instantaneous vorticity distribution, and the instantaneous location of vortex breakdown.

Global control at short time-scales of the order of the inherent frequency of the shear layer separating from the leading-edge and the natural frequency of vortex breakdown shows that "resonant" response of the excited shear layer-vortex breakdown system is attainable. The spectral content of the induced disturbance is preserved not only across the entire core of the vortex, but also along the axis of the vortex into the region of vortex breakdown. This unsteady modification results in time-mean alteration of the axial and swirl velocity fields and the location of vortex breakdown.

Localized control at long and short time-scales involves application of various transient forms of suction and blowing using small probes upstream and downstream of the location of vortex breakdown, as well as distributed suction and blowing along the leading-edge of the wing applied in a direction tangential to the feeding sheet. These local control techniques can result in substantial alteration of the location of vortex breakdown; in some cases, it is possible to accomplish this without net mass addition to the flow field.

II. EXPERIMENTAL TECHNIQUES

The unsteady flow structure from the leading-edge of a delta wing subjected to various forms of active control has been characterized using new types of laser-diagnostic systems and image-processing techniques. These methods are integrated with active control systems, driven by central microcomputers. Using these approaches, it is possible to impose active control of arbitrary functional form and examine the response of the instantaneous flow structure. The two- and three-dimensional flow structure is interpreted with the aid of newly-released graphics supercomputers.

III. GLOBAL CONTROL AT LONG TIME SCALES

The concept of a phase shift between the unsteady motion of the wing and the development of the leading-edge vortex is well known. In qualitative visualization studies, Lambourne et al. (1969), Gad-el-Hak and Ho (1985a,b, 1986), and Atta and Rockwell (1989) reveal various features of the visualized cross-section of the vortex during its unsteady

[1]Submitted for presentation at the NASA/AFOSR/ARO Workshop on Physics of Forced Separation, April 17-19, 1990.

development. There also occurs a phase shift of the location of vortex breakdown relative to the wing motion; it has been characterized from various perspectives by Woffelt (1986), Rockwell et al. (1987), Atta and Rockwell (1987), Reynolds and Abtahi (1987), Gilliam, Robinson, Walker, Wisser (1987), and Lemay, Batill, and Nelson (1988).

The following unresolved issues are the focus of this investigation: the effect of arbitrary forms of pitching maneuver on the instantaneous structure of the leading-edge vortex including trajectories of feeding sheets and distributions of vorticity; the influence of vortex breakdown over a portion of the cross-section of the vortex; and the response of the axial location of vortex breakdown in relation to all of these features.

Concerning the nature of the instantaneous structure of the leading-edge vortices, obtained from particle tracking techniques, the following represent the major findings:

(i) For locations upsteam of vortex breakdown, the shape, degree of concentration, and the location of the maxima of the instantaneous vorticity distribution across the vortex core are quite different for the up- and downstrokes of the continuous pitch-up-down maneuvers of the wing. This finding emphasizes the importance of accounting for the instantaneous cross-sectional structure of the vortex, and not simply the instantaneous location of vortex breakdown, in determining the overall loading on the wing.

(ii) Comparison of the vorticity distribution of the leading-edge vortex with the trajectory of the feeding sheet from the edge of the wing shows the relationship between the possible trajectories of the feeding sheet and the corresponding vorticity field. A major factor is the occurrence or non-occurrence of vortex breakdown within the core of the vortex.

Figure 1 shows an excerpt from the current investigation. Contours of constant vorticity were obtained by direct particle tracking and image processing techniques. The experimental parameters correspond to a pitching motion of $15^\circ \leq \alpha \leq 40^\circ$ for a continuous pitch-up-down motion at a pitching rate $\dot{\alpha}C/2U_\infty = 0.15$. The surface of the wing is indicated by the bold horizontal line. The contours of constant vorticity on the left side correspond to the pitch-up portion of the maneuver, and those on the right side to the pitch-down portion. The differences in elevation, orientation, and scale of the vorticity distributions are evident. They are dependent upon the history of the wing motion and appear to be most pronounced at the smallest angle of attack $\alpha = 20^\circ$.

The importance of accounting for vortex breakdown within the core of the vortex is illustrated in Figure 2. Instantaneous positions of the feeding sheets and contours of constant vorticity are shown for the same parameters as in Figure 2, but at $\alpha = 40^\circ$ for two different types of maneuvers. The shaded black region represents the extent of breakdown within the vortex. For the simple pitch-down motion, $\alpha = 40^\circ$ represents the static condition immediately preceding the onset of the maneuver, while the pitch-up-down case at $\alpha = 40^\circ$ includes the integrated history of the upstroke portion of the maneuver. It is evident that the positions of the feeding sheet and the contours of vorticity are substantially different for these two cases.

The structure of the leading-edge vortex at a given cross-section must, of course, be considered in conjunction with the axial movements of the location of vortex breakdown. Magness, Robinson, and Rockwell (1989) preliminarily addressed the effect of the type of pitching maneuver on the general response of the vortex breakdown location as a function of angle of attack. Recent studies have focussed on the vortex response to different classes of maneuver, and the detailed structure of the leading-edge vortices. Regarding the response of the location of the vortex breakdown, the major findings are:

(i) Continuous pitch up-down motions of the wing can preclude occurrence of vortex breakdown on the upstream portion of the wing, relative to that occurring for simple pitch-up and pitch-down motion where relaxation processes having long time scales are allowed to occur.

(ii) For the continuous pitch-up-down maneuver of the wing, the consequence of not allowing the vortex breakdown to relax to its equilibrium state is to produce upstream movements of the vortex breakdown location towards the apex for initial decreases in angle of attack α.

(iii) Combinations of simple ramp-type motions to form a hybrid pitching motion produce overshoots of the static characteristic of vortex breakdown location versus angle of attack, beyond that attainable with any of the simple ramp motions alone.

Figure 3 shows plots characterizing the first two of these three principal findings at two extreme values of reduced frequency. This sort of characterization of the breakdown location serves as a basis for detailed investigations of the flow structure of the leading-edge vortices.

IV. GLOBAL CONTROL AT SHORT TIME SCALES

Perturbation of a delta wing in the pitching mode at sufficiently high frequency and very low amplitude allows control of the detailed flow structure of the leading-edge vortex. In essence, the vortex development and breakdown on a delta wing involves two classes of characteristic frequencies: the inherent instability frequency of the shear layer from the leading-edge; and the frequency at which vortex breakdown occurs. The major issues here are: the structure of the perturbed feeding sheet; the nature of the perturbed onset of vortex breakdown; and the corresponding alteration of the time-mean vortex flow.

Simple considerations of hydrodynamic instability show that the processes of disturbance amplification in the shear layer and in the vortex core during the breakdown process are receptive to a wide range of excitation frequencies. As a consequence, it is possible to attain "resonant" excitation, leading to large alteration of the separating shear layer from the edge of the wing and the breakdown of the vortex core. The preliminary phase of this investigation was reported by Rockwell et al. (1987). This work is described in its completed form by Kuo, Magness, and Rockwell (1989).

The principal findings of this investigation are, in short:

(i) Small amplitude perturbations of the leading-edge lead to substantial alteration of the structure of the shear layer separating from it without occurrence of the classical mechanism of small-scale vortex coalescence.

(ii) The spectral content of the disturbance induced in the shear layer separating from the leading-edge is preserved not only across the core of the vortex, but also along the streamwise extent of the core into the region of vortex breakdown.

(iii) Substantial alteration of the time-mean characteristics of the leading-edge vortex include changes in the axial and swirl velocity fields and modification of the location of vortex breakdown.

Selected excerpts describing certain of the foregoing phenomena are given in Figures 4 through 6. Figure 4 shows the visualization obtained by locating a vertical hydrogen bubble wire along the leading-edge of the wing. The laser sheet that illuminated the marker bubbles was translated to the downstream locations x/C indicated in the photos. Excitation frequency

f_e is normalized with respect to the inherent instability frequency f_i of the shear layer separating from the leading-edge. Large-scale vortical structures are induced over the cross-section of the vortex in the presence of excitation at the inherent instability frequency of the feeding sheet. No small-scale vortex coalescence occurs.

Figure 5 shows spectra of the streamwise component $\tilde{u}$, i.e. $S_{\tilde{u}}$, taken at various locations upstream and downstream of the onset of vortex breakdown. The edge excitation frequency f_e is normalized by the inherent vortex breakdown frequency f_b. For excitation at the first harmonic of the vortex breakdown frequency, i.e. at $f_e/f_b = 2$, the spectral content shows predominance of the excitation frequency and its associated higher harmonics in regions before and after occurrence of vortex breakdown. In this case, the higher harmonic content persists well downstream of the onset of breakdown. For excitation at $f_e/f_b = 1$, there also occur a large number of higher harmonics due to the strong nonlinearity of the shear layer response. This spectral content is maintained over the entire cross-section of the vortex core prior to the occurence of breakdown, emphasizing the nonoccurence of vortex-vortex interactions (i.e. coalescence) in the shear layer as it is wrapped inwards toward the center of the core. Downstream of vortex breakdown, the predominant excitation peak at $f_e/f_b = 1$ persists, but the coherent higher harmonic components are attenuated.

Figure 6 shows contours of constant mean axial velocity $\bar{u}$ and constant fluctuating velocity $\tilde{u}$ over the entire cross-section of the leading-edge vortex at values of excitation frequency f_e, relative to the inherent vortex breakdown frequency f_b, i.e. $f_e/f_b = 1$ (left column) and 2 (right column). The effect of the matched excitation at $f_e/f_b = 1$ is to induce large amplitude fluctuations in the separating shear layer surrounding the core of the vortex, located at the peak of the contours of constant $\bar{u}$ and designated by the symbol +. At $f_e/f_b = 2$, the location of the core of the vortex moves downward towards the surface of the wing and outward towards the leading-edge. The maximum amplitude of the fluctuation $\tilde{u}$ is coincident with the location of the core of the vortex. This coincidence of the maxima of $\bar{u}$ and $\tilde{u}$ corresponds to the early onset of vortex breakdown at the higher excitation frequency $f_e/f_b = 2$.

V. LOCAL CONTROL AT MODERATE AND LONG TIME SCALES

Local control involves localized injection or suction of the flow at defined locations in the flow field and/or the surface of the wing. In a practical sense, this can be achieved by use of small probes, whose tips are located at crucial locations in the vortex core, or slits along the leading-edge of the wing. In essence, these techniques simulate localized point sources/sinks or distributions of them. The major issues here are: determination of the most sensitive location of the applied control; and optimization of the functional form of the unsteady control in the form of blowing/suction.

For the case of localized blowing along the leading-edge of the wing, Wisser, Iwanski, Nielson, and Ng (1988) most recently have revealed an increase in length of the vortex core prior to breakdown and an increase in lift acting on the wing. Not until this past year has the case of localized suction been explored; such simulations of a localized sink are described by Parm nter and Rockwell (1989). Location of a probe in the region downstream of vortex breakdown allows efficient restabilization of the vortex core. Among the principal findings are:

(i) Locations of the simulated point sink downstream of the occurrence of vortex breakdown produces stabilization of the core; such stabilization is attainable at relatively low values of dimensionless suction coefficient C_μ. The transient response time of the stabilization process due to an imposed transient (unsteady sink flow) scales as the magnitude of the imposed transient suction.

(ii) Hysteresis effects occur due to relaxation of the vortex breakdown (on a stationary wing) after abrupt onset or cessation of suction. These hysteresis effects simulate those on a pitching delta wing.

Localized control involving simulations of distributed sources/sinks in the form of a blowing/suction slit along the leading-edge have received little attention except for the steady blowing experiments of Wood and Roberts (1987), Wood, Roberts and Lee (1987) and Roberts, Hesselink, Kroo, and Woods (1987), and the (high frequency) sinusoidal perturbations employed in the investigation of Gad-el-Hak and Blackwelder (1987). The consequences of this type of control on the structure of the large-scale vortex have remained unexplored. Moreover, the possible modification of the nature and location of onset of vortex breakdown has not been pursued. Important considerations in our recent investigations include not only the case of steady blowing, but also the corresponding case of steady suction and, most significantly, the case of cyclic blowing and suction. The major findings of this investigation are:

(i) Both steady suction and steady blowing are effective at low values of C_μ, i.e. both result in lengthening of the vortex core prior to the onset of breakdown.

(ii) The most effective and robust control involves cyclic suction and blowing at an appropriate frequency. This approach involves no net mass addition to or from the flow.

The use of cyclic blowing and suction applied tangentially in the form of a jet $V_j(t)$ at the rounded leading-edge is represented in Figure 7; it is compared with the case of no blowing/suction, i.e. $V_j(t) = 0$. (These data were acquired by Professor W. Gu, a member of our research group.) Comparison of these velocity fields of Figure 7 suggests that application of the control results in restabilization of the vortex from a stalled condition to a well-defined, large-scale vortical structure and downward deflection of the separation streamline from its approximately horizontal position. These trends are associated with downstream movement of the *location of vortex breakdown*.

VI. ACKNOWLEDGEMENTS

The authors gratefully acknowledge support of the Air Force Office of Scientific Research, as part of a program monitored by Captain H. Helin.

VII. LIST OF REFERENCES

Atta, R. and Rockwell, D. 1987 "Hysteresis of Vortex Development and Breakdown on an Oscillating Delta Wing", *AIAA Journal*, Vol. 25, No. 11, pp. 1512-1513.

Atta, R. and Rockwell, D. 1989 "Leading-Edge Vortices Due to Low Reynolds Number Flow Past a Pitching Delta Wing", *AIAA Journal* (in press).

Gad-el-Hak, M. and Blackwelder, R. F. 1987 "Control of the Discrete Vortices from a Delta Wing", *AIAA Journal*, Vol. 25, No. 8, pp. 1042-1049.

Gad-el-Hak, M. and Ho, C.-M. 1985a "The Pitching Delta Wing", *AIAA Journal*, Vol. 23, No. 11, pp. 1660-1665.

Gad-el-Hak, M. and Ho, C.-M. 1985b "Three-Dimensional Effects on a Pitching Lifting Surface", AIAA Paper No. 85-0041, presented at the AIAA 23rd Aerospace Sciences Meeting, January 14-17, Reno, Nevada.

Gad-el-Hak, M. and Ho, C.-M. 1986 "Unsteady Vortical Flow Around Three-Dimensional Lifting Surfaces", *AIAA Journal*, Vol. 24, No. 5, May, pp. 713-721.

Gilliam, F., Robinson, N., Walker, J., and Wissler, J. 1987 "Visualization of Unsteady Separated Flow About a Pitching Delta Wing", AIAA 25th Aerospace Sciences Meeting, January 12-15, Reno, Nevada.

Kuo, C.-H., Magness, C., and Rockwell, D. 1989 "Control of Vortex Structure on a Delta Wing by Small-Amplitude Perturbations of Angle-of-Attack", submitted for publication.

Lambourne, N. C., Bryer, D. W., and Maybrey, J. F. N. 1969 "The Behavior of Leading-Edge Vortices Over a Delta Wing Following Sudden Change of Incidence", The Aeronautical Research Council Technical Report, Report and Memorandum 3645.

LeMay, S. P., Batill, S. M., and Nelson, R. C. 1988 "Leading-Edge Vortex Dynamics on a Pitching Delta Wing", AIAA Paper No. AIAA-88-2559-CP, AIAA Sixth Applied Aerodynamics Conference, June 6-8, Williamsburg, Virginia.

Magness, C., Robinson, O., and Rockwell, D. 1989 "Control of Leading-Edge Vortices on a Delta Wing", AIAA Paper No. 89-0999, presented at AIAA 2nd Shear Flow Conference, March 13-16, Tempe, Arizona.

Parmenter, K. and Rockwell, D. 1989 "Response of Leading-Edge Vortices to Localized Suction", *AIAA Journal* (in press).

Reynolds, G. A. and Abtahi, A. A. 1987 "Instabilities in Leading-Edge Vortex Development", AIAA Paper No. 87-2424, AIAA Applied Aerodynamics and Atmospheric Flight Dynamics Conference, August 17-19, Monterey, California.

Roberts, L., Hesselink, L., Kroo, I., and Wood, N. 1987 "The Control of Vortical Flows Over a Delta Wing", Proceedings of Workshop on Unsteady Separated Flows at U. S. Air Force Academy. Also see Frank J. Seiler Research Laboratory Report FJSRL-TR-88-0004, September 1988, Air Force Systems Command, United States Air Force.

Rockwell, D., Atta, R., Kuo, C.-H., Hefele, C., Magness, C., and Utsch, T. 1987 "On Unsteady Flow Structure from Swept Edges Subjected to Controlled Motion", Proceedings of Workshop on Unsteady Separated Flows at U. S. Air Force Academy. Also see Frank J. Seiler Research Laboratory Report FJSRL-TR-88-0004, September 1988, Air Force Systems Command, United States Air Force.

Wisser, K., Iwanski, K. T., Nelson, R. C. and Ng, T. T. 1988 "Control of Leading-Edge Vortex Breakdown by Blowing", AIAA Paper No. 88-0504, AIAA 26th Aerospace Sciences Meeting, January, Reno, Nevada.

Wolffelt, K. W. 1986 "Investigation on the Movement of Vortex Burst Position with Dynamically Changing Angle of Attack for a Schematic Delta Wing in a Water Tunnel with Correlation to Similar Studies in Wind Tunnel", AGARD Conference Proceedings #413, Aerodynamic and Related Hydrodynamic Studies Using Water Facilities, Symposium of the Fluid Dynamics Panel, Monterey, California, 20-23 October, 1986.

Wood, N. J. and Roberts, L. 1987 "The Control of Vortical Lift on Delta Wings by Tangential Leading-Edge Blowing", AIAA Paper 87-0158, January.

Wood, N. J., Roberts, L., and Lee, K. T. 1987 "The Control of Vortical Flow on a Delta Wing at High Angles of Attack", AIAA Paper 87-2278, August.

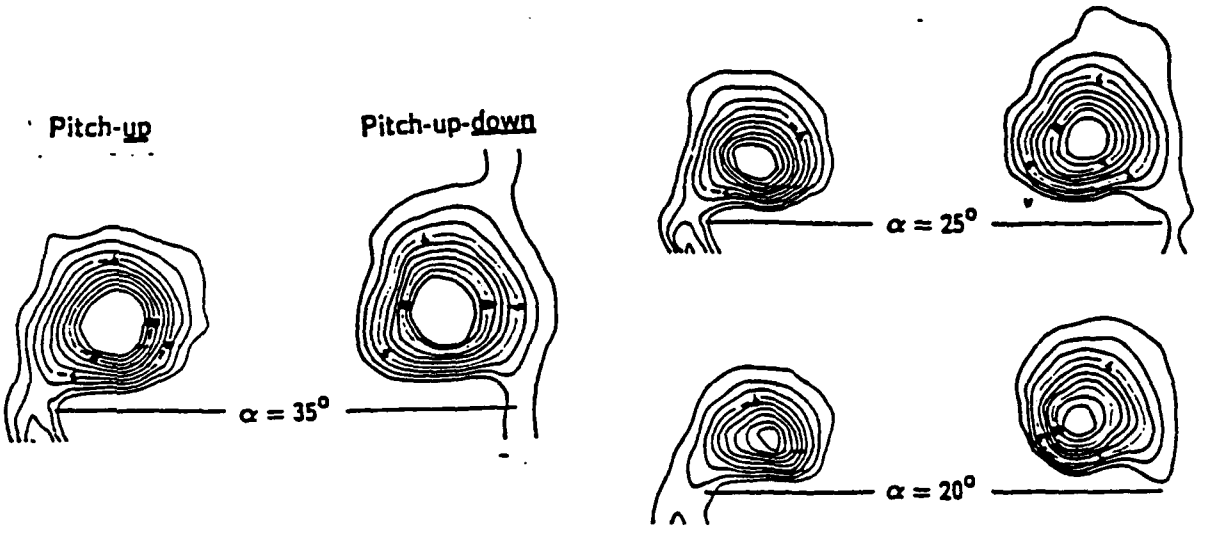

Figure 1: Instantaneous contours of constant vorticity at midchord for continuous pitch-up-down maneuver of delta wing. Sweep angle = 75°; pitch rate $\dot{\alpha}C/2U = 0.15$; pitching axis at midchord.

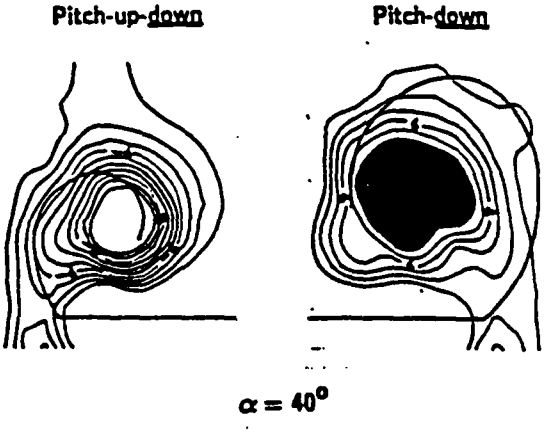

Figure 2: Instantaneous contours of constant vorticity and positions of feeding sheet at $\alpha = 40°$ for continuous pitch-up-down and pitch-down maneuvers. Sweep angle = 75°; pitch rate $\dot{\alpha}C/2U = 0.5$; pitching axis at midchord.

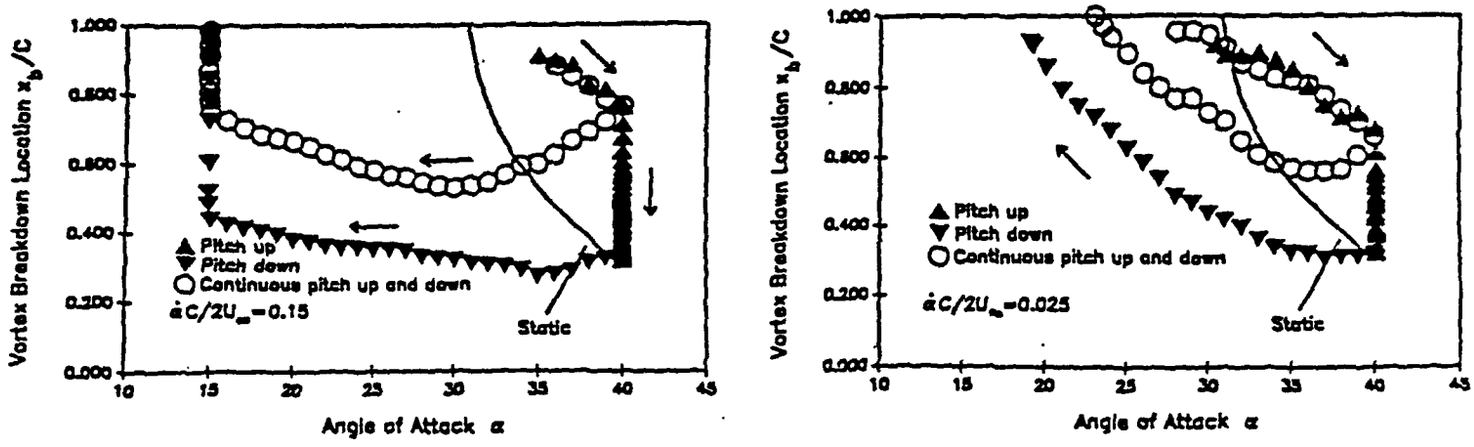

Figure 3: Instantaneous location of vortex breakdown as function of angle of attack for three basic types of delta wing maneuvers and two extreme values of dimensionless pitching rate. Sweep angle of delta wing = 75°.

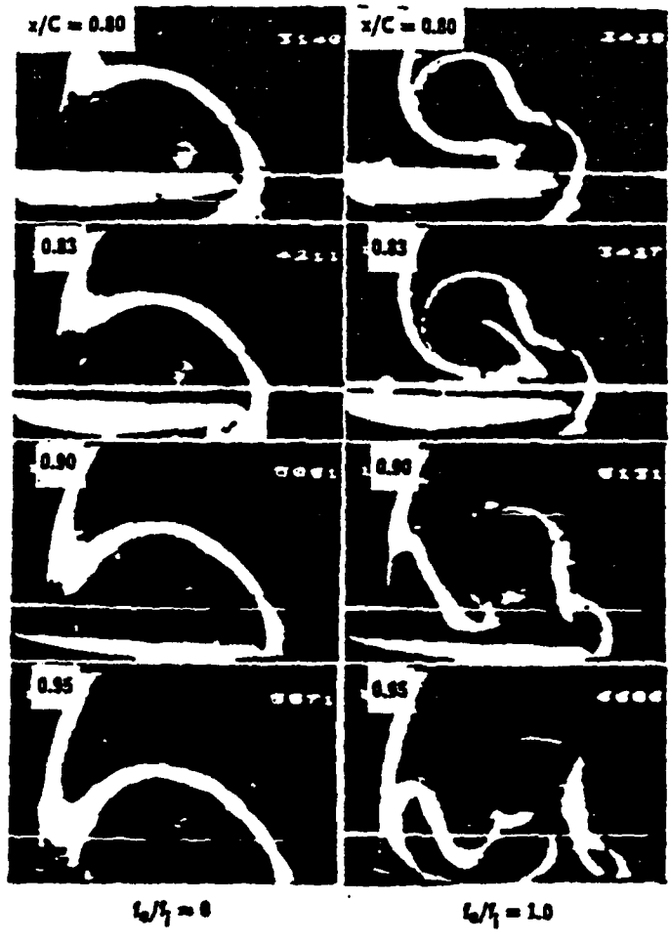

Figure 4: Visualization of flow structure of separating shear layer at several cross-sections along leading-edge of delta wing. Ratio of excitation frequency f_e to inherent instability frequency f_i of separating shear layer is: 0 (left column); 0.5 (middle column); and 1.0 (right column). Angle of attack $\alpha = \bar{\alpha} + \alpha_0 \sin 2\pi f_e t$; $\bar{\alpha} = 20°$, $\alpha_0 = 1°$.

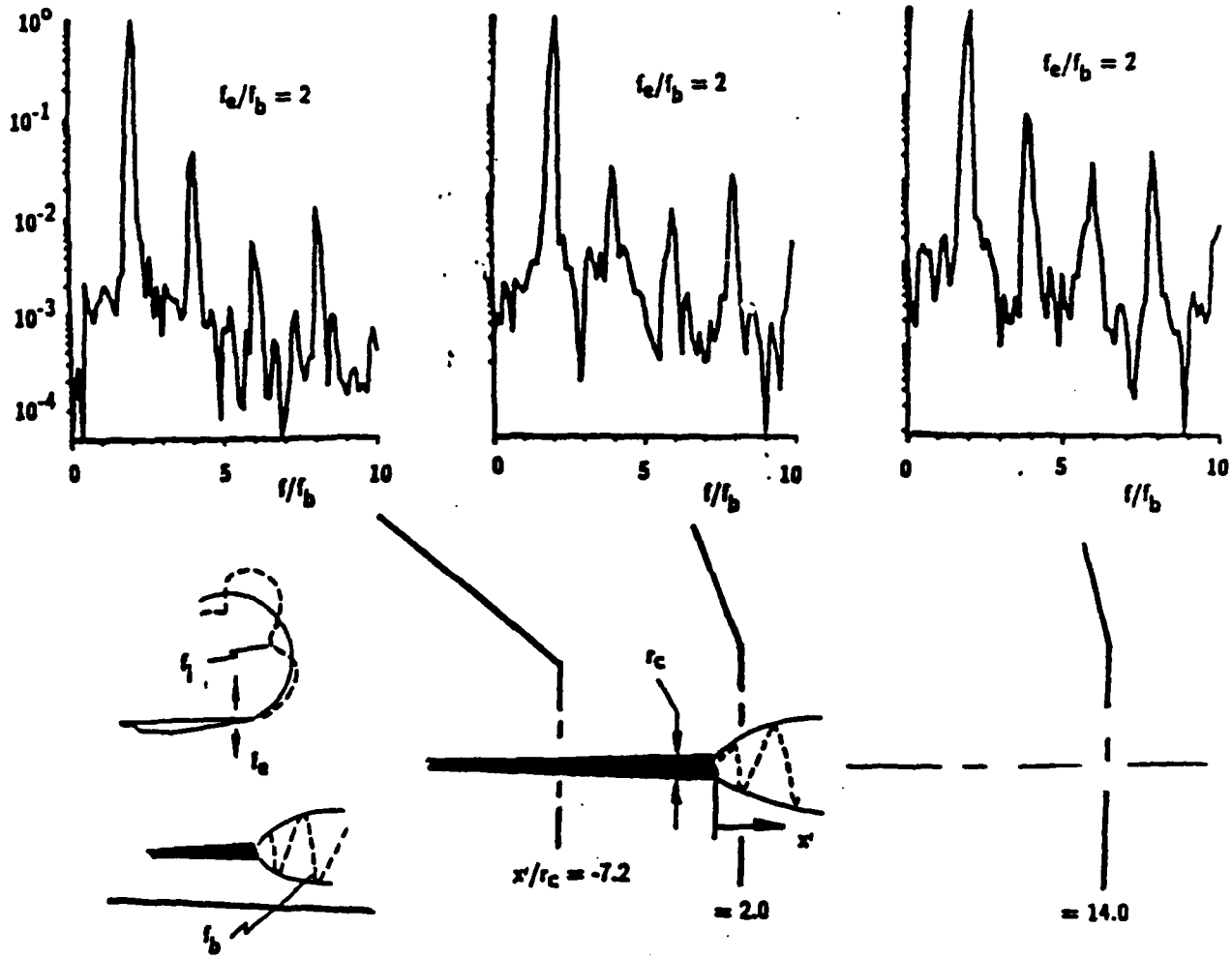

Figure 5: Overview of evolution of spectral content of vortex core upstream and downstream of vortex breakdown. Ratio of excitation frequency f_e to vortex breakdown frequency f_b has values indicated. $f_i/f_b = 2$.

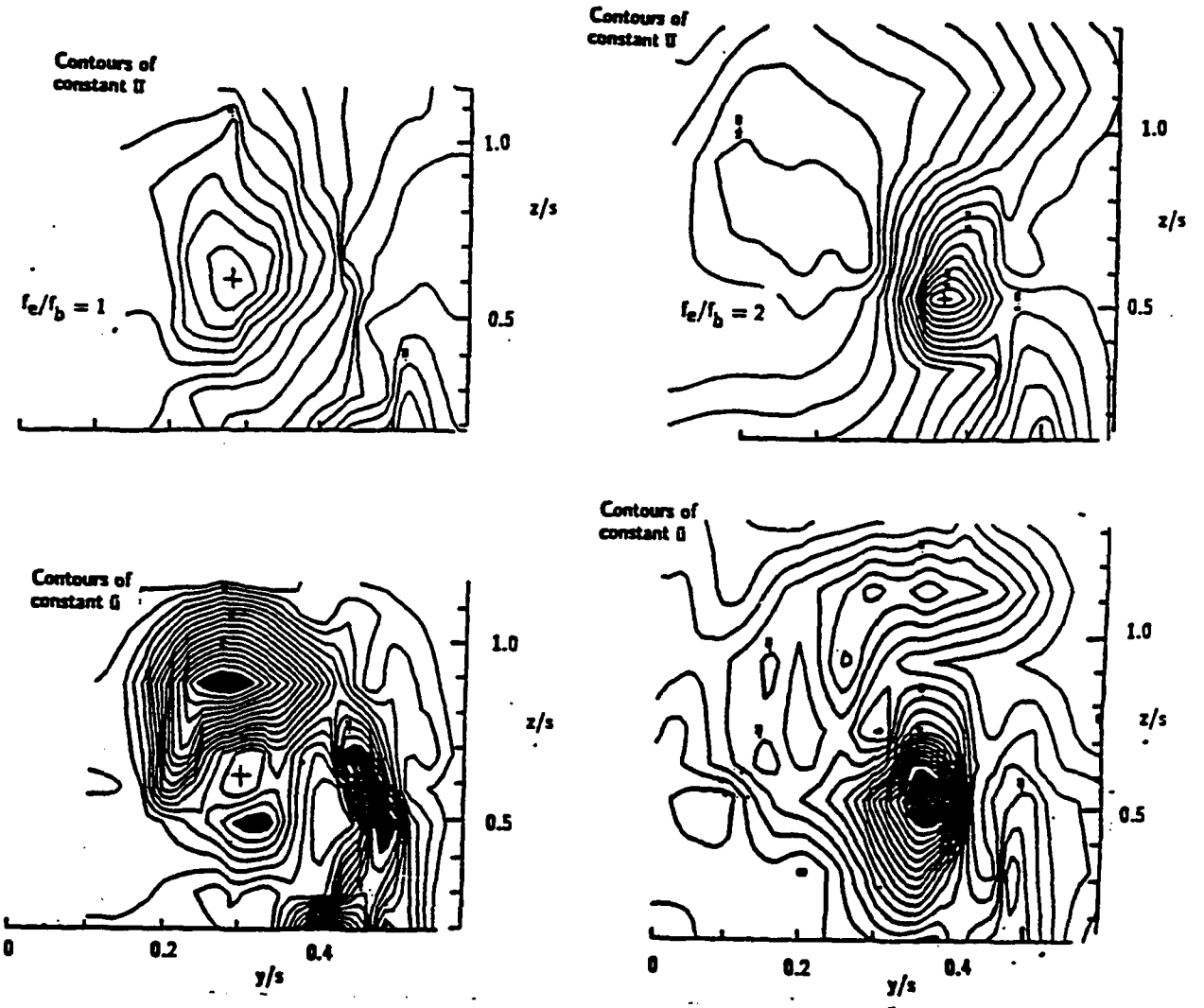

Figure 6: Distribution of mean U component of axial velocity over cross-section of vortex upstream of occurrence of vortex breakdown. Data acquired at reference station $x/C = 0.38$ upstream of vortex breakdown. Ratio of excitation frequency f_e to frequency f_b of inherent vortex breakdown is $f_e/f_b = 1$ (left column) and $f_e/f_b = 2$ (right column). Ratio of inherent instability frequency f_i of separating shear layer to frequency f_b is $f_i/f_b = 2$.

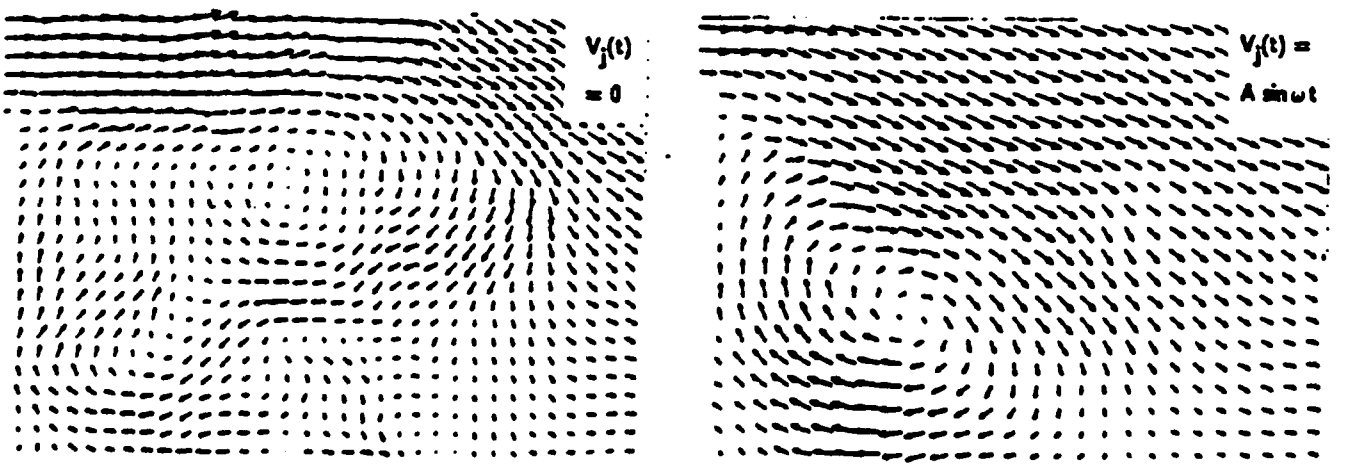

Figure 7: Comparison of velocity fields over cross-section of half delta wing at $\alpha = 45^\circ$ for cases with and without sinusoidal suction/blowing applied tangentially at rounded leading-edge. Laser sheet defining cross-section of visualized vortex located at approximately one-third chord.